LONGITUDINAL SLAB SPLITTING IN COMPOSITE GIRDERS

By

Jason M. Piotter

Thesis submitted to the faculty of
The Virginia Polytechnic Institute and State University
in partial fulfillment of the requirements for the degree of

Master of Science
in
Civil Engineering

APPROVED:

_____
W. Samuel Easterling, Chairman

_____ _____
Thomas M. Murray Carin Roberts-Wollmann

April 2001
Blacksburg, VA 24061

Keywords: **Longitudinal Shear, Longitudinal Splitting, Composite Girders, Composite Floor Systems, Transverse Reinforcement**

LONGITUDINAL SLAB SPLITTING IN COMPOSITE GIRDERS

By

Jason M. Piotter

Committee Chairman: W. Samuel Easterling

Via Department of Civil and Environmental Engineering

(ABSTRACT)

Longitudinal slab splitting in composite hot rolled girders and joist girders was investigated. Two different type of framing configurations were studied with two tests conducted per configuration. The framing configurations were designated as either flush-framed or haunched, which describes the framing of the joists into the joist girders or H-shape. Each floor system consisted of at least one exterior or spandrel joist girder, one interior joist girder, and in three of the four tests, an exterior or spandrel H-shape. The nominal lengths of the girders were 30 ft 4 in. with a centerline spacing of 7 ft for the flush-framed tests and 6 ft 9 in. for the haunch tests. Varying amounts of transverse reinforcement were used in the slab over each girder. Shear connectors were all 0.75 in. diameter headed shear studs of varying lengths. The results of these tests were used to determine the minimum amount of transverse reinforcement required to prevent longitudinal splitting from controlling the strength of the section.

A comparative analytical study was performed to generate a design procedure for determining the appropriate amount of transverse reinforcement. This consisted of adapting existing procedures in reinforced concrete for similar shear problems and generating alternative procedures based on existing research for composite construction. Results from these methods were then calibrated against experimental data obtained in this study.

ACKNOWLEDGEMENTS

I would like to extend my gratitude to Dr. W. Samuel Easterling for his guidance, patience, and depth of knowledge with regard to this research. His input and mentorship have helped me tremendously. I would also like to thank Dr. Thomas M. Murray for his advice, knowledge, and his willingness to take part in my academic and professional development. I would like to thank Dr. Carin Roberts Wollman for her input on the issues relating to the concrete slab and her availability at a moments notice. I would like to thank David Samuelson and Nucor Research and Development for sponsoring this research. I would also like to thank Dr. Hari Turner for helping me discover Virginia Tech and Dr. Raymond Plaut for making the process of getting here easier. I would also like to thank the Via family for the generous contribution that made my graduate education possible.

I would like to extend thanks to my fellow students within the structures division who have helped me and challenged me in ways that are unparalleled. Specifically, I would like to thank Alvin Trout, J.R. Mujagic, Thad Chapman, Marcela Guirola, Ben Mason, Grace Shen, and Emmett Sumner. I would also like to thank laboratory staff Brett Farmer, Dennis Huffman, and Denson Graham for their assistance in the construction and testing of the specimens and components.

I would like to thank my family of my parents, Jess and Vickie, and my brother Shawn in addition to the Kitzmann family of Roy, Joyce, Andy, and Jane for all the support they have given me throughout my academic career. I would not have made it this far if it weren't for them. Specifically, I want to above all thank my wife Amy; for just being there when things got difficult, for giving me the support I needed to continue my education, and the understanding to know that this journey will be worth it in the end.

TABLE OF CONTENTS

TABLE OF CONTENTS (cont.)

TABLE OF CONTENTS (cont.)

LIST OF FIGURES

LIST OF FIGURES (cont.)

LIST OF FIGURES (cont.)

LIST OF FIGURES (cont.)

LIST OF TABLES

LIST OF SYMBOLS

a	Depth of equivalent stress block in concrete slab, distance from end of span to load point
A_{BC}	Cross sectional area of bottom chord in joist girder
A_c	Cross sectional area of concrete perpendicular to plane of bending
A_{cs}	Area of concrete between shear planes or between the slab edge and shear plane
A_{cv}	Cross sectional area of slab in longitudinal shear plane
A_s	Cross sectional area of steel element
A_{sc}	Cross sectional area of headed shear stud
A_{TC}	Cross sectional area of top chord in joist girder
b	Effective width of concrete slab
b'	Width of concrete between shear planes of between shear plane and edge of slab
C	Total compressive force in concrete slab
C_1	Compressive force in steel member
d	Depth of steel joist or joist girder measure out to out
E	Modulus of elasticity of steel member
E_c	Modulus of elasticity of concrete
f'_c	Concrete cylinder strength
f_{mesh}	Yield strength of steel mesh
f_u	Ultimate tensile strength of steel member
f_y	Yield strength of steel member
f_{yr}	Yield strength of transverse reinforcement
I	Moment of inertia
I_{chords}	Moment of inertia of the top and bottom chords in joist
I_{comp}	Composite moment of inertia
I_{eff}	Total effective moment of inertia
I_s	Moment of inertia for steel member
I_s'	Adjusted moment of inertia for steel member
I_t'	Adjusted moment of inertia for composite section
in^2	Square inches

K_1	ACI shear constant equal to 400 psi in normal weight concrete
kip	One thousand pounds
ksi	Kip per square inch
l	Span of member
L_v	Length of shear span
P	Load at third point or end reaction including dead load and live load
M_{dn}^{calc}	Total design moment calculated with nominal material properties (60% M_n^{calc})
M_n^{calc}	Total ultimate moment calculated with nominal material properties
M_u^{calc}	Total ultimate moment calculated with actual material properties
M_u^{exp}	Total experimental ultimate moment
M_u'	Calculated moment considering only the concrete between shear planes
mm^2	Square millimeters
N	Newtons
n	Total number of welded shear studs in a shear span
psi	Pounds per square inch
Q_n	Total shear strength of a single welded shear stud
ΣQ_n	Limiting load for calculating the moment capacity of a composite section. The minimum of Asfy, 0.85f'c Ac, or nQn
T	Total tensile force in joist bottom chord or H-shape
T_1	Total tensile force in joist top chord
V_r	Longitudinal shear resistance
V_u	Applied longitudinal shear
v_u	Applied longitudinal shear stress
V_n^{calc}	Ultimate longitudinal shear stress calculated with nominal material properties
V_u^{calc}	Ultimate longitudinal shear stress calculated with actual material properties
V_u^{calc}	Ultimate longitudinal shear stress determined from chord, web, and flange strains
y_{BC}	Distance to bottom chord centroid measured to outstanding legs
y_{TC}	Distance to top chord centroid measured to outstanding legs
Δ_{MS}	Total midspan deflection
ρ	Reinforcement ratio; expressed as a ratio of As_{rebar} / A_{cv}

CHAPTER 1
INTRODUCTION

1.1 Background

Although composite steel and concrete members have been studied extensively and also used in steel-framed construction since the late 1960's, the limit states and design procedures with respect to strength and serviceability are still being researched. With respect to flexural members, the main body of research has focused on the strength and behavior of composite hot-rolled beams with or without profiled steel decking (A composite "beam" has the composite steel deck oriented perpendicular to the beam span, while a "girder" has the deck oriented parallel to the girder span). As a result, the American Institute of Steel Construction (AISC) provisions, in addition to European and Canadian steel codes, have covered this type of composite construction extensively. Composite hot-rolled girders or joist girders illustrated in Figure 1.1, however, have not been studied extensively. Ultimate strength methods have been developed for composite flexural members, but the methods used in the United States do not account for longitudinal shear and tensile cracks that develop in the slab.

Figure 1.1 Composite Girder Floor System

If longitudinal cracks occur due to high splitting forces caused by shear studs or negative transverse moment, there is a likelihood that a non-ductile failure will occur. This is due to a loss of continuity at critical shear planes in a portion of the top

compression flange of the composite member. The end result is the inability of the longitudinal shear force to disperse in the slab. The effective width concept is essentially invalid without the presence of transverse reinforcement to maintain the integrity of the slab if longitudinal or herringbone cracks are present.

Longitudinal shear strength of concrete elements was the subject of research by Hofbeck et al. (1969) and was adapted by Oehlers and Bradford (1995). They developed a mechanism for longitudinal shear, which defines the slab as initially cracked or uncracked. An initially uncracked section is analogous strut and tie model used in reinforced concrete analysis and design. A longitudinal shear force along one face of the slab induces a shear deformation which in turn introduces tensile forces along the principal directions. This resulting tensile force in the concrete forms characteristic herringbone cracks oriented 45 degrees to the direction of the longitudinal shear as illustrated in Figure 1.2. When transverse reinforcement is present, it completes the "strut and tie" model and inhibits premature failure. The system works by transfer of horizontal shear to concrete struts in compression. As the strut rotates, it induces tension in the transverse reinforcement, which prevents the slab from failing along the herringbone cracks until one of two events occur: the crushing of the concrete, or the yielding of the transverse reinforcement.

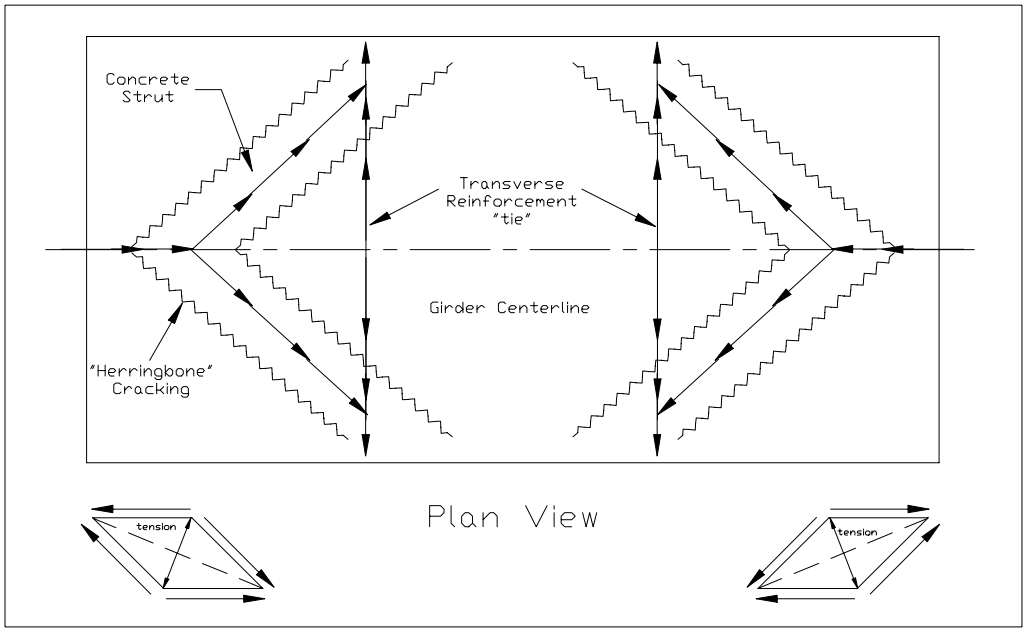

Figure 1.2 Strut and Tie Model

Initially cracked slabs in composite flexural members are characterized by the presence of longitudinal cracks parallel to the span of the steel member near a critical plane. The critical plane in general occurs at the thinnest portion of the slab over the steel deck flute nearest the girder centerline as illustrated in Figure 1.3. These cracks are assumed to form at or near the outset of the application of the superimposed dead loads or live loads due to negative transverse moments and concrete shrinkage. The crack face has three components resisting slip: aggregate interlock, dowel action, and friction. Interlock is considered a passive friction mechanism and is dependent on the axial stiffness of the transverse reinforcement and the concrete strength. The governing parameter is assumed to be concrete strength, while the transverse reinforcement needs only to prevent the formation of wide cracks.

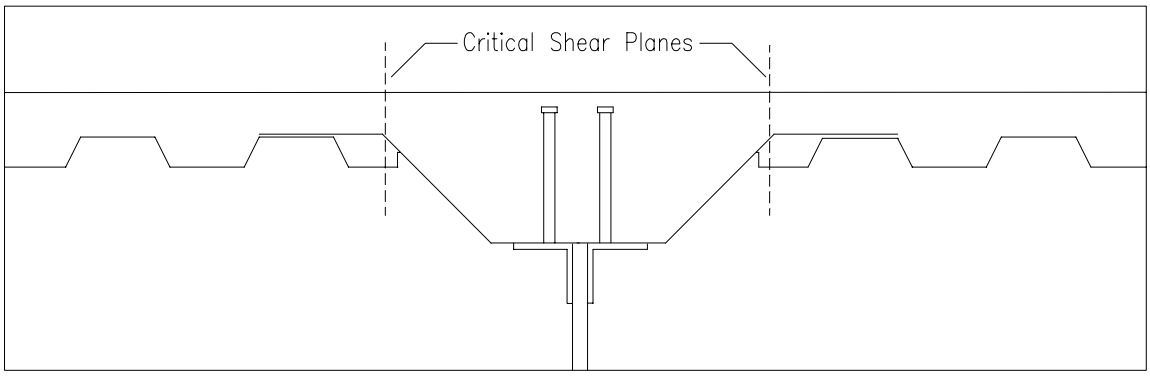

Figure 1.3 Critical Shear Planes

Active friction can contribute to the shear strength as well. This mode consists of an applied lateral compressive stress across the interface that keeps the crack faces in close proximity to allow for frictional resistance. Dowel action is provided by the transverse reinforcement passing across the crack interface. It is dependent on the yield strength of the steel reinforcement and the required development length of the rebar.

The focus in previous research has been on the initially longitudinally cracked section due to the nature of the type of failure that can occur and the likelihood of it occurring. It should be noted that in general, longitudinal slab splitting only applies to girders rather than beams. The explanation for this is that beams have steel deck oriented

with the flutes perpendicular to the axis of the steel beam. This effectively provides transverse reinforcement over the entire span.

The presence of negative transverse bending moment in addition to the extremely high shear forces that must be transferred, present a situation that can compromise the flexural strength of the girder. Excessive widening of the herringbone cracks is not likely due to the absence of large negative transverse moments in regions where the cracks propagate. Alternatively, longitudinal cracks in the slab have a higher likelihood of widening due to the negative transverse moment, which in effect reduces the contribution of the slab to resist longitudinal shear. If the cracks are wide enough, the slab contribution becomes negligible and if transverse reinforcement is not present, the composite girder will fail prior to reaching the calculated ultimate load.

Research on multiple girder floor systems (as opposed to single girder tests) has not been reported on with regard to transverse reinforcement either experimentally or analytically. The following questions arise: does a multiple composite girder floor better model the effects of longitudinal slab splitting and can the existing research on single composite girders effectively simulate what happens in a real floor system? Also, is it sufficient to provide enough reinforcement to reach the ultimate strength or should an attempt be made to provide reinforcement to prevent all cracking up to a certain percentage of the ultimate load? While the scope of this research cannot answer these questions completely, it provides a method for designing the appropriate amount of transverse reinforcement to maintain the effective slab width.

1.2 Literature Review

1.2.1 General

The existing body of research has focused on longitudinal slab cracking with tests on individual girders and corollary research on push off tests (illustrated in Figure 1.4) that simulated the effects of shear studs, concrete cracking, and transverse reinforcement. Push off tests give a reasonable estimate of local behavior around shear studs including crack formation. Specific push off tests presented in the following section have focused on the effect of direct shear normal to the embedded transverse reinforcement and also configurations where the existing crack and shear plane is oblique to the transverse

reinforcement. The research on longitudinal slab cracking has focused on single composite girders including joist girders, stub girders, and H-shapes. Single girder tests are similar to push off tests in that the results can be applied to composite behavior with reasonable results, but they do not model the true behavior of multiple member composite floor systems. Research on joist classification by Lauer et al. (1996) is presented because of the similarity in behavior of the chord and slab forces between composite joists and joist girders.

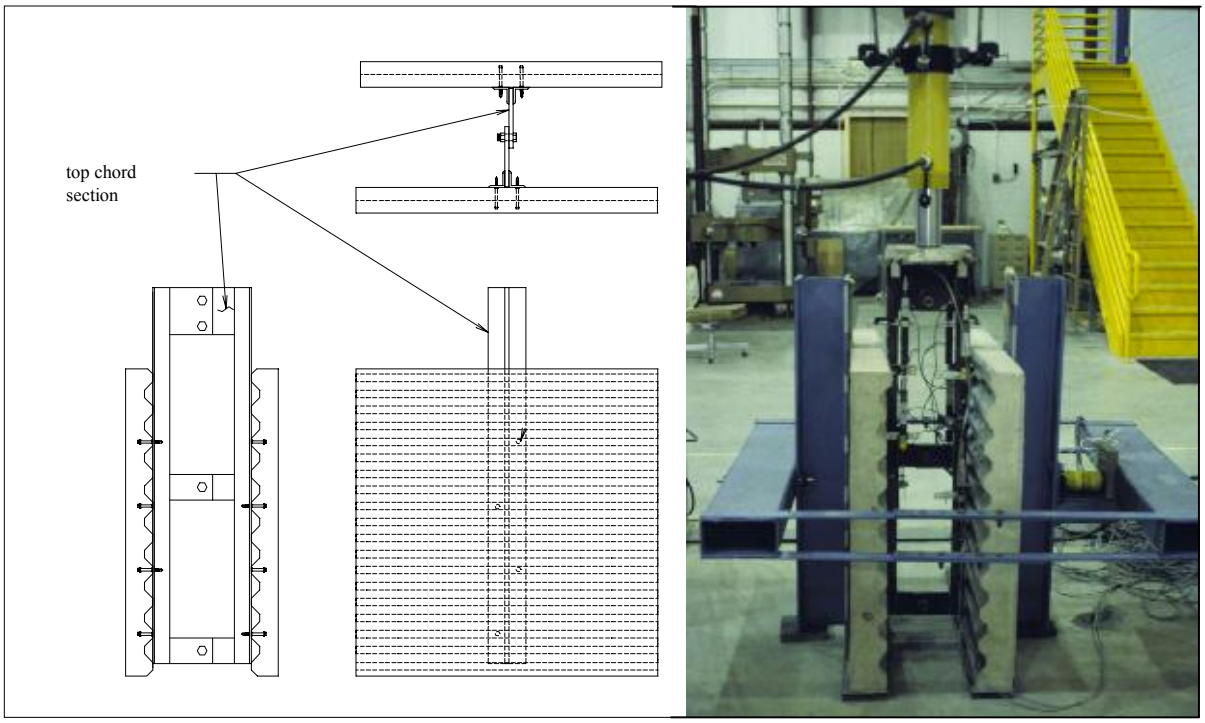

Figure 1.4 Push Off Test Setup

1.2.2 Existing Research

Johnson (1970) published one of the first papers dealing with longitudinal shear strength of composite beams. Specifically, he proposed a preliminary design method for the total amount of transverse reinforcement in composite slabs. This recommendation was based on a study of test results with positive and negative moment influence and without negative transverse bending.

The design method (Johnson 1970) utilizes conclusions drawn by Hofbeck et al. (1969). First, all transverse reinforcement, whether at the top or bottom of the slab,

contributes to longitudinal strength. Second, longitudinal bending moment does not need to be accounted for when determining the longitudinal shear strength. The parameters included in the design equations are the mean ultimate longitudinal shear stress on the governing shear plane (v_u) and ρF_{yr} which is the total transverse shear reinforcement per unit area of slab (ρ) times the yield strength of the steel (F_{yr}). The equations Johnson developed were for top and bottom reinforcement and represent minimum required reinforcement. Equations 1.1 and 1.2 correspond to the total reinforcement that is to be provided and Equations 1.3 and 1.4 correspond to the amount of reinforcement that is to be provided in the bottom of the slab.

$$\rho * F_{yr} \geq 1.26 v_u - 3.8\sqrt{f'c} \qquad \text{[Eq. 1.1]}$$

$$\rho * F_{yr} \geq 80 \qquad \text{[Eq. 1.2]}$$

$$\rho_b * F_{yr} \geq 0.63 v_u - 1.9\sqrt{f'c} \qquad \text{[Eq. 1.3]}$$

$$\rho_b * F_{yr} \geq 40 \qquad \text{[Eq. 1.4]}$$

Johnson (1970) also concluded that the need for transverse reinforcement is greatest when there is no negative transverse bending. This is in conflict with the assumption that as concrete protrusions sliding over one another separate an existing crack widens, inducing tensile stresses in the transverse reinforcement. Negative transverse moments will also cause the cracks to widen inducing additional tensile stresses in the transverse reinforcement.

Taylor et al.(1970) reported results from a series of push out tests including single sided and double-sided specimens and full-scale composite beam tests with haunched slabs over the steel member. The parameters that varied were haunch width, amount of transverse reinforcement, and number of shear studs. The test specimens were detailed to ensure that the stud height would remain short enough so that it would not extend fully into the slab but remain in the haunch. In the push out tests, an applied lateral load was applied to prevent separation (uplift) of the slab/haunch and the steel. Formation of cracks, effect of haunch reinforcement, number of studs, and effect of uplift were all noted and commented on in the results. Observation of the crack formation was

facilitated by not utilizing cold-formed steel deck. Load-slip and load-deflection curves were generated.

Taylor et al. concluded that push-off tests are a suitable way of generating data to study deep haunch behavior, but that they should not be used alone because they cannot replicate the complex stress conditions present in beams. They also concluded that to use the full strength of 0.5 in. diameter studs, a side cover of 3 inches is desirable but when this is not possible, lower stud strengths can be specified. It was also noted that stud forces that could cause bursting depend on the reinforcement of the haunch and must be taken into account for design.

El-Ghazzi et al. (1976) developed a design proposal that would introduce enough transverse shear reinforcement so that the first cracks form at the same time the ultimate moment is reached. The method, which uses a Cowan's failure criterion to determine the amount of shear stress that needs to be resisted, was developed for full and partial composite action. The stress distribution is idealized as the typical stress block concept used in reinforced concrete T-beams. The depth of the stress block (a) is given by:

$$a = \frac{\Sigma Q_n}{0.85 f`c * b} \qquad \text{[Eq. 1.5]}$$

Where

$$\Sigma Q_n = \min \begin{vmatrix} 0.85\ f'_c\ A_c \\ A_s F_y \\ nQ_n \end{vmatrix} \qquad \text{[Eq. 1.6]}$$

El Ghazzi et al. used these equations to develop a design equation for transverse reinforcement that relates the concrete strength (f'_c), effective width (b), and shear span (L_v) to the reinforcement ratio and the yield stress of the transverse reinforcement. The original equation based on a shear model equation was only valid for a certain range of parameters so El Ghazzi simplified it to an analytical method and then generalized it for a variety of variables utilizing design charts.

This method was then used to verify tests results reported by Davies (1969) on the effects of transverse reinforcement. It was shown that there was good agreement between the analytical method presented by El Ghazzi et al. and the empirical method put forth by Davies. El Ghazzi et al. concluded that longitudinal compressive strength, (effective) slab width b, and shear span L_v cannot be neglected when determining the amount of transverse reinforcement.

Robinson (1981) tested two composite girders with stub H-shapes framing in at the third points for slab support. The test specimens differed in the amount of transverse reinforcement and concrete strength. The girders in each test were W21x 62 with a nominal length of 41 ft and simply supported length of 40 ft. Twenty-nine shear studs (0.75 in. by 4.5 in.) were evenly spaced in each half span and 2 studs were placed on each side of the girder on the stub H-shapes. The formed metal deck was 3 in. deep, 8 ft wide, and was placed with the deck flutes parallel to the long axis of the girder. The nominal concrete slab thickness was 5 in. and the 28-day concrete strengths were reported as 3660 psi and 2530 psi for Girders 1 and 2 respectively. The slab reinforcement consisted of a total of eight No. 3 bars placed transverse to the girder; two located on either side of the stub H-shapes and two on either side of the load points which were located just inside the third points. The rebar was chaired to a height of 1.25 in. below the slab surface. Additionally, wire mesh (6 x 6 10/10) was used as a single layer in Girder 1 and a double layer in Girder 2. The girders were tested to failure with a hydraulic ram that applied load to a spreader beam that in turn applied two concentrated loads to 4 in. by 12 in. pin load applicators at 15 ft from either end of the girder.

The results of the test showed that cracks occurred in both specimens with a single wide crack in Girder 1 and two narrower cracks in Girder 2 which had twice the amount of wire mesh. This however did not affect the experimental strength of either girder as they reached 1.08 and 1.07 times the predicted strength. Both girders showed loss of interaction with Girder 2 having a greater loss of interaction despite having more transverse reinforcement. It should be noted that at the time this research was reported, it was assumed that the transverse reinforcement had some effect on the ultimate strength of the shear connectors.

Buckner et al. (1981) tested a 26 ft stub girder with a W10x72 girder section and three 5 ft W10x33 stub sections with shear studs welded to the stubs. The slab was 3.5 in. thick and contained No. 3 bars 12 in. on center placed at mid-depth of the slab. Each stub section had a total of 36 studs (0.625 in. by 2.5 in.) arranged in twelve rows of three with a lateral center-to-center spacing of 2.5 in. The stub girder failed by longitudinal shear and the compressive force in the concrete of 298 kips was below the ultimate compressive force of 500 kips based on $0.85f'_c A_c$ or 514 kips based on nQ_n. Buckner et al. concluded that transverse reinforcement should be provided for temperature and shrinkage and for crack control but that the presence of such steel would not likely be adequate for developing the required slab shear strength and additional transverse reinforcement would be required.

Elkelish and Robinson (1986) conducted an analytical study of longitudinal cracking of composite beams. They varied six parameters in a layered finite element analysis including type of loading, compressive strength of concrete, beam span to slab width ratio, slab thickness above the deck, percentage of transverse reinforcement, and the existence of metal deck. The method was verified by applying it to six tests conducted by Barnard (1965), Robinson and Wallace (1973), and Henderson (1976). All showed good agreement in terms of determining the flexural moment at which the initial longitudinal crack occurs. Elkelish and Robinson concluded that the ratio of the concrete compressive strength to the yield strength of steel is an important parameter in determining the longitudinal cracking behavior of a composite beam / slab. They also concluded that the presence of welded wire mesh was negligible in the resistance to initial longitudinal cracking, and that the beam to slab width ratio, the thickness of the unfluted deck, and the presence of transverse reinforcement all influence the longitudinal cracking of composite slabs.

Oehlers and Park (1992) studied the shear connection in longitudinally cracked slabs by testing 25 push out specimens with various amounts and positions of transverse reinforcement. Three of the four groups of specimens had a single line of shear connectors, while the fourth group had a double line of connectors. Longitudinal spacing of 100 and 200 mm was investigated for both the single and double lines of shear connectors. The transverse reinforcement was looped and welded to longitudinal bars to

ensure complete anchorage. The slabs were intentionally left thin so that longitudinal shearing failure occurred prior to dowel failure of the shear connectors. They concluded that the number of lines of connectors and their longitudinal spacing determines the failure mechanism that controls the amount of transverse reinforcement that is necessary. In the case of single lines of shear connectors with large longitudinal spacing, dowel failure of the shear connectors controls the design, and in the case of a multiple line of connectors with reduced longitudinal spacing, shear plane failure controls the design. They also concluded that reduction in strength of individual shear connectors is dependent on the stiffness of the transverse reinforcement and not its strength. This means that designing transverse reinforcement for equilibrium may prevent a global failure, but this method will not prevent localized dowel action failure of the shear connectors.

Lauer et al. (1996) studied 11 full-scale single composite joists and refined a joist classification system previously presented by Azmi (1972). The joists were tested to failure and used a variety of proprietary and non-proprietary shear connectors. Spans ranged from 20 ft to 40 ft and joist depths ranged from 8 in. to 20 in. The specimens were found to range from 27% to 149% percent composite, defined as the ratio of calculated shear connector strength to measured bottom chord yield force. This ratio indicated whether the specimen was under-connected or over-connected based on the balanced condition of 100%, which meant that the strength of the shear connectors was equal to the bottom chord yield strength.

Lauer et al. modified Azmi's original three-category classification system (over-connected, under-connected, and balanced) by considering the involvement of forces in the top chord. He concluded that Azmi's flexural models were indeed valid for composite and partially composite systems so long as the top chord is considered. To achieve this, Lauer et. al. concluded the top chord strength had to be better understood so that it did not limit the design of the composite joist. Lauer et al. also concluded that the shape of the load-deflection plot could be linked to the failure mode of the joist. If bottom chord yielding was the controlling mode of failure, then the plot showed a well defined yield point. Also, top chord performance was linked to the amount of shear connection provided. In typical cases where the amount of shear connection was at or

near 80% of the bottom chord force, it was shown that the top chord had little or no contribution in resisting applied loads.

Showalter (1999) investigated the ultimate strength of three different types of open-web composite joist girders. These systems were designated as flush-framed, stub-girder, and haunched and had various amounts of transverse reinforcement and shear studs. The flush-framed configuration consisted of all framing members (joists and girders) having top chords at the same elevation. The three joist girders were nominally 30 ft in length, 30 in. in depth, and were spaced on 7 ft centers. At the third points, 7 ft long joists were placed between the interior member and each of the spandrel members. Eighteen gage, 2 in. deep, galvanized steel deck was used with the flutes parallel to the top chords/flange of the girders. The spandrel members had 14 welded shear studs in the 10 ft shear span between the support and the joist bearing location and the interior joist girder had 27 welded shear studs in the shear span. The transverse reinforcement consisted of 6 No. 4 rebar at 21 in. on center over each girder.

The haunched system is characterized by a 45-degree sloping side haunch (concrete), which results in an increased slab thickness of 5 in. over the two joist girders. This is illustrated in Figure 1.5. This is achieved with haunch flashing and by placing the cross joists in bearing on the top chord of the joist girders with the deck material bearing on the joists and shored at the end of the span with a channel.

The third girder in this test was an H-shape (W24x55) that did not have a haunch. The H-shape had 17 welded shear studs in the shear span and had no transverse reinforcement other than the welded wire mesh. The other spandrel member was a joist girder that had 26 welded shear studs, and transverse reinforcement consisting of 6 No. 4 rebar at 21 in. on center in the shear span. The interior member was a joist-girder with 52 welded shear studs in the shear span and the transverse reinforcement consisted of 11 no. 4 rebar at 12 in. on center and 27 no. 5 rebar at 4.5 in. on center.

The spandrel joist girders reached 92% and 90% of their predicted ultimate load and the interior joist girder reached 97% of its predicted ultimate loadfor the flush-framed test. For the haunch test, the spandrel joist girder and interior joist girder reached 98% and 117% of the predicted ultimate load, respectively. The spandrel H-shape, however, only reached 74% of its predicted ultimate load.

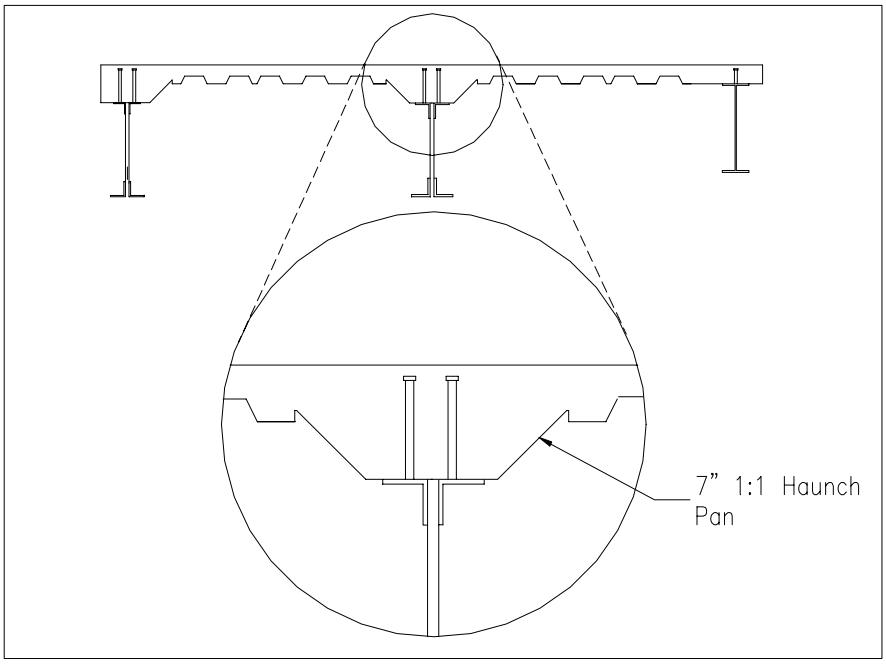

Figure 1.5 Haunch Detail

Showalter concluded that the design model was effective in predicting the ultimate strength for the flush-framed test. He also concluded that the installation of transverse reinforcement over the interior and exterior joist-girders can reduce the development of longitudinal shear cracks over the joist girders; thus reducing the potential for a decrease in flexural strength. Showalter noted that these conclusions are valid for this particular floor system but may not be fully valid for typical construction. In the haunch joist-girder test, Showalter concluded that the configuration was conservative in that the experimental strength significantly exceeded the predicted strength when compared to the flush-framed case.

The research presented represents the bulk of the literature that explicitly addresses the issue of transverse reinforcement and longitudinal slab cracking. It can be concluded that the issues regarding longitudinal slab cracking have yet to be fully explained as they relate to real floor systems with multiple composite girders and joists. The research presented here does provide an adequate starting point for applying the knowledge gained from single composite girder systems to more complex composite girder systems.

1.3 Nomenclature

The tests presented in this document are labeled FF-1, FF-2, H-1 and H-2. Tests FF-1 and FF-2 correspond to two flush-framed tests that were reported by Kigudde et al. (1996) and Piotter et al. (2001) respectively and H-1 and H-2 correspond to haunch tests that were reported by Showalter (1999) and Piotter et al. (2001), respectively. The joist and joist-girder nomenclature is based on an alphanumeric system that began at the left end of the elevation view of the member in question. For convenience and consistency, the members are oriented and referenced to compass coordinates (N, S, E, & W) at the Structures and Materials Research Laboratory at Virginia Polytechnic Institute and State University. The end or cross-section view is viewed from the east end looking west and the profile or elevation view is viewed from the south looking north. As shown in Figure 1.6, all joist-girders are oriented longitudinally on the east-west direction and the joists are oriented longitudinally in the north-south direction.

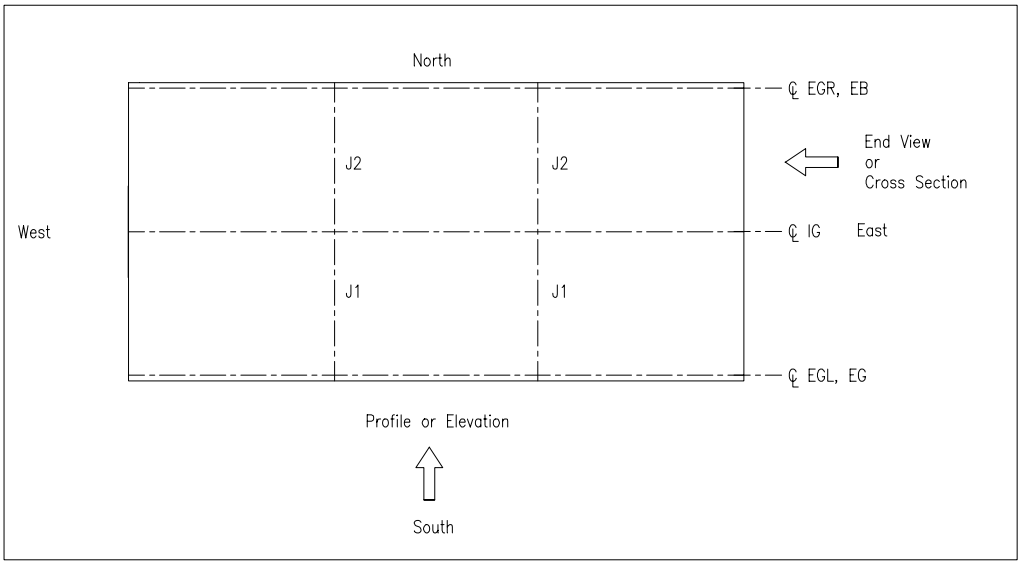

Figure 1.6 Plan View of Floor System

The joists and joist girders were given designations based on the location in the setup relative to the other structural framing members. In all setups, IG refers to the interior joist girder or the middle member of the three girders in the floor system. In FF-1, the exterior joist girders are referred to as EGL and EGR which were the joist girders on the south and north side of the specimen, respectively. In FF-2 and H-1, EG refers to the exterior joist-girder located on the south side of the specimen while EB refers to the

H-shape located on the north side of the specimen. In H-1, EGL refers to the exterior joist-girder on the south side of the specimen and EB was the designation for the H-shape. The individual elements of the joists and joist girders are designated by the location relative to the end of the member and the centerline. The joist girder shown in Figure 1.7 depicts the nomenclature for the individual chord and web elements for the flush-framed tests. The top chord and bottom chord are referred to as TC and BC, respectively. The diagonal web members are designated with a W followed by a number starting at 2 and progressing from left to right (west to east) by increments of 1 to the number 9. Just to the right (east) of midspan the web members have an additional designation of R added to the member name to distinguish them from the left (west) end members and the numbers begin at 9 and decrease by increments of 1 to the number 2. Vertical web members are assigned the letter V followed by numbers beginning at 1 and increasing by 1 to the number 8. This begins at the first vertical member at the left (west) end and progresses to the right (east) end.

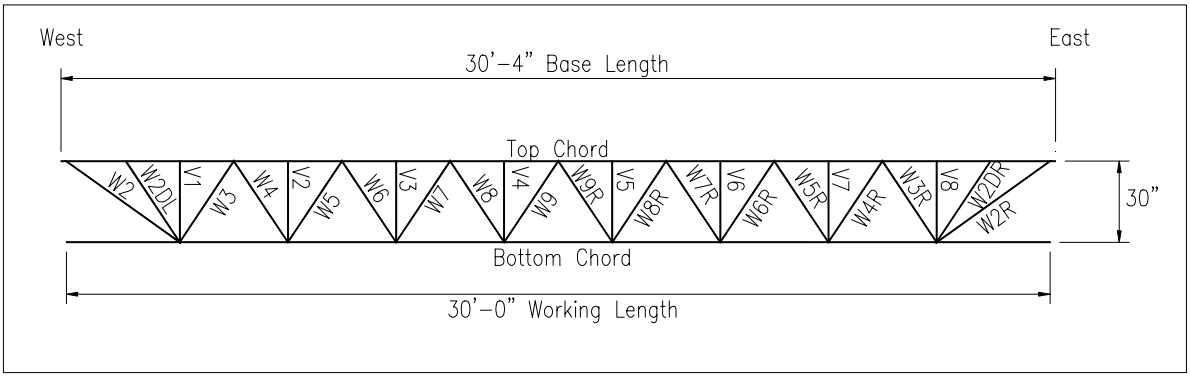

Figure 1.7 Flush-Framed Joist Girder Nomenclature (FF-1, FF-2)

The joist girder shown in Figure 1.8 depicts the nomenclature for the individual chord and web elements for the haunch tests. The top chord and bottom chord are referred to as TC and BC respectively. The diagonal web members are designated with a W followed by a number starting at 2 and progressing from left to right (west to east) by increments of 1 to the number 7. Just to the right (east) of midspan the web members have an additional designation of R added to the member name to distinguish them from the left (west) end members and the numbers begin at 7 and decrease by increments of 1 to the number 2. Vertical web members are assigned the letter V followed by numbers

beginning at 1 and increasing by 1 to the number 6. This begins at the first vertical member at the left (west) end and progresses to the right (east) end.

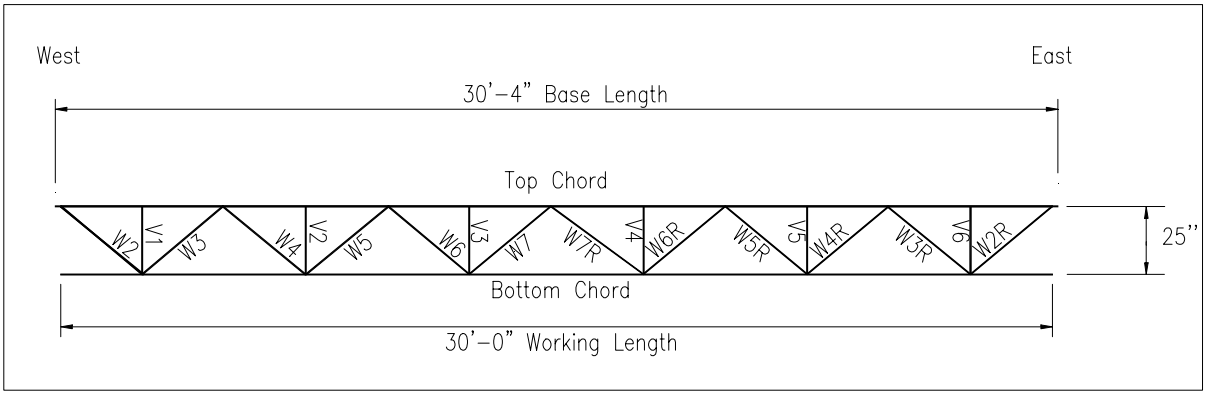

Figure 1.8 Haunched Joist-Girder Nomenclature (H-1, H-2)

The element designations for the joists are presented in Figures 1.9 – 1.12. The layout for tests FF-1, H-1, H-2 is the same with regard to the member elements. The top chords and bottom chords are designated TC and BC respectively, and the web members are labeled as indicated in the figures.

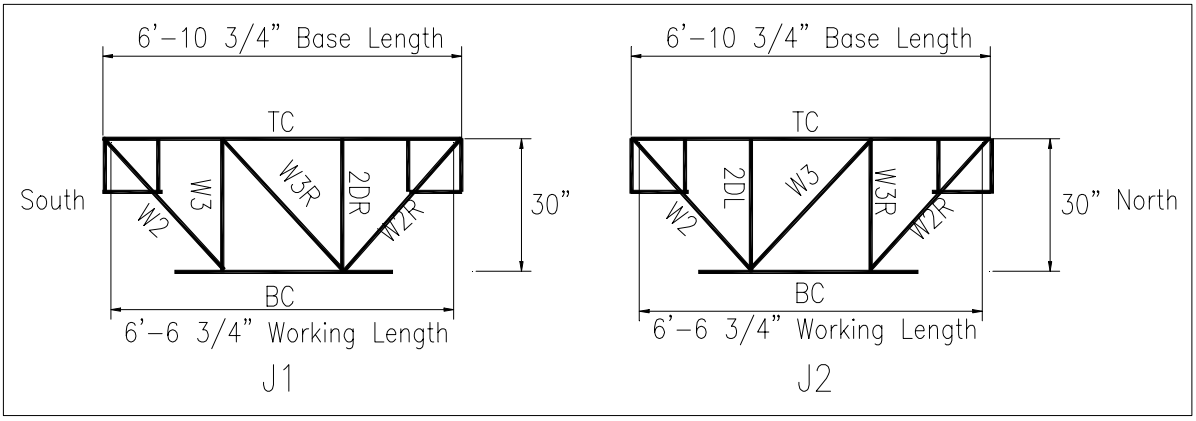

Figure 1.9 Flush-Framed Joist Nomenclature (FF-1)

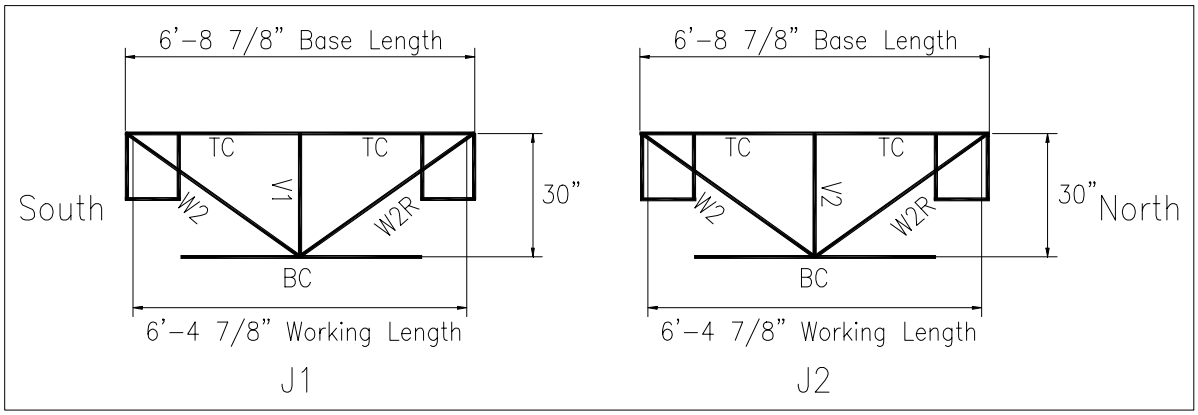

Figure 1.10 Flush-Framed Joist Nomenclature (FF-2)

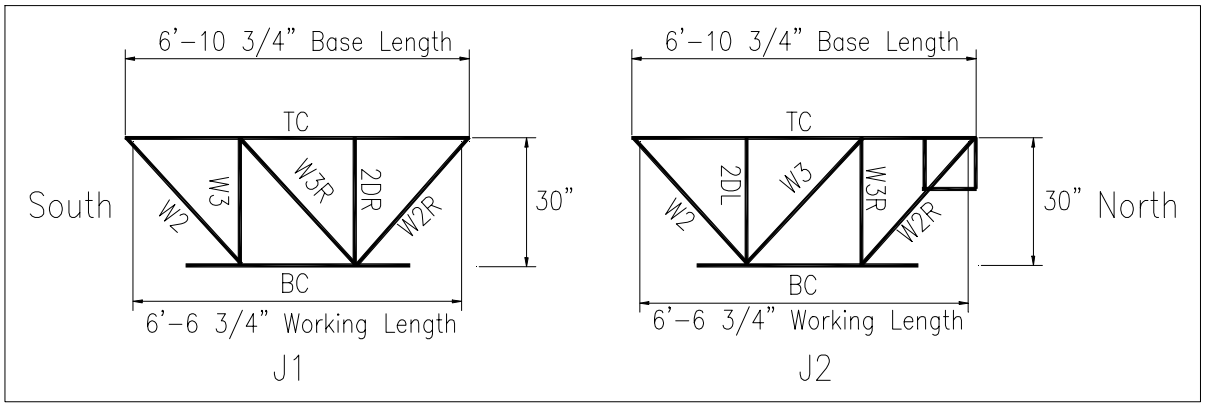

Figure 1.11 Haunched Joist Nomenclature (H-1)

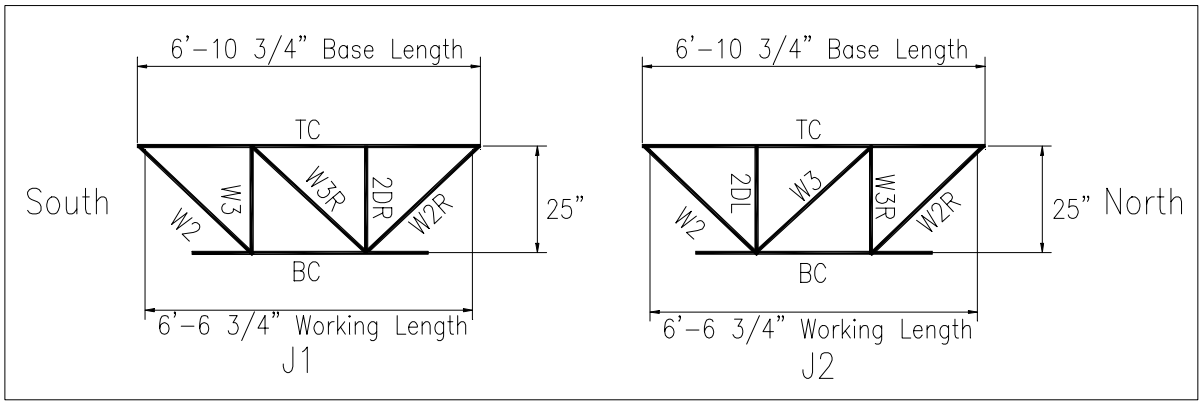

Figure 1.12 Haunched Joist Nomenclature (H-2)

1.4 Scope of Research

The results of testing presented in this study describe the physical behavior and implication of the amount of transverse reinforcement present in composite floor systems. Specifically, the focus is on the longitudinal shear strength and its effect on the ultimate flexural strength of the joist girders with the presence of longitudinal cracks. A procedure is presented to design the appropriate amount of transverse slab reinforcement for both open-web composite joist girders and composite H-shapes.

This document is organized into five chapters. Chapter 1 presents introductory material relevant to the research that was conducted. This includes a literature review of material pertaining to existing literature on composite and concrete structural systems and general organization of the test specimens. Chapter 2 gives detailed descriptions of each test setup including specimen layout, instrumentation, and testing procedures. Chapter 3 presents the results of the tests conducted. Chapter 4 presents analytical methods and a general analysis of each of the four setups. Chapter 5 is a summary of what was accomplished in each test with conclusions and recommendations based on the test results. A transverse reinforcement design example, test summaries, an evaluation of joist girder stiffness, and sample calculations are presented in the Appendices. The details of these tests are presented in project reports by Kigudde et al. (1996) and Piotter et al. (2001) and also a thesis by Showalter (1999). These details include strain gage readings for all members, load cell readings, concrete slip measurements, and deflection measurements.

CHAPTER 2

EXPERIMENTAL SETUP

2.1 General

The series of tests studied were designed to simulate a two-bay floor system. The main structural members consisted of an interior joist girder flanked by a spandrel joist girder or a spandrel H-shape at 7 ft centers for the flush-framed configuration and 6 ft 9 in. centers for the haunched configuration. The main members were joined together at the third points by joists that were fabricated with depths of 30 in. for tests FF-1, FF-2, H-1, and 25 in. for H-2. The joists were bolted to the girder sections for the flush-framed configuration and were bearing on the girder top chords and welded in place for the haunched configuration. The joist-girders were positioned such that the top chord joist seats were centered over the load cells and the web centerline of the support stand.

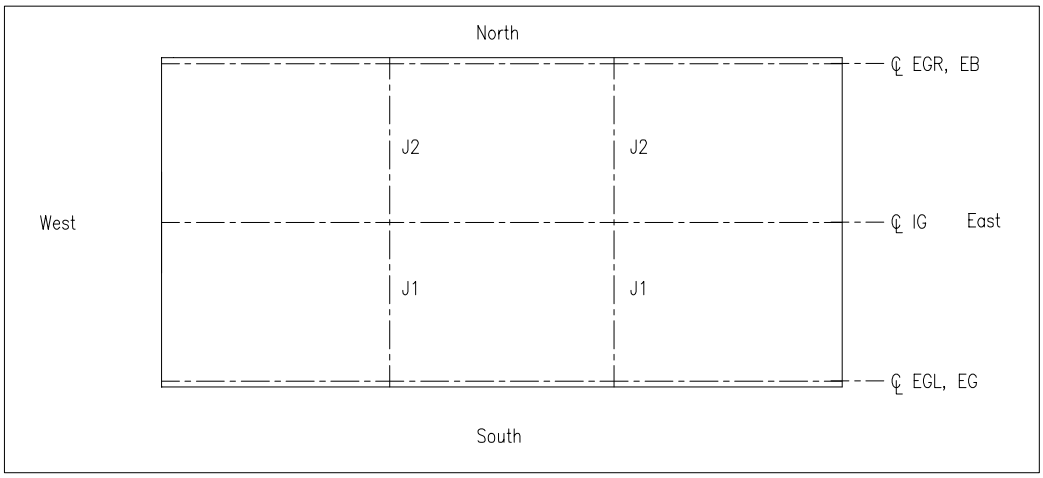

Figure 2.1 Plan View of Layout

The 18 gage, 2 in. deep steel deck used for the four tests was nominally 30 ft 4 in. long and 3 ft. wide. The deck at the end of the span between joist-girders was supported by channels welded to a 1 in. flat bar tack welded to the joist seat and bearing on the load cells. Pour stop was installed to achieve a nominal slab thickness of 5 in. The haunched joist-girders had 7 in., 1:1 haunch pans positioned over the top chords illustrated in

Figure 2.2. This detail increased the effective concrete depth over the joist-girders from 5 in. to 10 in. The joist seats were supported by a 2 in. roller positioned between two 0.5 in. restraint plates that were placed on top of a load cell at each bearing point for the floor system, as illustrated in Figure 2.3. The bottom chords were restrained laterally by a stiffener plate attached to the support stand, which fit in the gap between the chord angles.

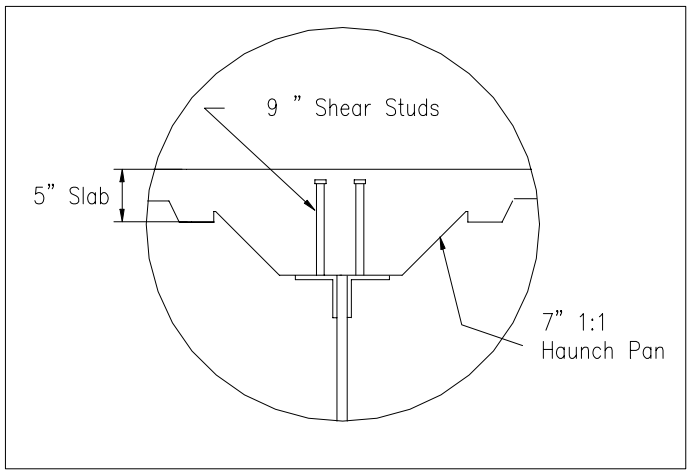

Figure 2.2 Haunch Detail

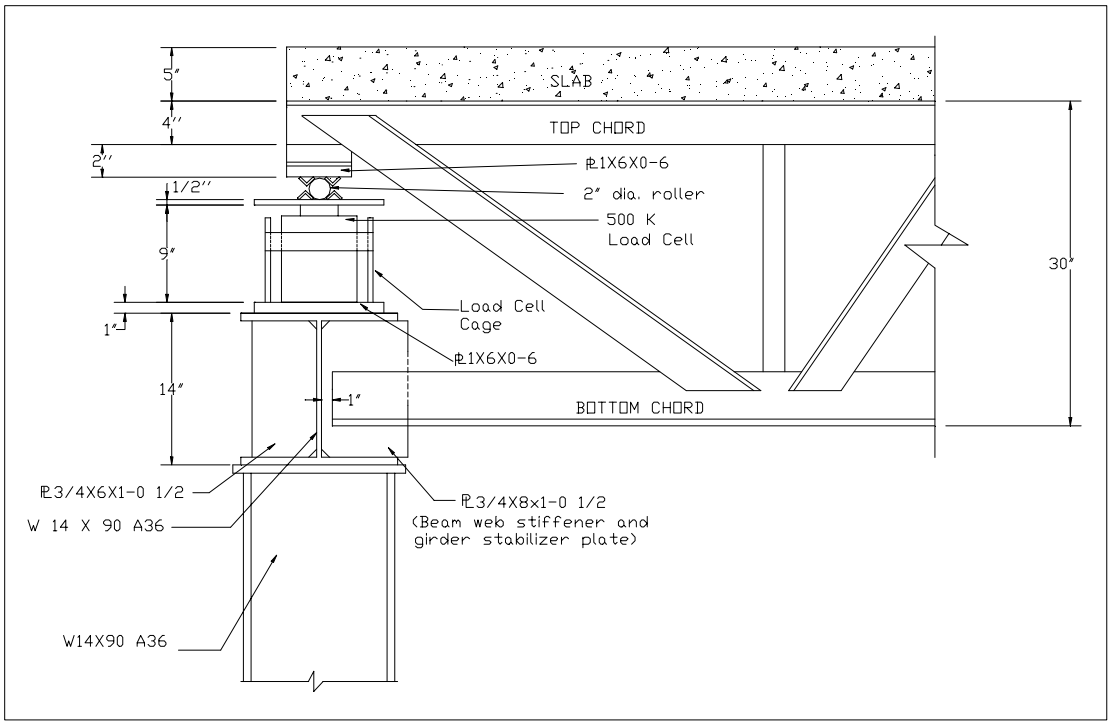

Figure 2.3 Support Stand Detail

Figure 2.4 Framing Layout (H-2)

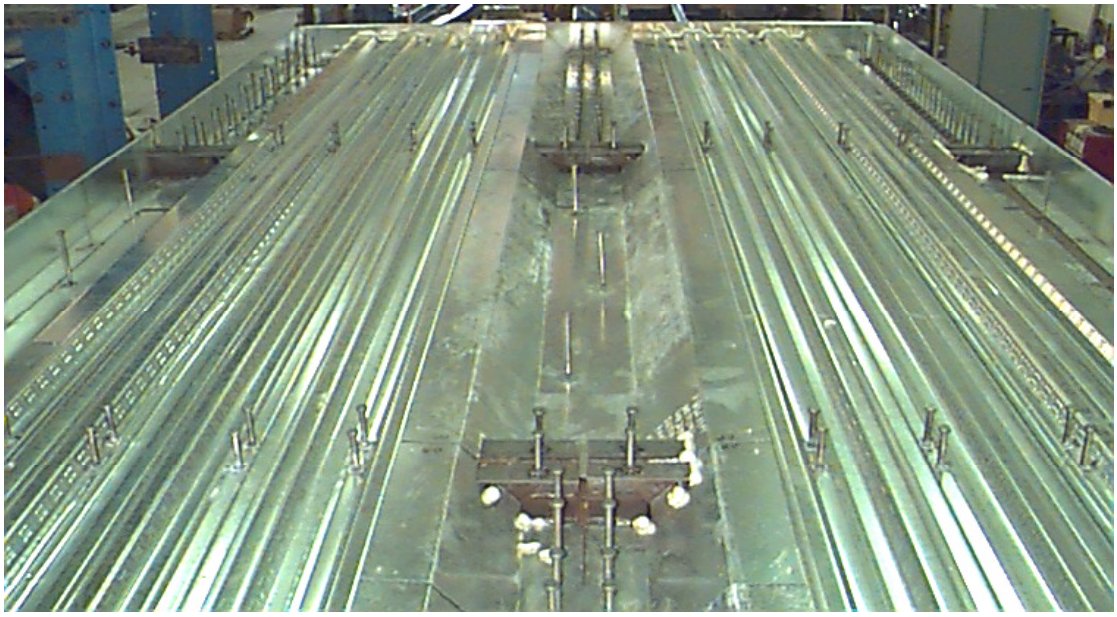

Figure 2.5 Haunch Pans and Steel Deck (H-2)

2.2 Description of Specimen Configurations

2.2.1 Flush-Framed Joist-Girder (FF-1)

The first flush framed joist girder test setup had three 30 ft 4 in. joist girders on 7 ft centers with 18 gage, 2 in. deep, deck with a total slab thickness 5 in. The four joists were 30 in. deep and were bolted to specially fabricated joist girder vertical web members (V3 and V6).

The welded shear studs were (0.75 in. dia.) 4.5 in. in length after welding and were placed as illustrated in Figure 2.6. The interior joist girder (IG) had 28 welded shear studs in each shear span and the exterior joist girders (EGL, EGR) had 14 welded shear studs in each shear span. Shear studs were also provided on the joists to ensure the entire floor was composite. They were placed 2 per rib between joist-girder centerlines and had a final height after welding of 4.5 in.

The exterior joist girders had transverse reinforcement of six no. 4 bars in each shear span and the interior joist girder had ten no. 4 bars for transverse reinforcement. This was in addition to the welded wire fabric present for temperature and shrinkage reinforcement. The layout for the transverse steel is shown in Figure 2.7.

Nominal chord and web sizes for the joists and joist girders are shown in Tables 2.1 and 2.2. Complete details of this test can be obtained in the project report by Kigudde et al. 1996.

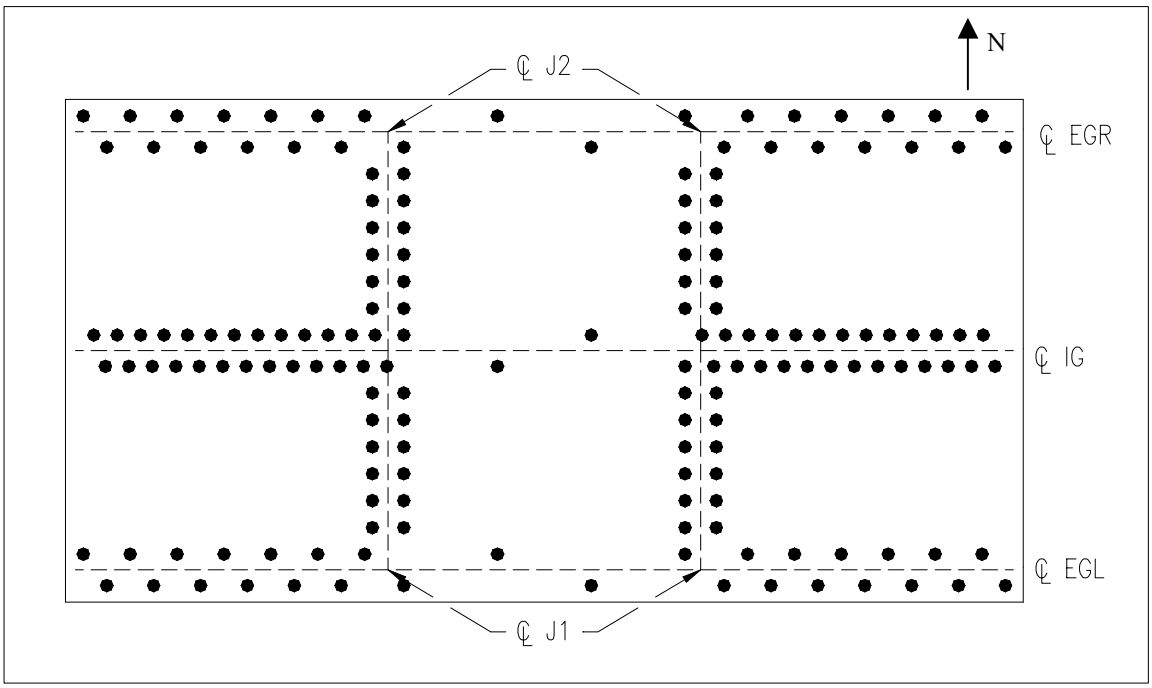

Figure 2.6 Shear Stud Layout (FF-1)

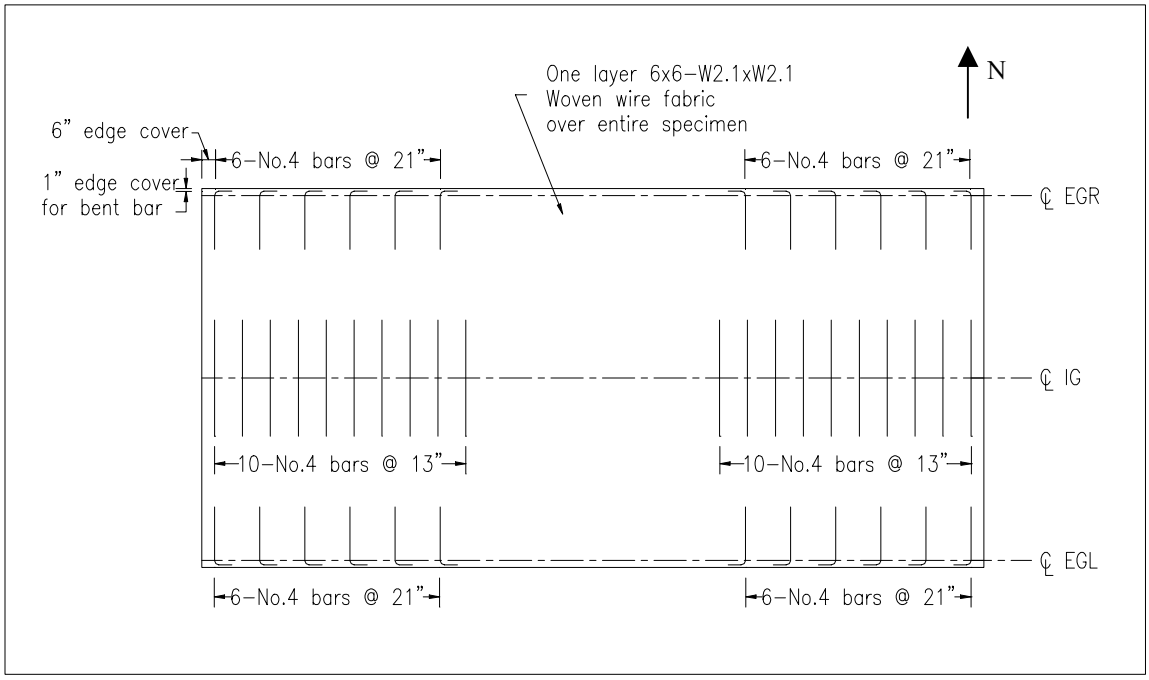

Figure 2.7 Transverse Reinforcement Layout (FF-1)

Table 2.1 Composite Joist-Girder Member Sizes (FF-1)

Member	Nominal Size	
	EGL and EGR	IG
Top Chord	2L-3.00 x 3.00 x 0.250	2L-4.00 x 4.00 x 0.375
Bottom Chord	2L-4.00 x 4.00 x 0.375	2L-5.00 x 5.00 x 0.625
W2 , W2R	2L-3.00 x 3.00 x 0.250	2L-4.00 x 4.00 x 0.375
W2DL , W2DR	1L-2.00 x 2.00 x 0.187	1L-1.75 x 1.75 x 0.170
W3 , W3R	2L-2.50 x 2.50 x 0.250	2L-3.50 x 3.50 x 0.344
W4 , W4R	2L-2.50 x 2.50 x 0.212	2L-3.50 x 3.50 x 0.344
W5 , W5R	2L-2.50 x 2.50 x 0.250	2L-3.50 x 3.50 x 0.344
W6 , W6R	2L-2.50 x 2.50 x 0.212	2L-3.50 x 3.50 x 0.375
W7 , W7R	2L-1.50 x 1.50 x 0.155	2L-2.00 x 2.00 x 0.176
W8 , W8R	2L-1.25 x 1.25 x 0.133	2L-1.50 x 1.50 x 0.170
W9 , W9R	2L-1.50 x 1.50 x 0.138	2L-2.00 x 2.00 x 0.176
V1 , V8	1L-1.75 x 1.75 x 0.155	1L-2.00 x 2.00 x 0.250
V2 , V7	1L-1.75 x 1.75 x 0.155	1L-2.00 x 2.00 x 0.250
V3 , V6	2L-5.00 x 5.00 x 0.438	2L-4.00 x 4.00 x 0.500
V4 , V5	1L-1.75 x 1.75 x 0.155	1L-2.00 x 2.00 x 0.250

Table 2.2 Composite Joist Member Sizes (FF-1)

	Member	Nominal Size		Member	Nominal Size
J1	Top Chord	2L-3.00 x 3.00 x 0.313	**J2**	Top Chord	2L-3.00 x 3.00 x 0.313
	Bottom Chord	2L-4.00 x 4.00 x 0.500		Bottom Chord	2L-4.00 x 4.00 x 0.500
	W2	2L-3.50 x 3.50 x 0.344		W2	2L-3.50 x 3.50 x 0.344
	W3	2L-3.00 x 3.00 x 0.313		V1	2L-3.50 x 3.50 x 0.375
	W3R	2L-2.50 x 2.50 x 0.250		W3	2L-2.50 x 2.50 x 0.250
	V2	2L-3.50 x 3.50 x 0.375		W3R	2L-3.00 x 3.00 x 0.313
	W2R	2L-3.50 x 3.50 x 0.344		W2R	2L-3.50 x 3.50 x 0.344

2.2.2 Flush-Framed Joist-Girder (FF-2)

The second flush-framed joist girder test had three 30 ft 4 in. joist girders on 7 ft centers with 18 gage, 2 in., steel deck and a total slab thickness of 5 in. The four joists were 30 in. deep and were bolted to specially fabricated joist girder vertical web members (V3 and V6) on the interior and exterior joist girders and to shear tabs welded to a W24x55 girder.

The welded shear studs were (0.75 in. dia.) 4.5 in. in length after welding and were placed as illustrated in Figure 2.8. The interior joist girder (IG) had 34 welded shear studs in the shear span. The first 18 were doubled into nine rows spaced at 4.5 in. on center with the remaining studs staggered at 4.5 in. on center. The exterior joist girder (EG) had 17 welded shear studs staggered a 4.5 in. on center in the shear span. The H-shape (EB) had 31 welded shear studs in the shear span. The first 12 were doubled up for 6 rows of 2 at 4.5 in. on center with the remaining studs in a single line over the web at 4.5 in. on center. Shear studs were placed two per rib between joist girder centerlines on the joists to ensure the entire floor was composite, and the final height after welding was 4.5 in.

The exterior joist girder had transverse reinforcement of six no. 4 bars in each shear span and the interior joist girder had eight no. 4 bars for transverse reinforcement. The H-shape had 26 no. 4 bars for transverse reinforcement. This was amount was determined based on the calculated longitudinal shear. Welded wire fabric was also present for temperature and shrinkage reinforcement. The layout for the transverse steel is illustrated in Figure 2.9.

Nominal chord and web sizes for the joists and joist girders are shown in Tables 2.3 and 2.4. More details of this test are presented in subsequent sections.

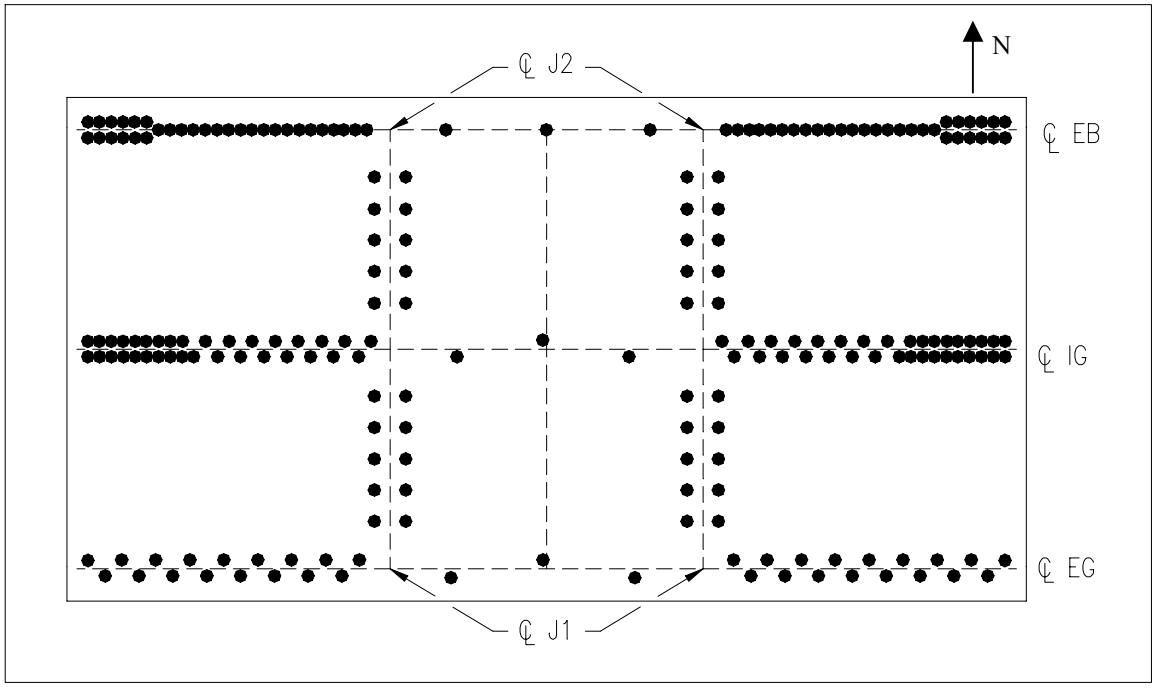

Figure 2.8 Shear Stud Layout (FF-2)

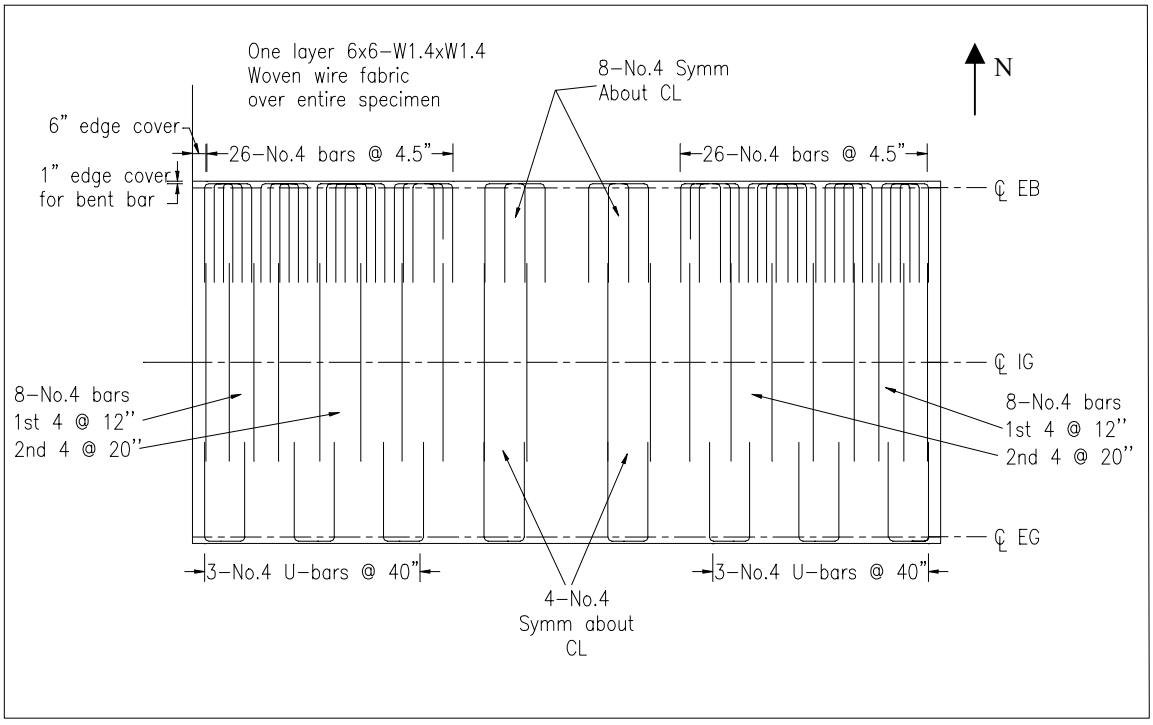

Figure 2.9 Transverse Reinforcement Layout (FF-2)

Table 2.3 Composite Joist-Girder Member Sizes (FF-2)

Member	EG	IG
Top Chord	2L-3.00 x 3.00 x 0.250	2L-4.00 x 4.00 x 0.375
Bottom Chord	2L-4.00 x 4.00 x 0.375	2L-5.00 x 5.00 x 0.625
W2 , W2R	2L-3.50 x 3.50 x 0.313	2L-4.00 x 4.00 x 0.500
W2DL , W2DR	2L-1.50 x 1.50 x 0.138	2L-2.00 x 2.00 x 0.176
W3 , W3R	2L-3.00 x 3.00 x 0.281	2L-4.00 x 4.00 x 0.375
W4 , W4R	2L-3.00 x 3.00 x 0.227	2L-4.00 x 4.00 x 0.375
W5 , W5R	2L-3.00 x 3.00 x 0.281	2L-4.00 x 4.00 x 0.375
W6 , W6R	2L-3.00 x 3.00 x 0.227	2L-4.00 x 4.00 x 0.375
W7 , W7R	2L-1.50 x 1.50 x 0.170	2L-2.00 x 2.00 x 0.232
W8 , W8R	2L-1.25 x 1.25 x 0.133	2L-2.00 x 2.00 x 0.176
W9 , W9R	2L-1.50 x 1.50 x 0.170	2L-2.00 x 2.00 x 0.232
V1 , V8	1.00 x 1.00 bar	2.00 x 1.00 bar
V2 , V7	1.00 x 1.00 bar	2.00 x 1.00 bar
V3 , V6	2L-4.00 x 4.00 x 0.438	2L-4.00 x 4.00 x 0.438
V4 , V5	1.00 x 1.00 bar	2.00 x 1.00 bar

Table 2.4 Composite Joist Member Sizes (FF-2)

J1	Top Chord	2L-4.00 x 4.00 x 0.375	**J2**	Top Chord	2L-4.00 x 4.00 x 0.375
	Bottom Chord	2L-4.00 x 4.00 x 0.375		Bottom Chord	2L-4.00 x 4.00 x 0.375
	W2	2L-4.00 x 4.00 x 0.500		W2	2L-4.00 x 4.00 x 0.500
	V1	2L-4.00 x 4.00 x 0.500		V1	2L-4.00 x 4.00 x 0.500
	W2R	2L-4.00 x 4.00 x 0.500		W2R	2L-4.00 x 4.00 x 0.500

2.2.3 Haunched Joist Girder (H-1)

The first haunch joist-girder test had three 30 ft 4 in. joist girders on 6 ft 9 in. centers with 18 gage, 2 in., steel deck and a total slab thickness of 5 in. Over the joists, 7 in. 1:1 haunch pans were used to form a trapezoidal haunch increasing the depth of the concrete to 10 in. The four joists were 30 in. deep and were bearing on the top chords of the interior and exterior joist girders. The joists were flush framed and bolted to shear tabs that were welded to the spandrel W24x55 girder.

The welded shear studs (0.75 in. dia.) on the girders were 9 in. in length after welding and were placed as illustrated in Figure 2.10. The interior joist girder (IG) had 52 welded shear studs in the shear span and the exterior joist girder (EG) had 26 welded shear studs in the shear span. The H-shape (EB) had 17 welded shear studs in the shear span for a total of 37. Shear studs were also provided on the joists to ensure the entire floor was composite. They were placed two per rib between joist girder centerlines. The stud height after welding over the joists was 4.5 in.

The exterior joist girders had transverse reinforcement of 14 no. 3 bars in each shear span and the interior joist girder had 27 no. 5 bars and 11 no. 4 bars for transverse reinforcement. The H-shape had no transverse reinforcement provided with the exception of welded wire fabric. The layout for the transverse steel is shown in Figure 2.11.

Nominal chord and web sizes for the joists and joist girders are shown in Tables 2.5 and 2.6. More details of this test can be obtained in Showalter (1999).

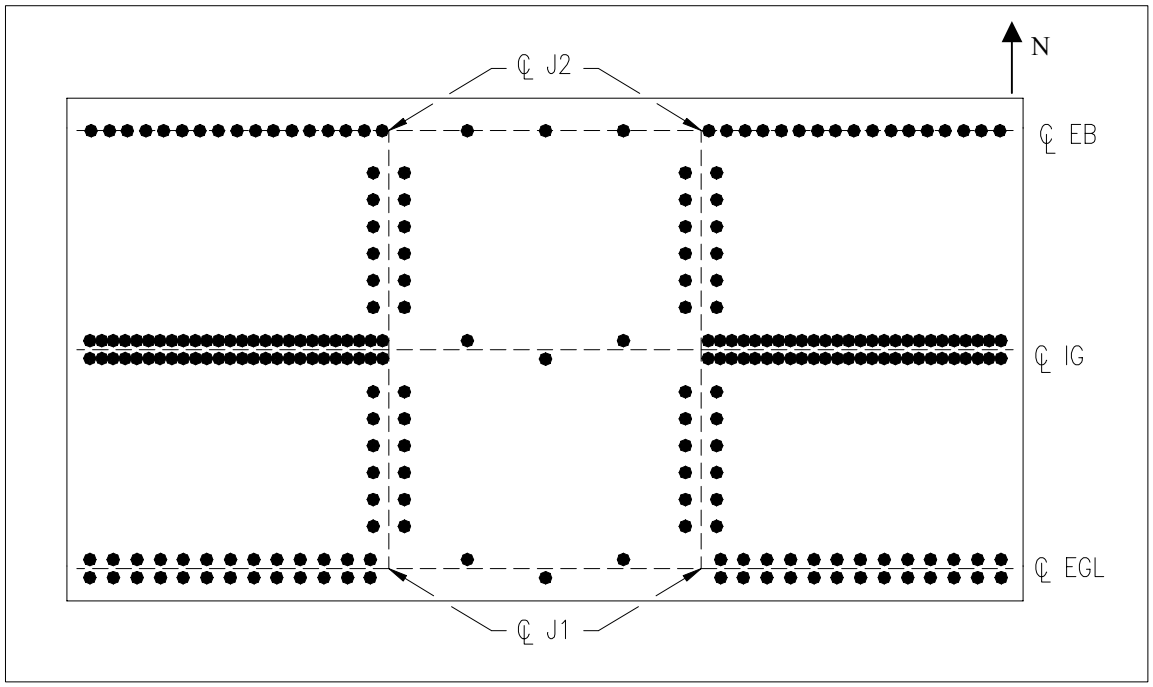

Figure 2.10 Shear Stud Layout (H-1)

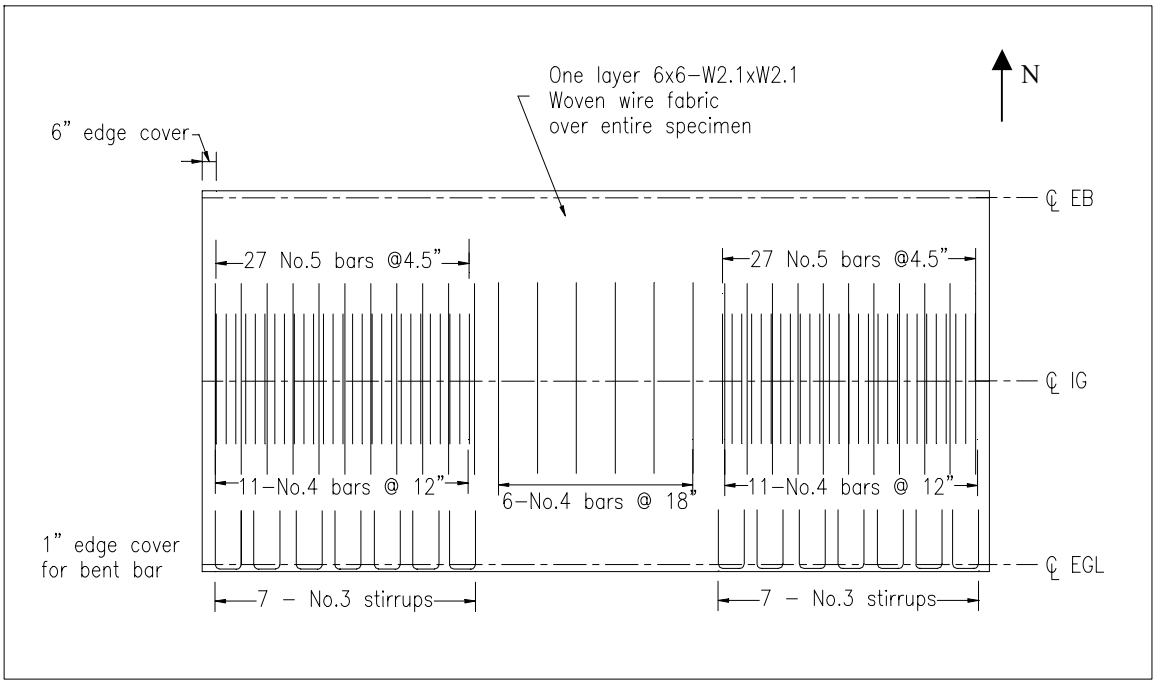

Figure 2.11 Transverse Reinforcement Layout (H-1)

Table 2.5 Composite Joist-Girder Member Sizes (H-1)

Member	Nominal Size	
	EGL	IG
Top Chord	2L-3.00 x 3.00 x 0.250	2L-4.00 x 4.00 x 0.375
Bottom Chord	2L-4.00 x 4.00 x 0.375	2L-5.00 x 5.00 x 0.625
W2 , W2R	2L-3.50 x 3.50 x 0.287	2L-4.00 x 4.00 x 0.500
W3 , W3R	2L-3.50 x 3.50 x 0.313	2L-5.00 x 5.00 x 0.438
W4 , W4R	2L-3.50 x 3.50 x 0.287	2L-4.00 x 4.00 x 0.500
W5 , W5R	2L-3.50 x 3.50 x 0.313	2L-5.00 x 5.00 x 0.438
W6 , W6R	2L-1.75 x 1.75 x 0.170	2L-2.50 x 2.50 x 0.212
W7 , W7R	2L-2.00 x 2.00 x 0.176	2L-2.50 x 2.50 x 0.250
V1 , V6	1L-1.50 x 1.50 x 0.155	1L-1.50 x 1.50 x 0.155
V2 , V5	1L-1.50 x 1.50 x 0.155	1L-1.50 x 1.50 x 0.155
V3 , V4	1L-1.50 x 1.50 x 0.155	1L-1.50 x 1.50 x 0.155

Table 2.6 Composite Joist Member Sizes (H-1)

	Member	Nominal Size		Member	Nominal Size
J1	Top Chord	2L-3.50 x 3.50 x 0.344	**J2**	Top Chord	2L-3.50 x 3.50 x 0.313
	Bottom Chord	2L-3.50 x 3.50 x 0.313		Bottom Chord	2L-3.50 x 3.50 x 0.287
	W2	2L-4.00 x 4.00 x 0.438		W2	2L-4.00 x 4.00 x 0.438
	W3	2L-3.50 x 3.50 x 0.287		V1	2L-4.00 x 4.00 x 0.375
	W3R	2L-3.50 x 3.50 x 0.344		W3	2L-3.00 x 3.00 x 0.313
	V2	2L-4.00 x 4.00 x 0.375		W3R	2L-4.00 x 4.00 x 0.375
	W2R	2L-4.00 x 4.00 x 0.375		W2R	2L-4.00 x 4.00 x 0.375

2.2.4 Haunched Joist-Girder (H-2)

The second haunched joist-girder test had three 30 ft 4 in. joist girders on 6 ft 9 in. centers with 18 gage 2 in. steel deck and a total slab thickness in the clear span of 5 in. Over the joists, 7 in. 1:1 haunch pans were used to form a trapezoidal haunch bringing the total thickness of concrete to 10 inches. The four joists were 30 in. deep and were in bearing on the top chords of the interior and exterior joist girders.

The welded shear studs (0.75 in. dia.) on the girders were 9 in. in length after welding and were placed as illustrated in Figure 2.12. The interior joist-girder (IG) had 40 welded shear studs in the shear span and the exterior joist-girder (EG) had 20 welded shear studs in the shear span. The H-shape (EB) had 26 welded shear studs in the shear span. Shear studs were also provided on the joists to ensure the entire floor was composite, and they were placed two per rib between joist-girder centerlines. The studs over the joists had a final height after welding of 4.5 in. and the studs over the joist-girders had a final height after welding of 9 in.

The exterior and interior joist girders and the H-shape had transverse slab reinforcement of four no. 3 bars in each shear span. This was in addition to the welded wire fabric present for temperature and shrinkage reinforcement. The layout for the transverse steel is shown in Figure 2.13.

Nominal chord and web sizes for the joists and joist girders are shown in Tables 2.7 and 2.8. More details of this test are presented in subsequent sections.

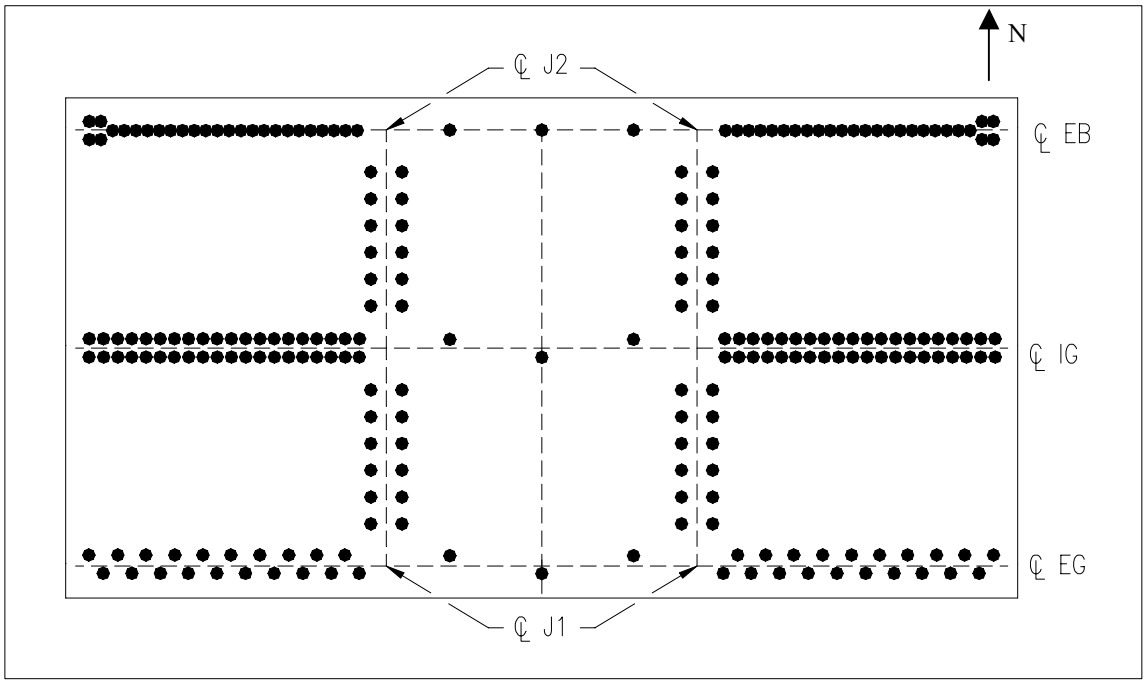

Figure 2.12 Shear Stud Layout (H-2)

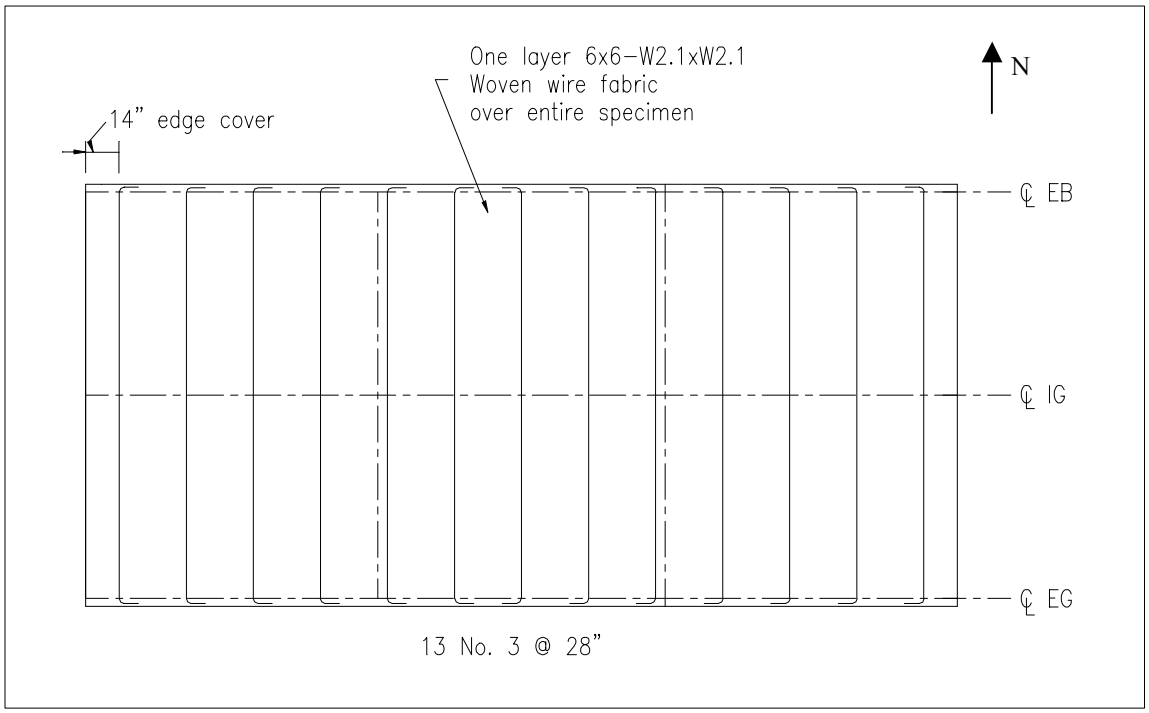

Figure 2.13 Transverse Reinforcement Layout (H-2)

Table 2.7 Composite Joist-Girder Member Sizes (H-2)

Member	Nominal Size	
	EG	IG
Top Chord	2L-3.00 x 3.00 x 0.250	2L-4.00 x 4.00 x 0.375
Bottom Chord	2L-4.00 x 4.00 x 0.375	2L-5.00 x 5.00 x 0.625
W2 , W2R	2L-3.00 x 3.00 x 0.250	2L-4.00 x 4.00 x 0.375
W2DL , W2DR	1L-2.00 x 2.00 x 0.187	1L-1.75 x 1.75 x 0.170
W3 , W3R	2L-2.50 x 2.50 x 0.250	2L-3.50 x 3.50 x 0.344
W4 , W4R	2L-2.50 x 2.50 x 0.212	2L-3.50 x 3.50 x 0.344
W5 , W5R	2L-2.50 x 2.50 x 0.250	2L-3.50 x 3.50 x 0.344
W6 , W6R	2L-2.50 x 2.50 x 0.212	2L-3.50 x 3.50 x 0.375
W7 , W7R	2L-1.50 x 1.50 x 0.155	2L-2.00 x 2.00 x 0.176
W8 , W8R	2L-1.25 x 1.25 x 0.133	2L-1.50 x 1.50 x 0.170
W9 , W9R	2L-1.50 x 1.50 x 0.138	2L-2.00 x 2.00 x 0.176
V1 , V8	1L-1.75 x 1.75 x 0.155	1L-2.00 x 2.00 x 0.250
V2 , V7	1L-1.75 x 1.75 x 0.155	1L-2.00 x 2.00 x 0.250
V3 , V6	2L-5.00 x 5.00 x 0.438	2L-4.00 x 4.00 x 0.500
V4 , V5	1L-1.75 x 1.75 x 0.155	1L-2.00 x 2.00 x 0.250

Table 2.8 Composite Joist Member Sizes (H-2)

	Member	Nominal Size		Member	Nominal Size
J1	Top Chord	2L-3.00 x 3.00 x 0.313	**J2**	Top Chord	2L-3.00 x 3.00 x 0.313
	Bottom Chord	2L-4.00 x 4.00 x 0.500		Bottom Chord	2L-4.00 x 4.00 x 0.500
	W2	2L-3.50 x 3.50 x 0.344		W2	2L-3.50 x 3.50 x 0.344
	W3	2L-3.00 x 3.00 x 0.313		V1	2L-3.50 x 3.50 x 0.375
	W3R	2L-2.50 x 2.50 x 0.250		W3	2L-2.50 x 2.50 x 0.250
	V2	2L-3.50 x 3.50 x 0.375		W3R	2L-3.00 x 3.00 x 0.313
	W2R	2L-3.50 x 3.50 x 0.344		W2R	2L-3.50 x 3.50 x 0.344

2.3 Construction Methods

The joist girders and joists for the four tests were fabricated by Vulcraft in Norfolk, Nebraska and shipped to the Virginia Tech Structures and Materials Research Laboratory. The joists were inspected, measured, and compared with the design specifications provided. One end of the bottom chord of the joist-girders was fabricated with additional material that could be cut off to obtain steel coupons prior to testing. Strain gages were attached to the joist girders on the top chords near the end of the span, the bottom chords at the midspan and third points, and the webs at the third points. Details of the instrumentation are presented in section 2.4

After the strain gages were attached, the joist girders were placed on the support stands. In H-1, H-2, and FF-2, an H-shape was used as a spandrel member in place of one of the joist girders. Due to the differences in the bearing condition of the H-shape and the joist girders, a special detail had to be fabricated at both ends of the H-shape as illustrated in Figure 2.14. Half-depth flange stiffeners were welded to the H-shape at the third points to prevent local buckling due to the concentrated loads from the joists.

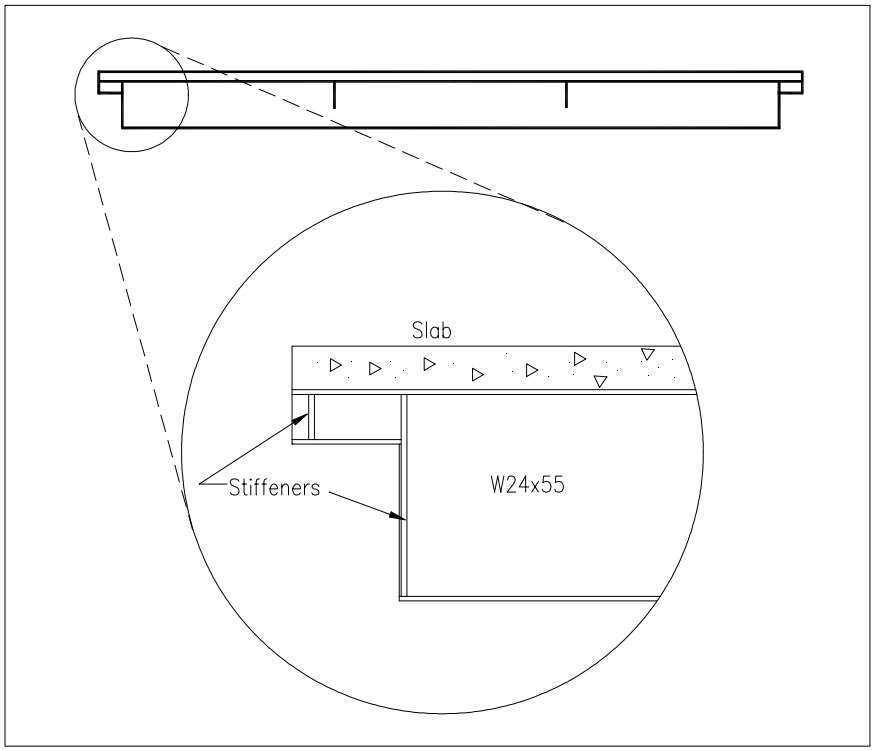

Figure 2.14 H-Shape bearing detail

In tests H-1 and FF-2, plates with bolt holes were welded to the inside of the H-shape to act as part of the joist to girder connection and as web stiffeners. After the beam fabrication was complete, it was placed on the support stands.

The joists were put in place after the joist girders were put in their final position and it was determined that the test setup was square. The joists were bolted to the joist girders in tests FF-1 and FF-2 as illustrated in Figure 2.15 and in tests H-1 and H-2, the joists were positioned on the spandrel joist girder and welded to the top chord along the edge of the joist seat as illustrated in Figure 2.16. The detail on both sides of the interior joist girder was the same as that for the spandrel joist girder for all four tests. The joist detail on the H-shape varied in the three tests in which it was included. In H-1, the joists were bolted into the H-shape with the top chord at the same elevation as the H-shape top flange. In H-2, the joist was bearing on the top flange with the joist seat welded to it. In FF-2, the joist was bolted to the H-shape with a detail similar to test H-2.

After the framing was complete, the deck was placed on the specimen. Tests FF-1 and FF-2 had the top chords and top flange at the same elevation, so no special provision needed to be made with regard to the steel deck. The deck sheets were positioned and fastened in place with puddle welds and then were button punched at the deck seams. In the case of FF-1, the deck was placed continuously from each spandrel girder. In test FF-2, two deck sheets were placed and positioned between the joist girders. The remaining gap between the edge of the deck sheets and the joist girder was closed by using girder fillers that were attached to the deck sheets with screws and to the joist girder top chords with puddle welds. The spandrel members had girder fillers to the inside and the pour stop leg covered the 1 in. gap between the top chord angles.

For H-1 and H-2, haunch pans were used to fill the gap between the deck and the joist girders. Due to the bearing detail of the joists on the joist girders, the deck was supported directly by the joists and the channels at the end of the span. As a result, the deck was 5 in. above the top chords of the joist girders. With the addition of a 2 in. deck, a 7 in. 1:1 haunch pan was required. It was positioned on either side of the interior joist-girder and to the inside of both spandrel members and was fastened with screws and

puddle welds. Considerable fabrication of the haunch pans was necessary to fit the haunch pans around the joist top chords.

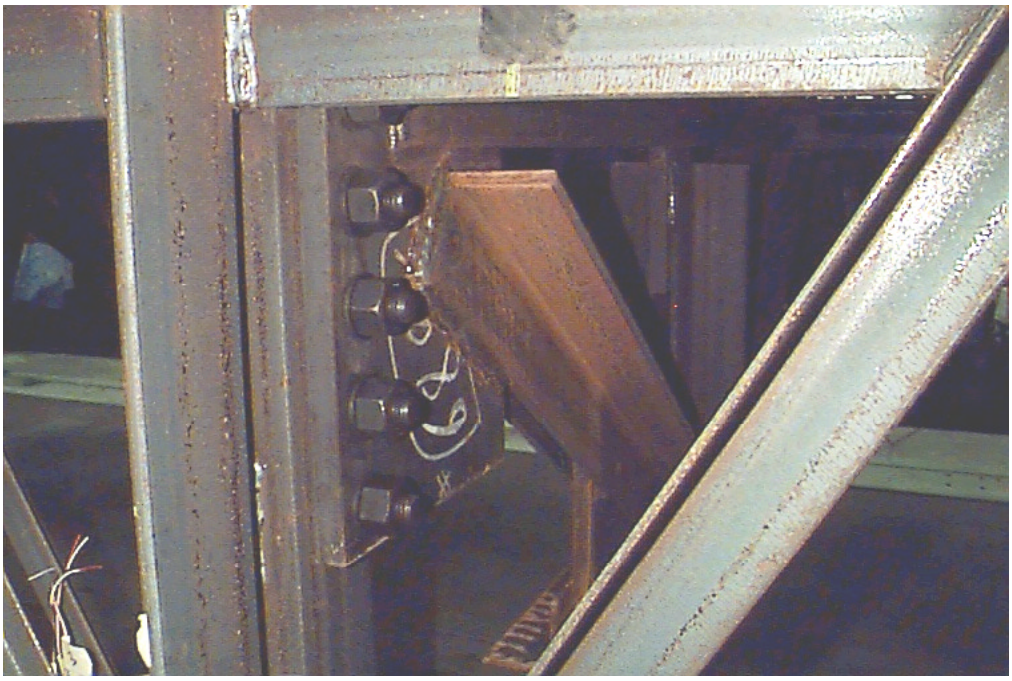

Figure 2.15 Bolted Connection Detail (FF-1,FF-2)

Figure 2.16 Joist Bearing Detail (H-1, H-2)

Holes were drilled in the haunch pans, girder fillers, or the deck for all the tests where necessary to accommodate the attachment of concrete slip gages. The placement of the holes coincided with the center of the first two panels on the joist-girders and was measured so placement on the H-shape would be consistent.

Galvanized cold-formed steel pour stop was installed around the edge of the entire specimen and remained in place through testing. Shear stud locations were marked on the specimen and the 0.75 in. diameter shear studs were welded to the joists, joist girders, and the H-shapes as indicated in each design. A specially designed welding gun provided by Nelson Stud Welding was used to attach the shear studs. The temperature and shrinkage reinforcement consisted of welded wire fabric (W1.4 x W1.4) placed over the entire specimen. The amount of transverse reinforcement varied from none over the H-shape in test H-1 to over 10 square inches over the interior girder in test H-1. Specific details can be found in the project reports by Kigudde et al. (1996) and Piotter (2001) and also in Showalter (1999).

After the reinforcement was placed, deflection transducers were calibrated and attached to the bottom chords/flange of the girders. The strain gages, load cells, and deflection transducers were wired to the data acquisition system, calibrated, and then zeroed. To get an accurate dead load reading of tests H-2 and FF-2, each bearing point was elevated slightly and the load cell corresponding to that point was re-zeroed and a load measurement was taken when the joist girder was bearing on the load cell. Concrete was then cast from the east end to west end and vibration was used to ensure uniform placement. A vibrating screed to facilitate a uniform distribution of concrete in tests H-2 and FF-2. Instrument readings were taken at the end of the casting day to account for the change in strain, deflection, and load from the concrete. Concrete cylinders were made for each test to determine the 7 and 28 day compressive strengths. After the concrete was finished and set, it was covered with plastic and the surface was watered for the first seven days after the casting date. At the end of seven days, the plastic was removed and the concrete continued to cure at the ambient temperature and humidity of the lab.

After seven days, the remaining test setup was completed. This included installing two load frames, load actuators, and the load distribution beams. Concrete strain gages were placed on the deck surface and plunge-type displacement transducers

were attached to nails embedded in the concrete through the holes previously drilled in the steel deck to measure slip between the concrete and top chord/flange. The steel sections were cleaned and whitewashed to provide a qualitative measure of yielding in the bottom chords, flanges and webs. All instrumentation was zeroed and readings were taken prior to loading, with the remaining instrumentation already in place.

2.4 Instrumentation

The instrumentation layout for the four test specimens is shown in Figures 2.17 – 2.19. The locations of the measuring devices vary slightly for each of the four tests due to geometric differences and observations made in previous testing. In general, bottom chord strains were recorded at the midspan of all specimens. After FF-1, strain gages were added at the third points of all the girders and in FF-2, two additional strain gages were added at the midspan at the extreme fiber to each girder. In FF-1, lateral deflections and joist bottom chord brace strain were measured; based on that test; the subsequent tests omitted this set of instrumentation. Concrete strains were measured over each girder member at the midspan and west third points for all four tests.

The strain gages were Measurements Group 120 Ohm foil gages with three wire lead and the concrete gages were Tokyo Sokkei 120 Ohm gages. Vertical deflections were measured with linear displacement transducers attached at the midspan and quarter points for FF-1, and the midspan and third points for FF-2, H-1, and H-2. Horizontal slips were measured approximately 2 ft and 4 ft from the end of the specimen with plunge type potentiometers. End reactions for each of the girders were measured with 150 kip load cells for the two spandrel members and a 200 kip load cell and 500 kip load cell for the interior girder.

The linear displacement transducers, potentiometers and load cells were all calibrated for deflection and load prior to testing using a dial caliper and universal testing machine.

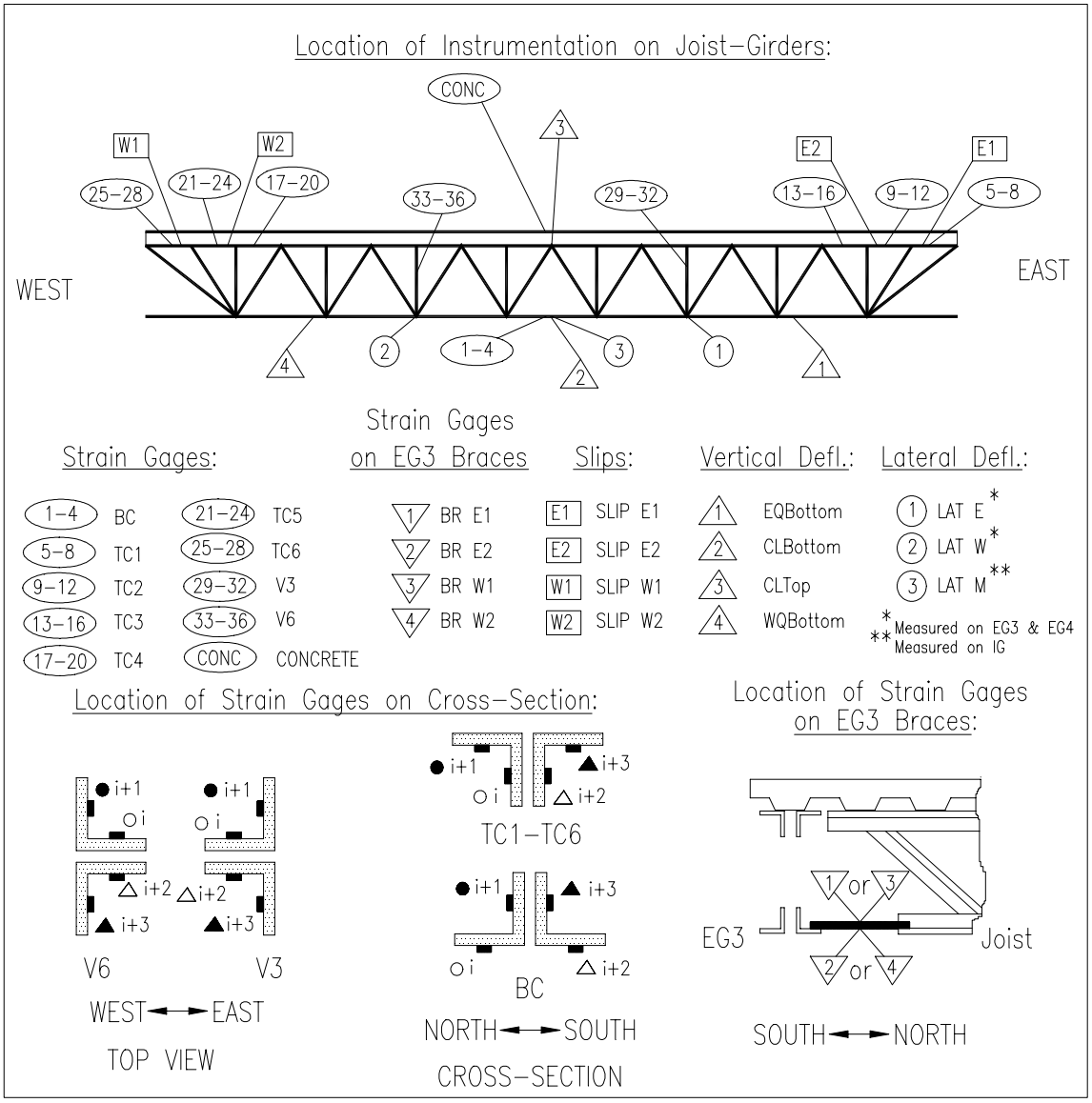

Figure 2.17 Instrumentation Summary (FF-1)

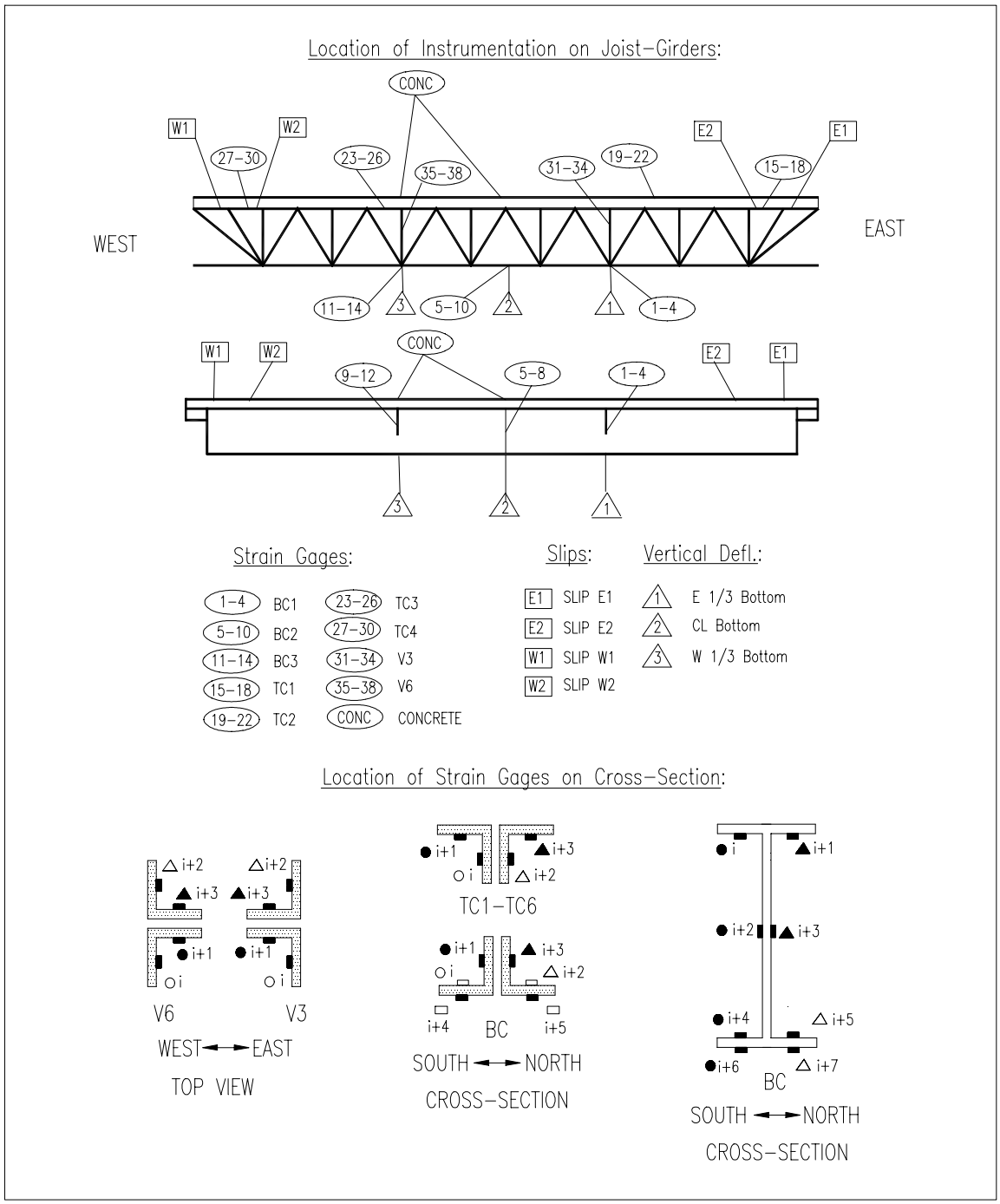

Figure 2.18 Instrumentation Summary (FF-2)

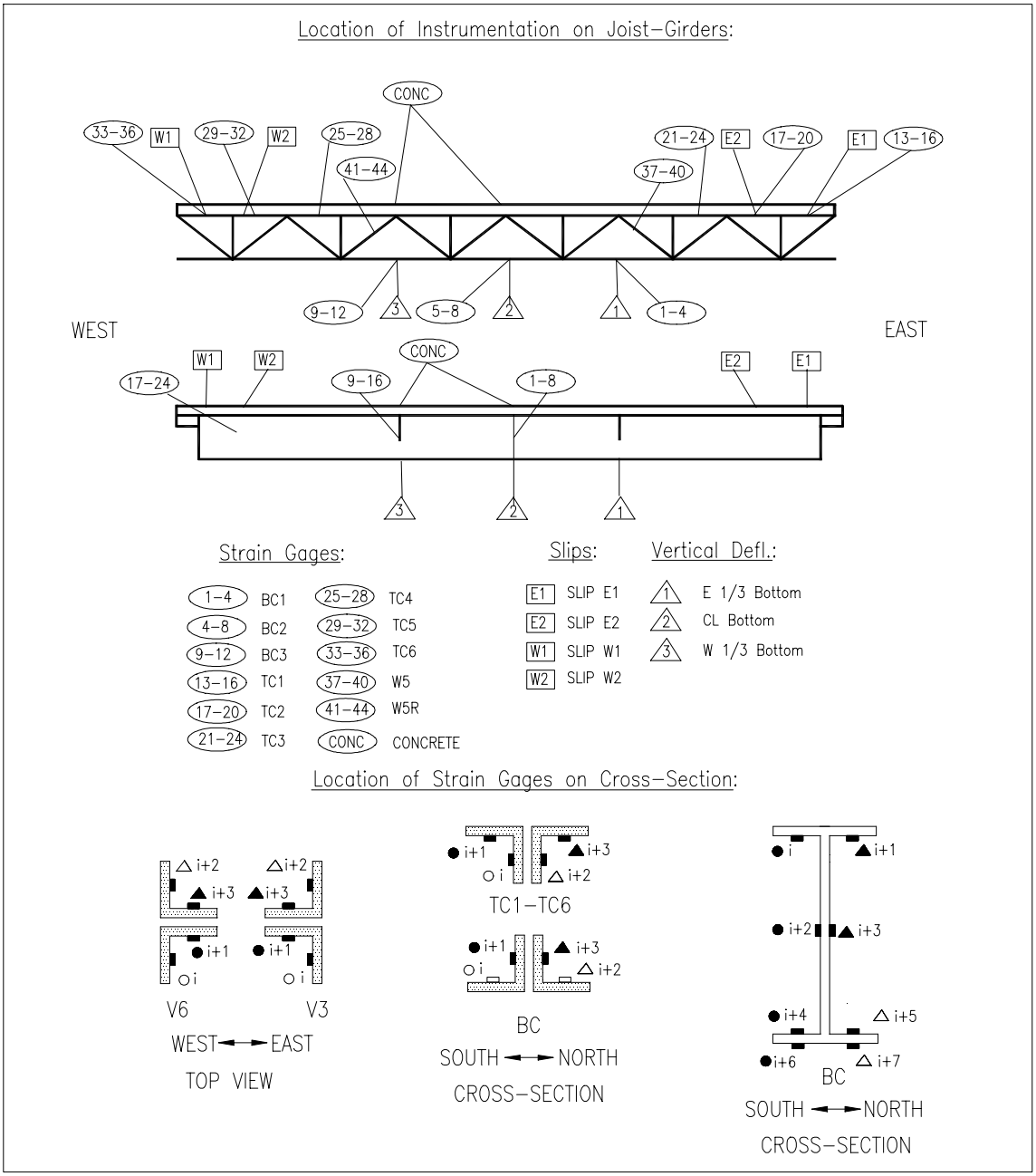

Figure 2.19 Instrumentation Summary (H-1, H-2)

2.5 Load Apparatus

The load apparatus for each test consisted of two load frames located at each third point illustrated in Figures 2.20-2.23, two 400 kip hydraulic rams, a set of spreader beams that were one or two tiers high, and support stands that supported the floor system. The load frame and support stands were bolted to the reaction floor. Figure 2.20 shows the cross-section view of the load apparatus with the load distribution beams oriented transverse to the centerline of the joist girders.

Hydraulic rams applied loads to two 15 ft W27x84 reaction beams that rested on a series of 6 in. by 6 in. or 12 in. by 12 in. plates bearing on elastomeric pads on the slab. This allowed for application of point loads that could be positioned per the required loading scenario, including direct loading of individual girders. In H-2, a second tier of spreader beams was used to apply a series of four point loads across the third points.

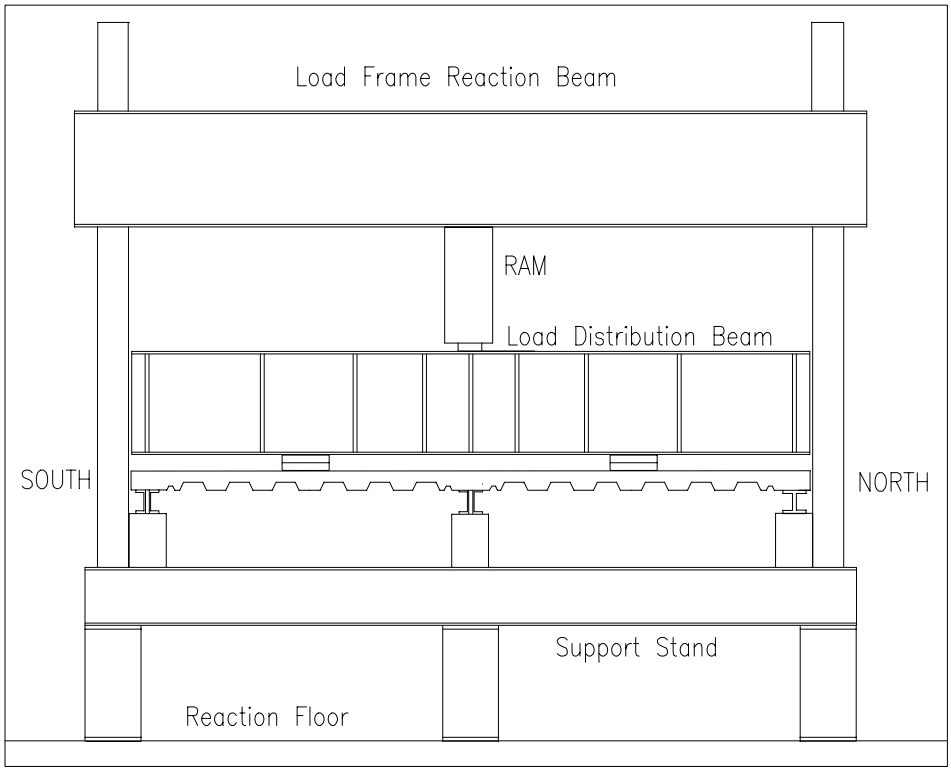

Figure 2.20 Load Apparatus (End View)

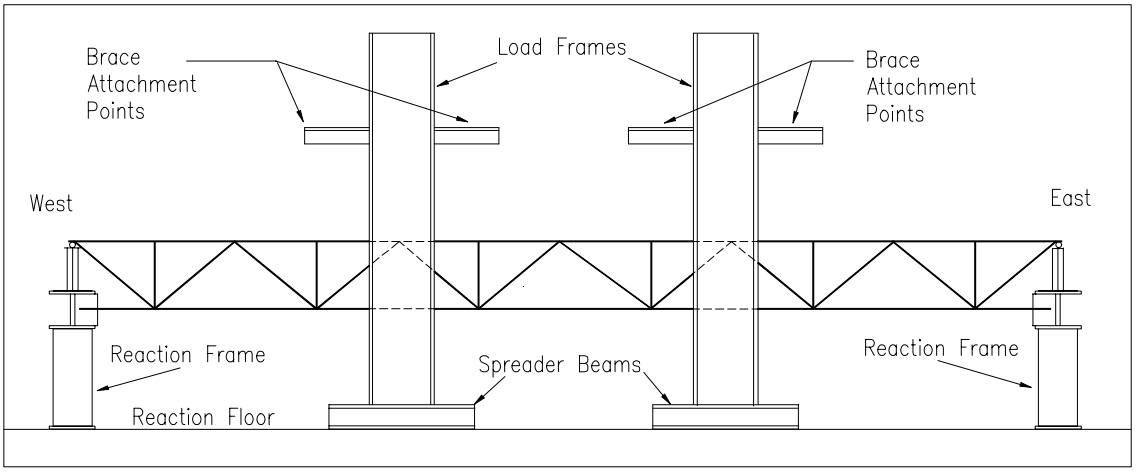

Figure 2.21 Load Apparatus (Elevation)

2.6 Testing Methodology - General

The testing methodology for each test was similar with the exception of small variations of where the load was applied relative to the girder centerlines.

Prior to testing, load distribution beams were put in place and the effect of the increased load was measured. Instrumentation was zeroed prior to application of load and the loads and strains that were recorded during concrete placement and setting of the distribution beams were added back in when the data was reduced. This allowed all phases of loading to be accounted for in each test. Application of live load to the floor system began with a preload of 10% of the predicted ultimate load to seat connections and to verify that the instrumentation was working properly. This load was then removed and the floor returned to its original unloaded position. Load vs. deflection plots were also generated to observe when the initiation of nonlinear behavior occurred and to determine when to change the load application from load controlled increments to deflection controlled increments.

Tests FF-1 and H-1 utilized multiple loading patterns that included moving the bearing plates under the distribution beam to various locations across each of the joist girders and H-shape third points. Details of these configurations and loadings can be obtained from the reports by Kigudde et al. (1996) and Showalter (1999).

In FF-2 and H-2, the load application points for the testing range are depicted in Figures 2.24 and 2.25. In FF-2, the two point loads were applied to the floor directly

over the single vertical web member on the each of the joists until failure. In H-2, a total of four point loads were applied to the floor with two point loads per joist directly over each of two vertical web members.

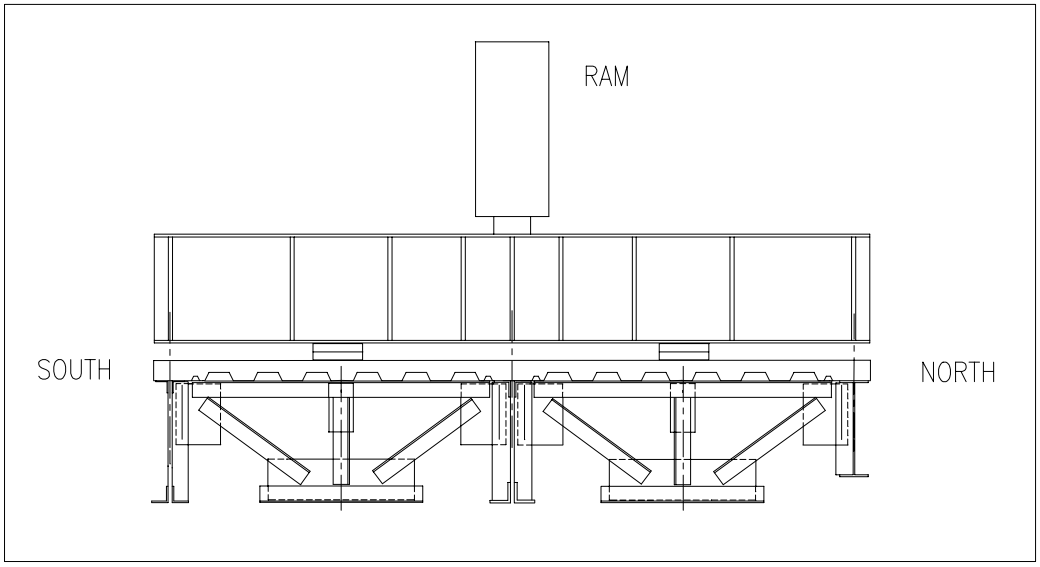

Figure 2.22 Location of Load Application (FF-2)

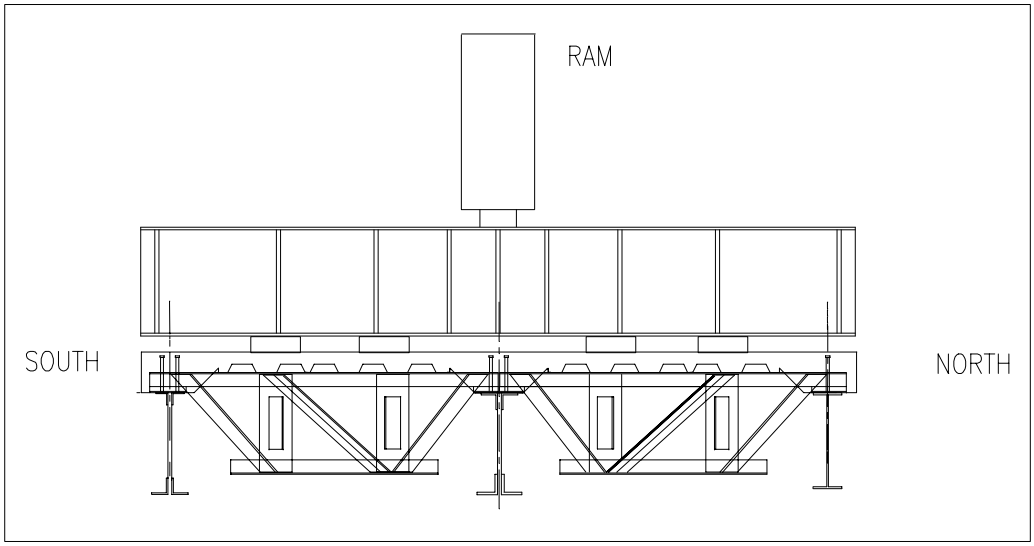

Figure 2.23 Location of Load Application (H-2)

2.6.1 Flush-Framed Test (FF-2)

After the preload was removed from the floor, the loading sequence for this test proceeded. The first phase of loading consisted of load increments of 30 to 40 kips of total load on the interior joist girders up to 1.43 times the design load (design load is ~60% of ultimate load), which was 274 kips of total load on the interior joist-girder and 136 kips on the exterior joist-girder and H-shape. At each load step, the applied load was allowed to stabilize for approximately 5 minutes. The floor was then fully unloaded and allowed to stabilize for 30 minutes, and the deflection at 1.43 times the design load was compared with the residual deformation in the unloaded floor resulting from plastic set. This was requested by the sponsor per the Steel Joist Institute (SJI) requirements for bare joists. The floor was then reloaded in the same manner with load increments of 30 to 40 kips. When the load reached 1.43 times design, the slab was inspected at each subsequent load step for cracks, and the steel framing was inspected for signs of yielding. The floor system was loaded to failure by deflection controlled increments when the load vs. deflection plot began to show nonlinear behavior.

2.6.2 Haunch Test (H-2)

After the preload was removed from the floor, the loading sequence for this test proceeded. The first phase of loading consisted of load increments of 10 to 15 kips of total load on the interior joist girders up to design load, which was approximately 60% of the ultimate load. At each load step, the applied load was allowed to stabilize for approximately 5 minutes. The floor was fully unloaded at the end of the first day of testing. On the second day of testing the floor was then reloaded in the same manner with load increments of 10 to 15 kips. When the load reached the design load, the slab was inspected periodically for cracks and the steel framing was inspected for signs of yielding. When the main body of testing had concluded and the ultimate (failure load) was reached, it was determined that additional data points beyond the ultimate load would be obtained. This was achieved by loading each girder individually by placing the ram loads directly over the girder third points.

CHAPTER 3
TEST RESULTS

3.1 General

The results of the four composite joist girder tests are summarized in this chapter. Plots of total load vs. deflection, total load vs. midspan bottom chord strain, total load vs. the end slip between the steel member and the concrete slab and total load vs. top chord strain are presented. All of the tests had unloading cycles during testing. The data points that are associated with unloading have been omitted from all of the plots. This was done so the plots would provide a clear indication of the behavior of each floor system. Complete plots of all phases of loading are presented in the project reports by Kigudde et al. (1996) and Piotter et al. (2001) and in Showalter (1999). Test summaries are presented in Appendix B.

Total load as defined here is the load on the floor system due to dead load, which includes the self-weight of steel framing, composite slab, and load distribution beams, and applied, or live, load from to the hydraulic actuators. In tests FF-1 and H-1, the load due to the load distribution beams is not included. In FF-2 and H-2, the data for all loads was acquired and included. Different levels of applied load are referred to in the following sections. They are the experimental ultimate load, the calculated ultimate load based on actual material properties, the calculated ultimate load based on nominal material properties, and the calculated design load. The experimental ultimate load is the maximum load sustained by the particular steel member. The calculated loads (moments) will be discussed and compared with measured experimental values in Chapter 4.

Bottom chord yielding was determined both qualitatively and quantitatively with strain gage measurements and flaking of whitewash, respectively. Yield strains were calculated based on tensile coupon yield stress and were compared to average bottom chord strain. The load deflection plot could not be used directly to determine if yielding had occurred. This was because the nonlinearity shown in the plots was due not only to bottom chord yielding but also due to the nonlinear behavior of the shear connection. A

well-defined yield plateau does indicate that a significant combination of bottom chord yielding and nonlinear behavior of the shear connectors had occurred.

3.1.1 Behavioral Trends

Three distinct behavioral trends illustrated by the plots of experimental data were identified and are discussed. The first is an explanation of how the load vs. deflection plots and load vs. bottom chord strain plots incorporated data that was not measured directly. The second is a discussion of load vs. strain behavior for the bottom chords of the joist girders with regard to yielding behavior. The final trend addresses variations in bottom flange strain on opposite sides of the web.

The plots in the following sections depict two separate loading stages for each member in the four test setups. The second two data points illustrated in Figure 3.1 are measures of the steel framing self-weight and the weight of the fresh concrete respectively.

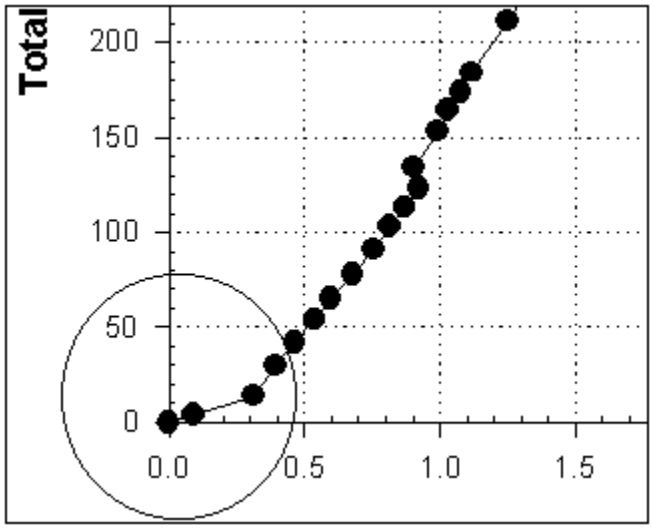

Figure 3.1 Self Weight and Concrete Placement Data

In FF-1 and H-1, steel self-weights were determined by extrapolating the load deflection plot, measured for concrete placement with calculated values of the framing self-weight from shop orders. A similar method was employed to determine the strain in the framing members due to their own self-weight. The loads, deflections, and strains

due to the weight of the fresh concrete were measured directly. In FF-2 and H-2, the procedure was the same except that the steel-framing member dead loads were measured directly as explained in Chapter 2.

Figure 3.2 shows the total load vs. midspan bottom chord strain for one of the joist girders in this thesis. This plot illustrates that at a certain range of loads, the values of measured strain do not increase while the load continues to increase. The reason for this has to do with the location of initiation of bottom chord yielding as it relates to the location of the strain gages on the bottom chord. The geometric layout of the web members positioned the panel points on the bottom chord symmetrically about the midspan of the girder. The midspan strain gages were located between two panel points, which explains the behavior, illustrated in Figure 3.2. Because of the extreme stress condition at the panel points due to web forces and bottom chord tension, the interior panel points yielded first. As the load increases, the yielding progresses from the panel points toward the midspan. The measured strains at the midspan do not increase until the yielding reaches the midspan at which point the plot will show a yield plateau if the experimental load increases enough to cause yielding to propagate.

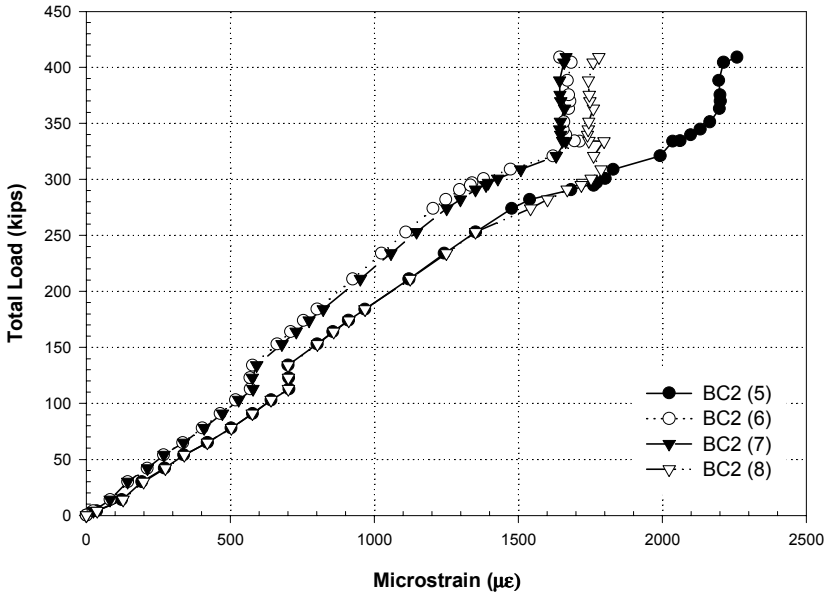

Figure 3.2 Total Load vs. Midspan Bottom Chord Strain

Figures 3.3 and 3.4 are plots of total load vs. midspan bottom flange strain for two H-shapes in these tests. Figure 3.3 is the complete total load vs. strain plot and Figure 3.4 illustrates an area of detail that has significance with regard to the H-shape behavior. In Figure 3.4, it can be seen that the bottom flange strains for H-1 show a higher rate of increasing tensile strain on one side of the web compared to the other. One gage, BF1 (8) shows that the strain does not increase significantly over a large range of total load. The plot for the flush-framed test isn't as definitive in terms of showing a clear pattern similar to the haunch test. The last few data points, however, begin to show a similar trend as in the haunch test. Gages 14 and 16 are both on the same side of the web and begin to show the same behavior of increasing tensile strains while the gages on the opposite side of the web do not show any significant increase in strain. This behavior is not what was expected for bottom flange strains due to bending. Gages located on opposite sides of the web but in the same relative position vertically should show similar strain gage readings. In this case, one side of the flange is showing strains that are becoming more tensile while the other side of the flange is showing constant strain tending toward compression. This indicates that either some type of torsion or out of plane bending due to warping is occurring in the H-shape. This behavior is evident at other locations (third points) supporting this conclusion.

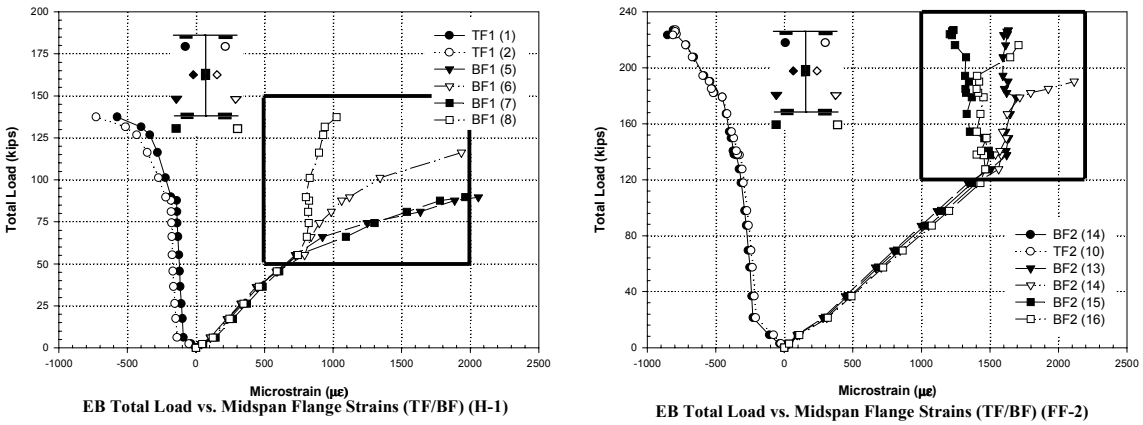

Figure 3.3 Bottom Flange Behavior

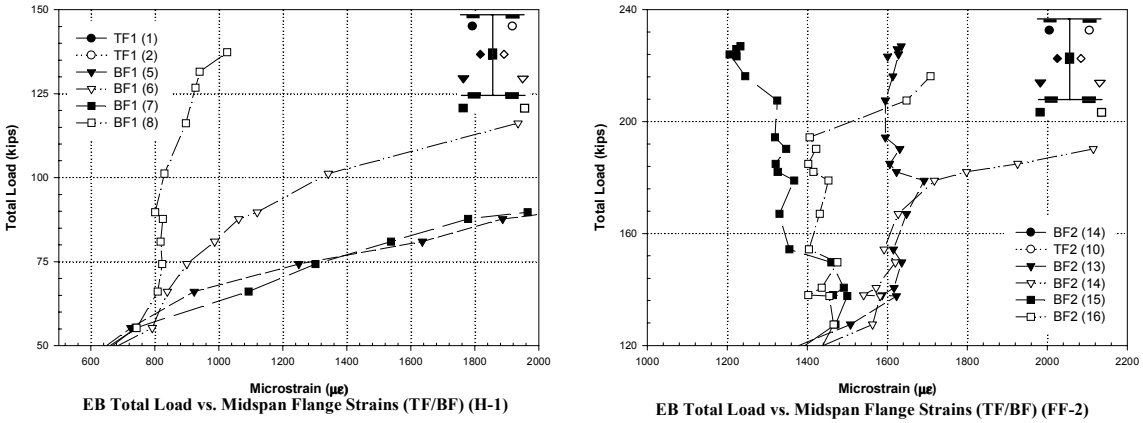

Figure 3.4 Area of Detail (Bottom Flange Behavior)

3.1.2 Material Properties

The measured values for the concrete compressive strength and steel tensile yield stress are presented in Table 3.1 and 3.2, respectively. The compressive strength for the concrete slabs was determined by averaging the compressive strengths for three or more concrete cylinders tested the same day as the composite girder tests. The yield and ultimate stresses are based on average results from two to four coupons per chord section. Tensile coupon tests were performed in a universal testing machine following ASTM A370 provisions.

Table 3.1 Concrete Compressive Strengths

Test	f'c (psi)
Flush-Framed (FF-1)	4 900
Flush-Framed (FF-2)	5 200
Haunch (H-1)	4 500
Haunch (H-2)	5 300

Table 3.2 Tensile Coupon Strengths

Member	Fy (psi)	Fu (psi)
(FF-1)		
EGL (bottom chord)	60 200	83 200
IG (bottom chord)	55 000	77 700
EGR (bottom chord)	60 000	82 500
(FF-2)		
EG (bottom chord)	63 000	85 500
IG (bottom chord)	57 000	87 200
EB (flange)	70 800	80 600
(H-1)		
EG (bottom chord)	55 300	82 100
IG (bottom chord)	53 400	83 700
EB (flange)	48 100	67 800
(H-2)		
EG (bottom chord)	60 800	84 500
IG (bottom chord)	54 700	80 300
EB (flange)	68 800	79 700

3.2 Flush-Framed Joist girder Tests (FF-1)

Kigudde et al. (1996) reported on the behavior of the flush-framed joist girder tests (FF-1) and complete results are presented therein.

3.2.1 Exterior Joist girder (EGL) (FF-1)

The exterior joist girder (EGL) had an experimental ultimate load of 174 kips and the load vs. midspan deflection behavior is illustrated in Figure 3.5. No distinct plateau can be seen on either the load vs. deflection plot or the load vs. bottom chord strain plot. The yield strain for the bottom chord was 2076 microstrain and is greater than strain gage readings of average bottom chord strain indicating that yielding had not occurred. No significant flaking of whitewash also shows that complete yielding of the bottom chord had not occurred.

The joist girder failed by buckling of W3R at a total load of 161 kips and a midspan deflection of 2.74 in. This means that buckling determined the strength of the joist girder based on the fact that no significant yielding was indicated.

The maximum end slip at failure illustrated in Figure 3.7 was approximately 0.10 in., indicating that the welded shear studs remained intact. This is based on a general criterion that assumes an end slip of 0.2 in. indicates that the shear studs had failed. The top chord behavior further verifies that the shear connection remained intact. The load vs. top chord strain plot illustrated in Figure 3.8 indicates that the top chord showed no strain reversal from tension to compression.

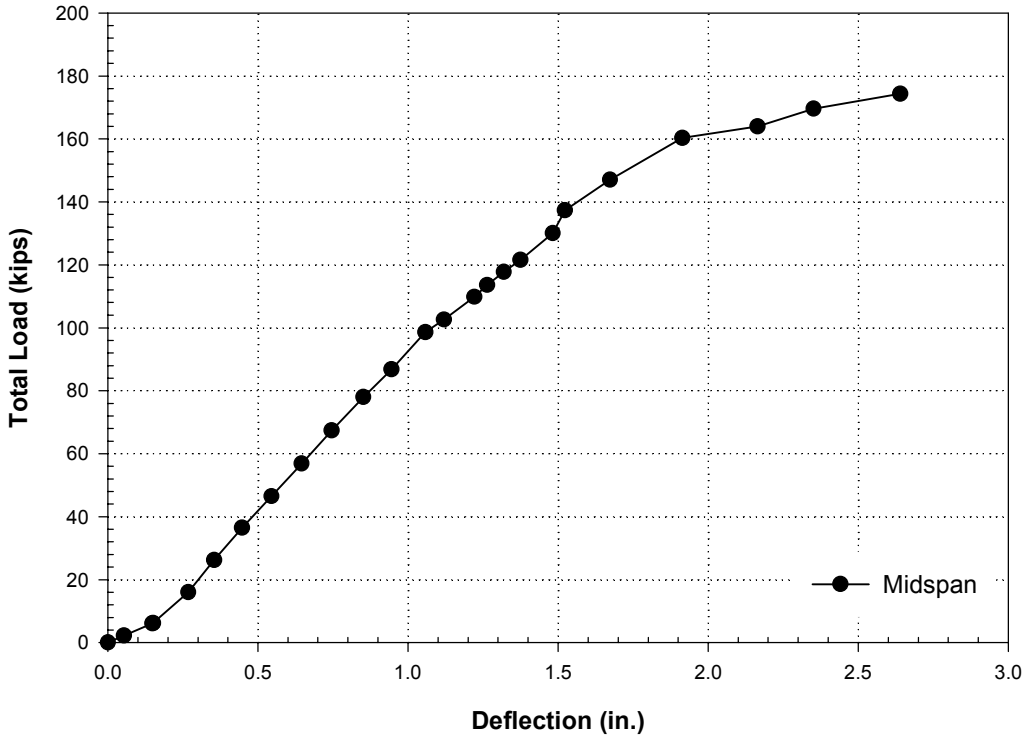

Figure 3.5 EGL Total Load vs. Midspan Deflection (FF-1)

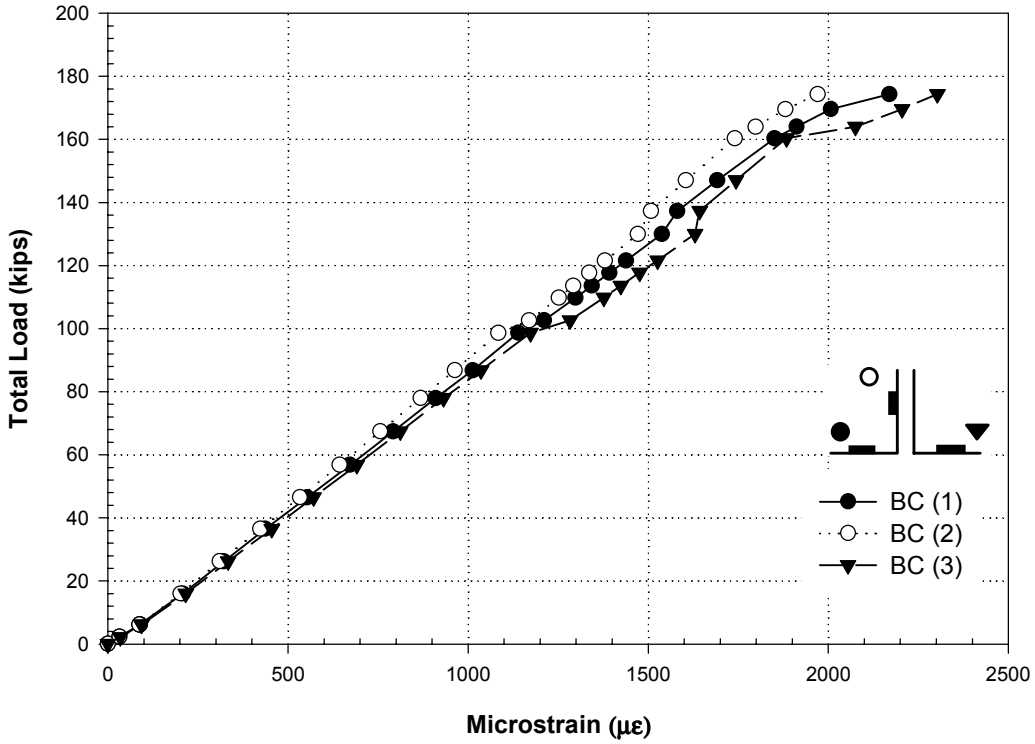

Figure 3.6 EGL Total Load vs. Midspan Bottom Chord Strain (FF-1)

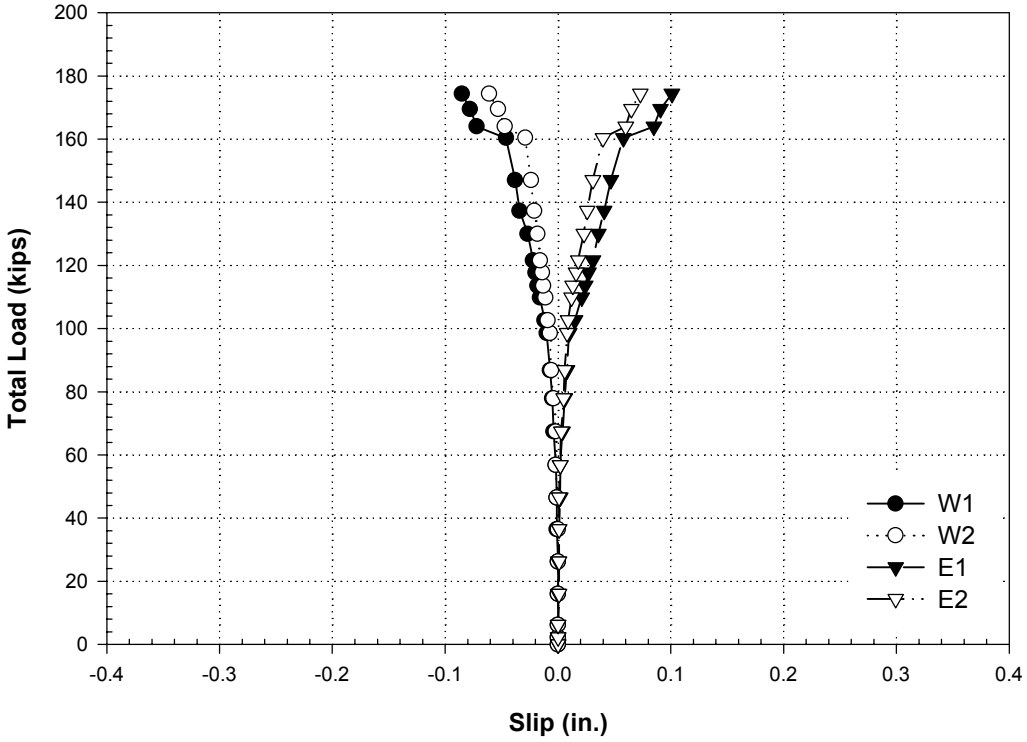

Figure 3.7 EGL Total Load vs. Slip (FF-1)

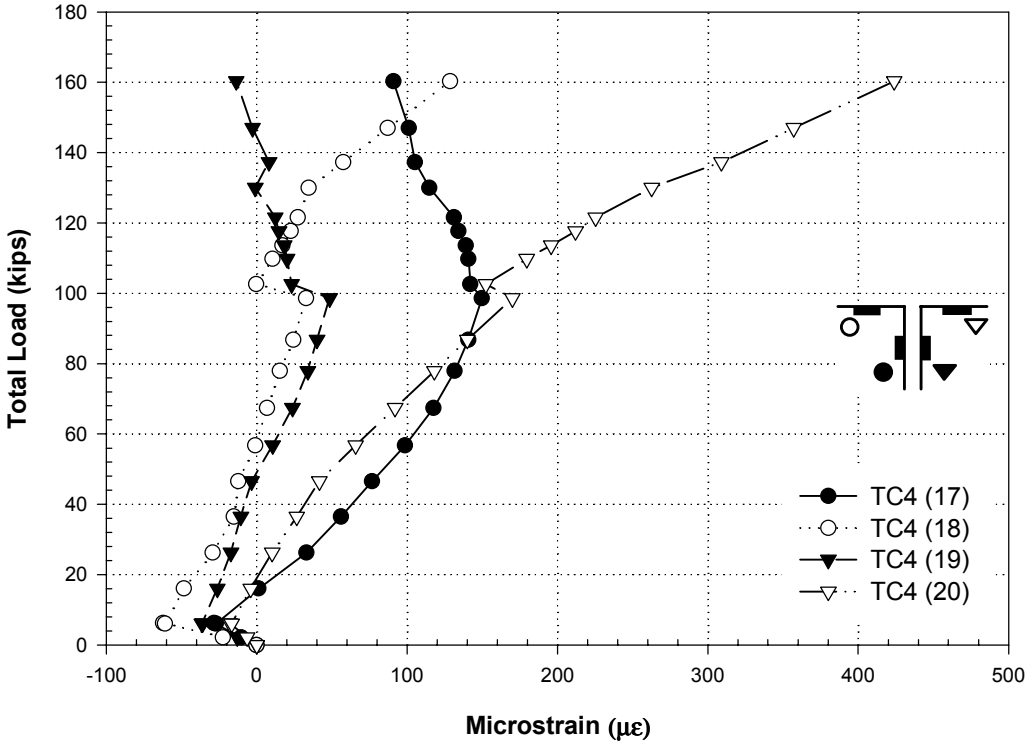

Figure 3.8 EGL Total Load vs Top Chord Strain (FF-1)

3.2.2 Interior Joist girder (IG) (FF-1)

The interior joist girder (IG) had an experimental ultimate load of 341 kips and Figure 3.9 illustrates the load vs. deflection behavior of the girder. The yield strain for the bottom chord was 1896 microstrain, which was slightly more than the average strain gage readings for the bottom chord strain illustrated in Figure 3.10. This result indicates that the bottom chord had not fully yielded. Yielding was also not indicated qualitatively by flaking of whitewash on the bottom chord.

The joist girder failed by weld fracture at the fillers of the double angle web members W3, W3R, W5, and W5R at a total load of 331 kips. Immediately following those failures, the webs began to show excessive buckling. Loading was terminated at a load of 329 kips at a midspan deflection of 7.2 in..

Figure 3.11 shows that the end slip reached approximately 0.4 in. near the ultimate load, indicating the shear connectors likely failed. The load vs. top chord strain plot illustrated in Figure 3.12 was inconclusive in terms of whether there was a strain reversal but based on the end slip, it can be concluded that some degree of shear connection failure had occurred.

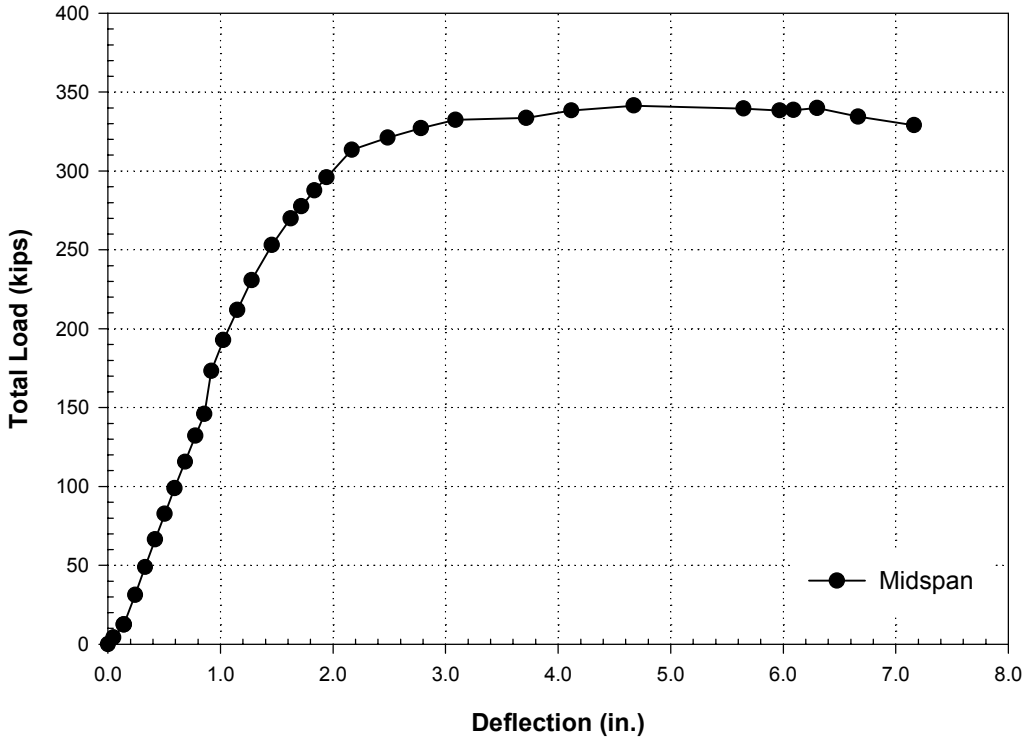

Figure 3.9 IG Total Load vs. Midspan Deflection (FF-1)

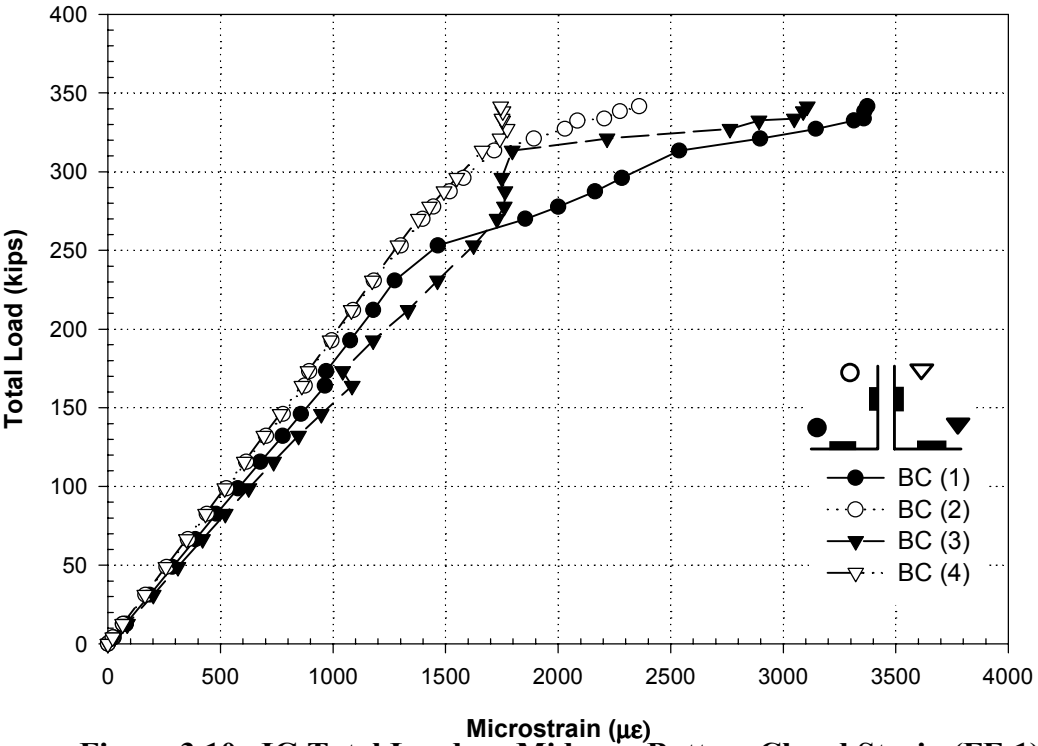

Figure 3.10 IG Total Load vs. Midspan Bottom Chord Strain (FF-1)

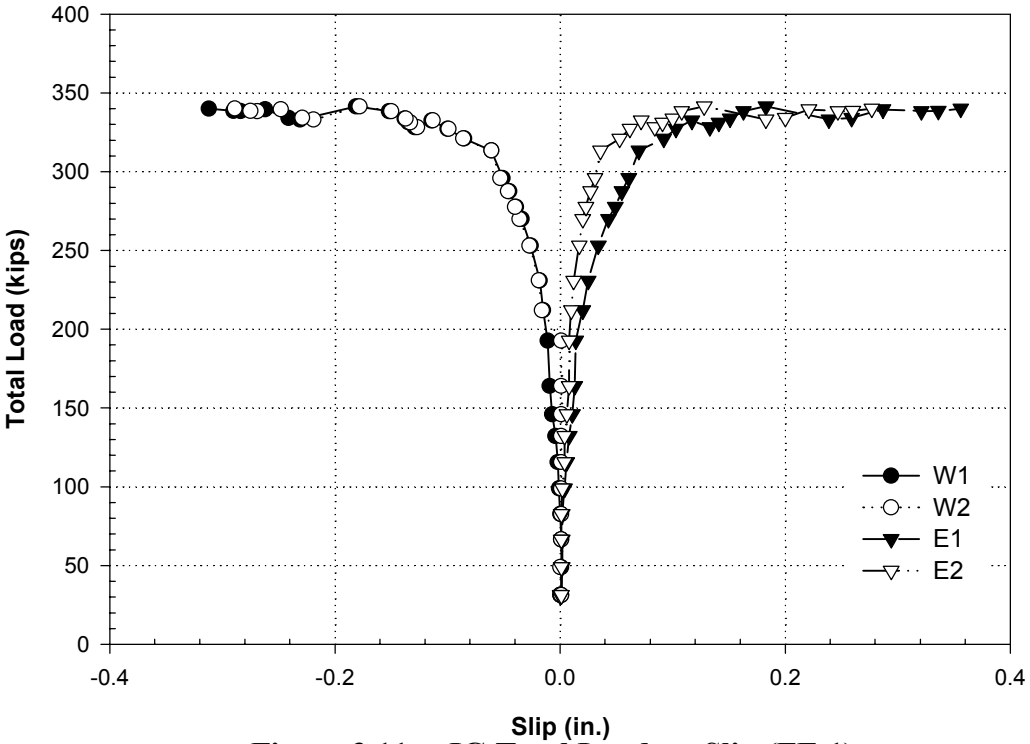

Figure 3.11 IG Total Load vs. Slip (FF-1)

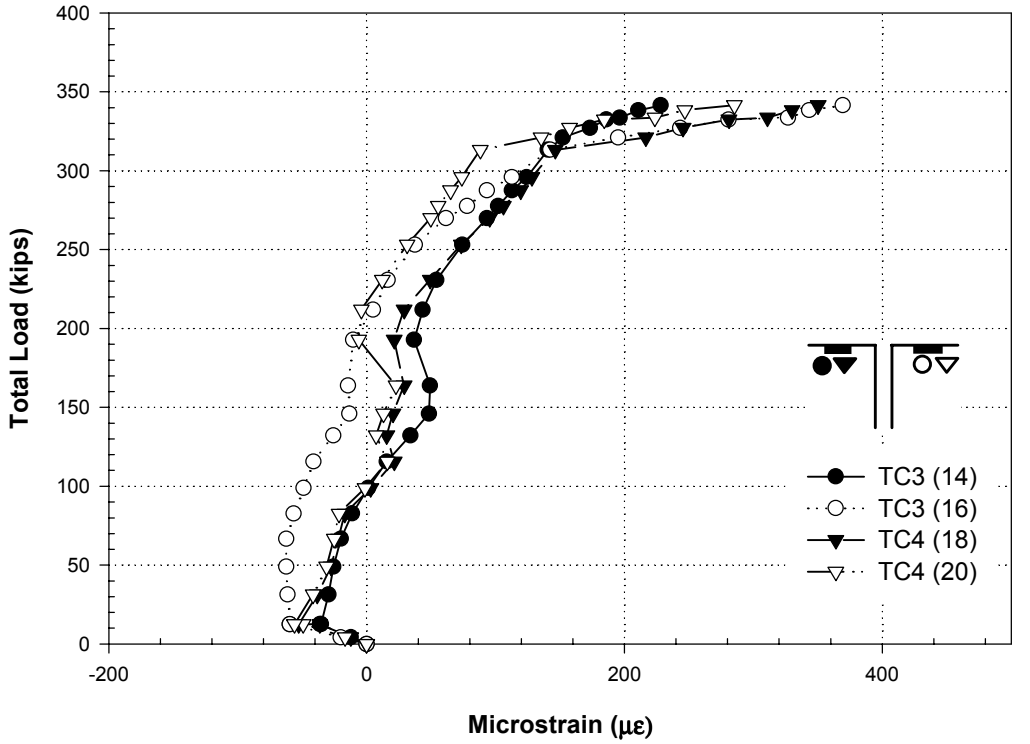

Figure 3.12 IG Total Load vs. Top Chord Strain (FF-1)(E/W 1/3 Pts)

3.2.3 Exterior Joist girder (EGR) (FF-1)

The exterior joist girder (EGR) had an experimental ultimate load of 173 kips as indicated by the load vs. midspan deflection plot in Figure 3.13. No distinct plateau can be seen on the load vs. deflection plot; however, some nonlinearity is indicated near the end of testing. The yield strain for the bottom chord was 2069 microstrain while strain gage readings show that the average bottom chord strain was less than the yield strain verifying that no yielding had occurred.

The joist girder failed by buckling of W3R at a total load of 165.9 kips and a midspan deflection of 3.10 in. The buckling failure controlled in this case as no significant yielding could be attributed to the bottom chord.

The maximum end slip at failure illustrated in Figure 3.15 was approximately 0.10 in., indicating that the welded shear studs remained relatively intact. The top chord behavior further verifies that the shear connection remained intact. The load vs. top chord strain plot illustrated in Figure 3.16 indicates that the top chord showed no strain reversal from tension to compression, also indicating no significant loss in shear connection.

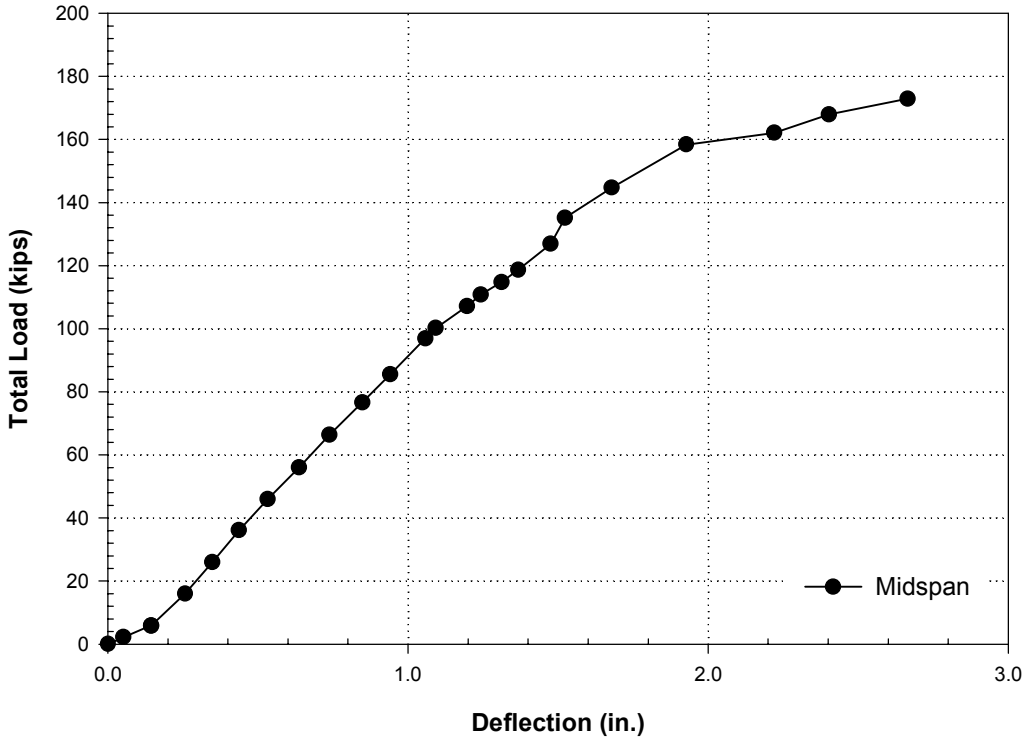

Figure 3.13 EGR Total Load vs. Midspan Deflection (FF-1)

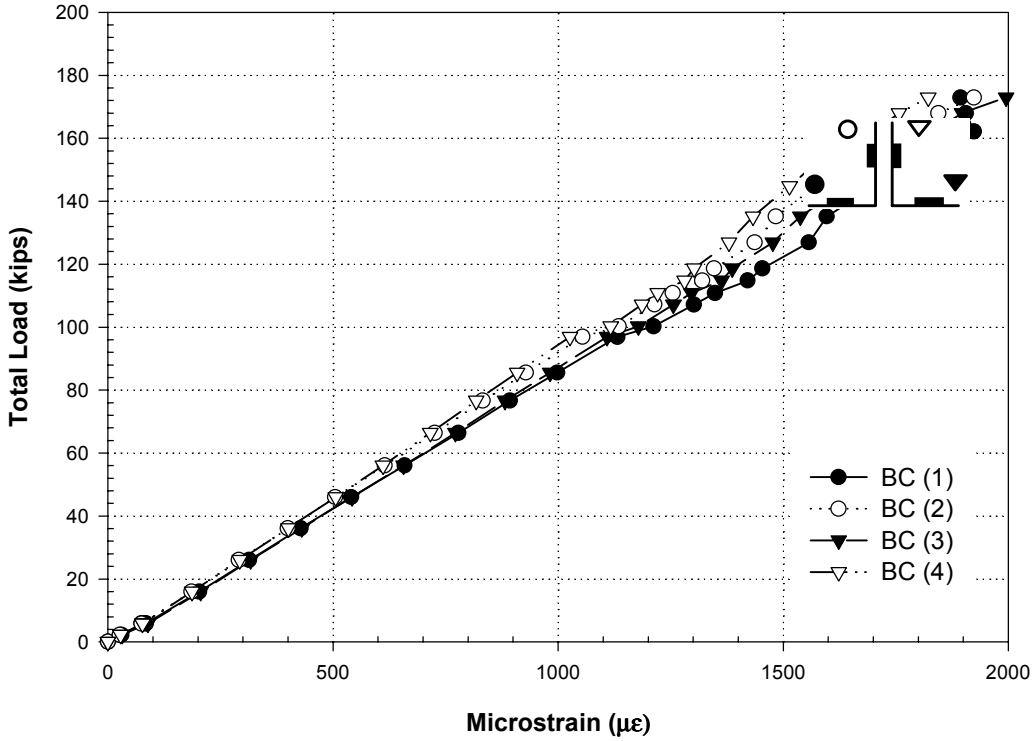

Figure 3.14 EGR Total Load vs. Midspan Bottom Chord Strain (FF-1)

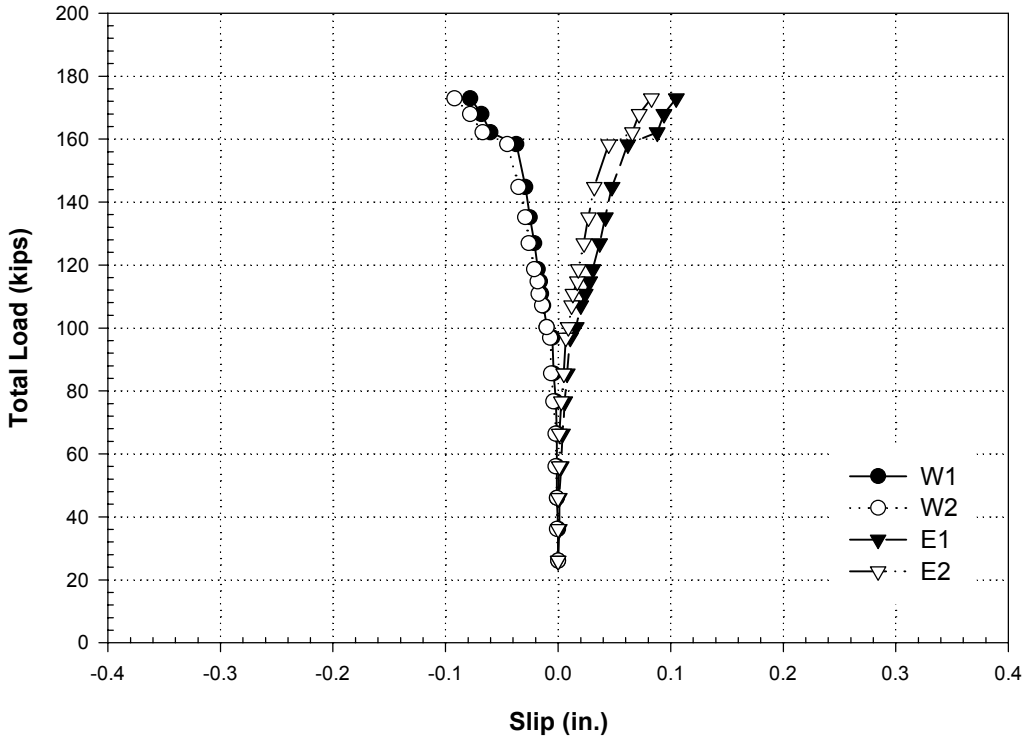

Figure 3.15 EGR Total Load vs. Slip (FF-1)

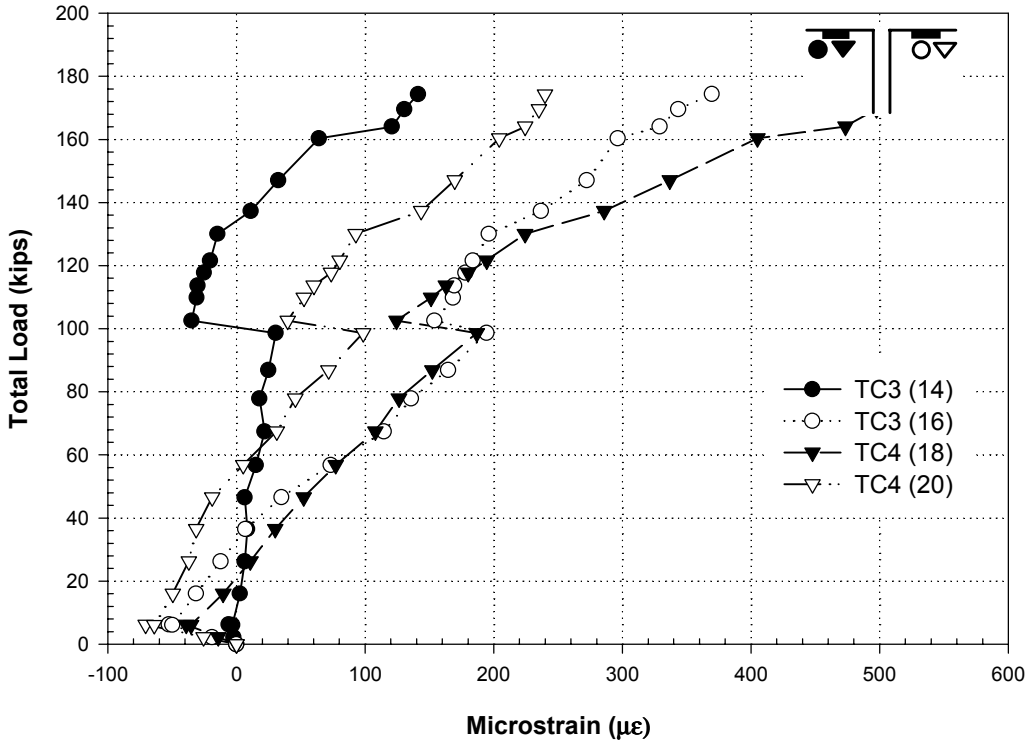

Figure 3.16 EGR Total Load vs. Top Chord Strain (FF-1)(E/W 1/3 Pts)

3.3 Flush-Framed Joist Girder Test (FF-2)

3.3.1 Exterior Joist girder (EG) (FF-2)

The exterior joist girder (EG) had an experimental ultimate load of 215 kips and the load vs. midspan deflection plot is illustrated in Figure 3.17. It should be noted that the joist girder showed some increase in strength beyond the plateau at a load of 180 kips. The top chord shows a strain reversal from compression to tension at 180 kips which gives some indication that the top chord began to pick up some of the load as bottom chord yielding progressed. The yield strain for the bottom chord was 2172 microstrain, which was exceeded by the actual bottom chord strain at failure. This verifies that yielding of the bottom chord had occurred.

Figure 3.19 shows that the end slip reached approximately 0.13 to 0.15 in. which was below the general limit of 0.2 in. of end slip indicating that the welded shear studs were intact at failure. Alternatively, based on the load vs. top chord strain illustrated in Figure 3.20, it is probable that the shear connection was beginning to fail based on the indications of the second strain reversal in the top chord. The plot shows a marked change from the strain becoming more tensile at a load of between 175 and 200 kips then reversing to become a compressive strain at a load of 210 kips.

The joist girder failed by crushing of the concrete slab at total loads of 179 kips and 215 kips respectively. Loading was terminated at a load of 215 kips, at which point the concrete at midspan crushed over the full width of the floor and no more load was being carried.

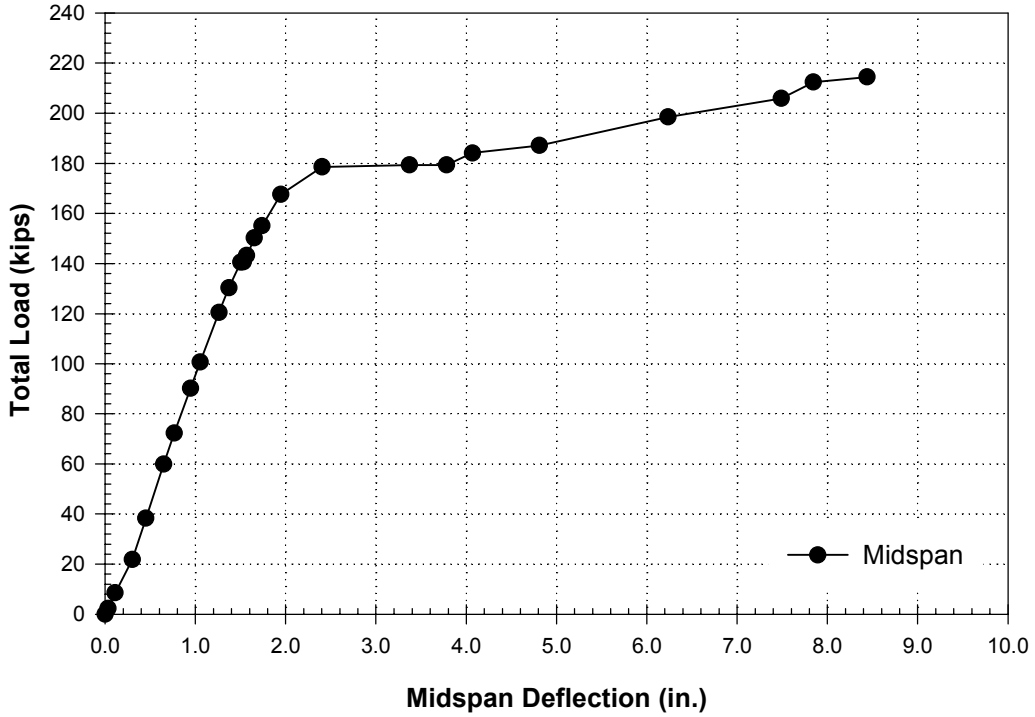

Figure 3.17 EG Total Load vs. Midspan Deflection (FF-2)

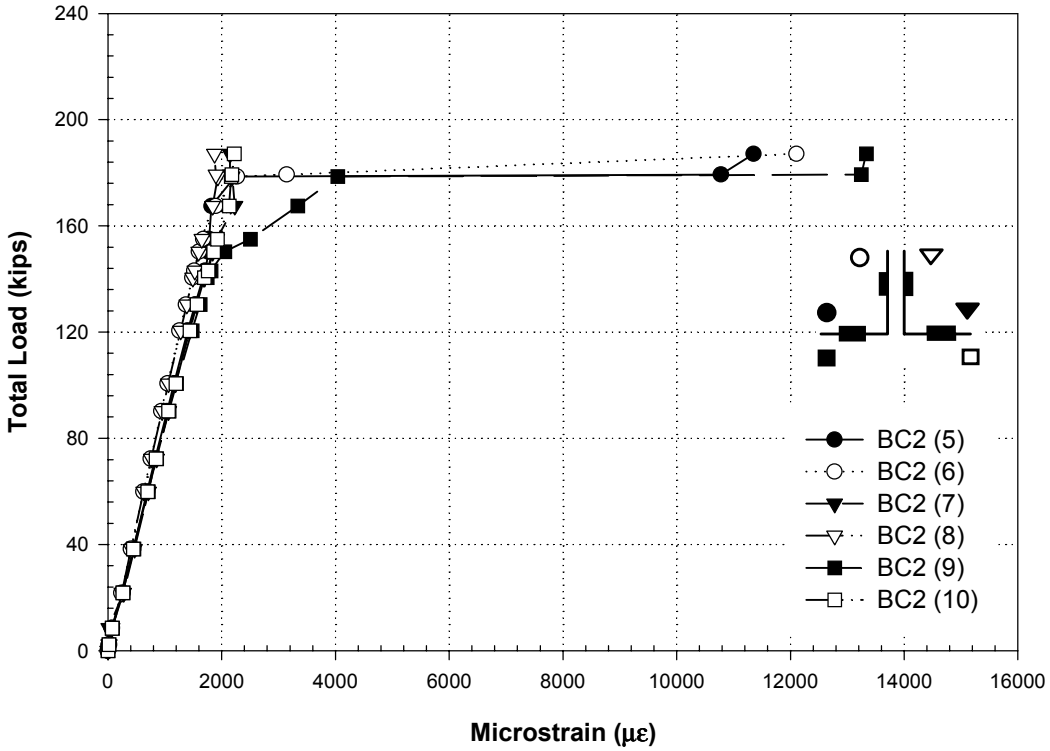

Figure 3.18 EG Total Load vs. Midspan Bottom Chord Strain (FF-2)

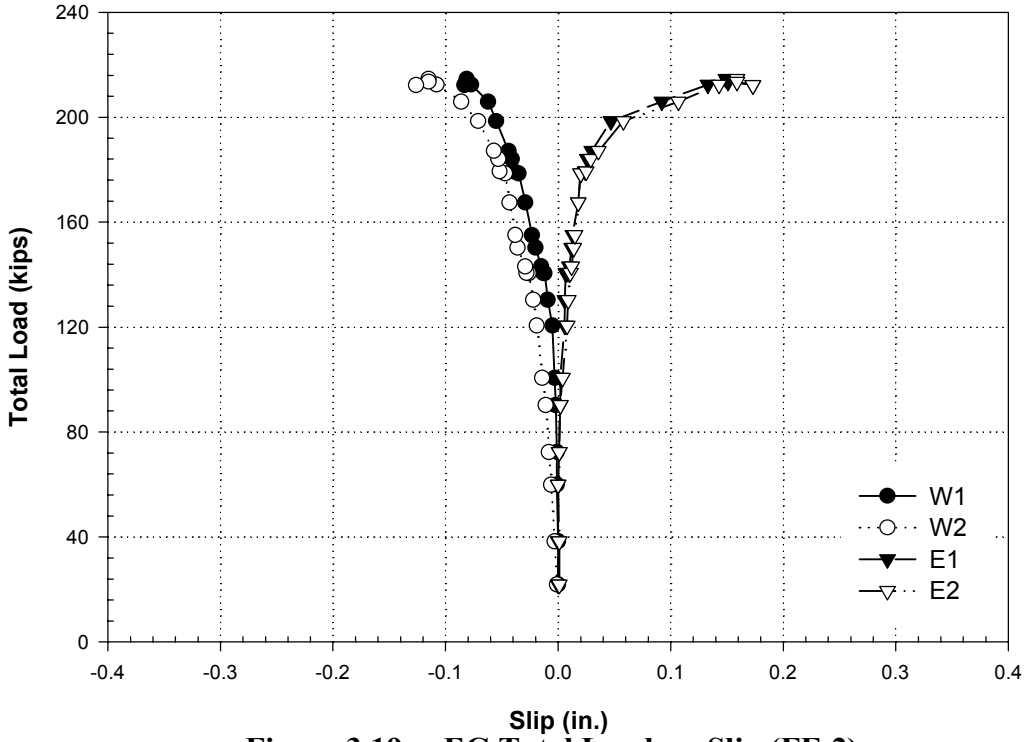

Figure 3.19 EG Total Load vs. Slip (FF-2)

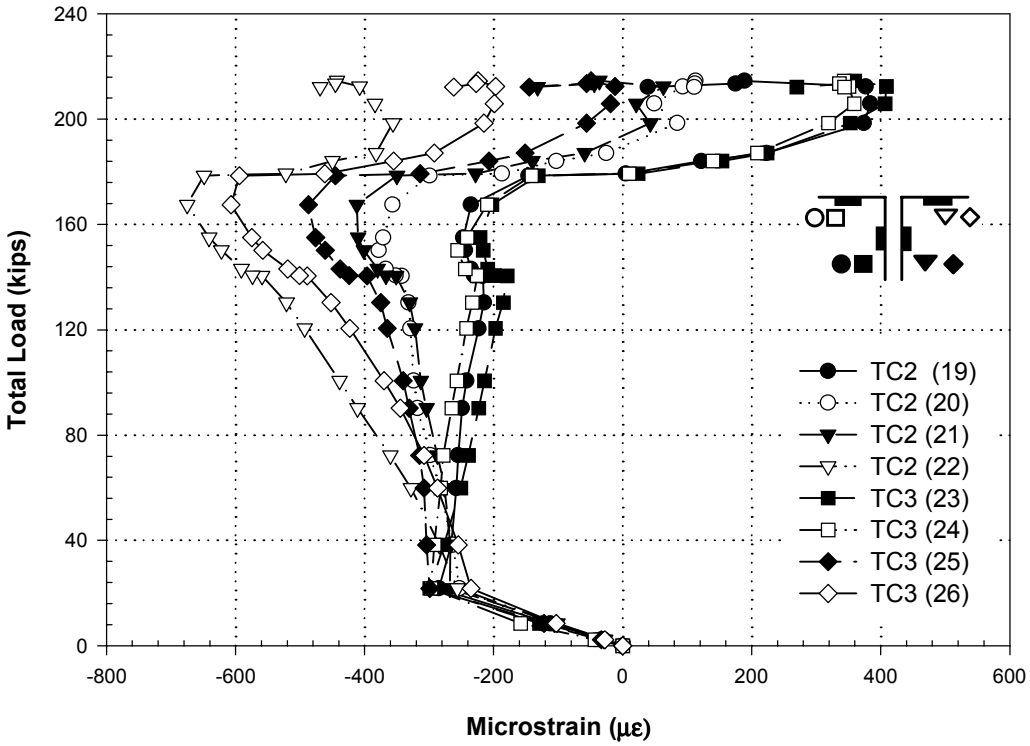

Figure 3.20 EG Total Load vs. Top Chord Strain (FF-2)(E/W 1/3 Pts)

3.3.2 Interior Joist girder (IG) (FF-2)

The interior joist girder (IG) had an experimental ultimate load of 388 kips as indicated in the load vs. midspan deflection plot illustrated in Figure 3.21. As with the exterior joist girder, the interior joist girder also showed some increase in strength beyond the plateau. Inspection of the load vs. deflection plot and the load vs. top chord strain plot show that at a load of 320 kips, the load began to increase as a strain reversal from compressive to tensile began in the top chord. This behavior, as with the exterior joist girder, indicates that as the bottom chord yielded, the top chord began to pick up load as shown by the top chord strain reversal. The yield strain for the bottom chord was 1965 microstrain, which was less than the measured bottom chord strain, verifying that yielding had occurred.

Figure 3.23 shows that the end slip reached approximately 0.15 to 0.19 in. at the west end, which indicates that the shear studs were approaching failure at the west end. The east end showed an end slip of approximately 0.05 in which indicates that the welded shear studs remained intact. The load vs. top chord strain illustrated in Figure 3.24 does not show a significant strain reversal for either the east or west end (TC3 East, TC4 West). Careful inspection indicates that the plots are beginning to show the same characteristic tendency toward tensile strain with the plot becoming more vertical at the last few data points. This vertical rise in the plot is exhibited in the exterior joist girder just prior to strain reversal.

The joist girder failed by bottom chord yielding and crushing of the concrete slab at a total load of 327 kips and 388 kips respectively. Loading was terminated at a load of 388 kips, at which point the concrete at the midspan crushed over the full floor width and no additional load could be applied.

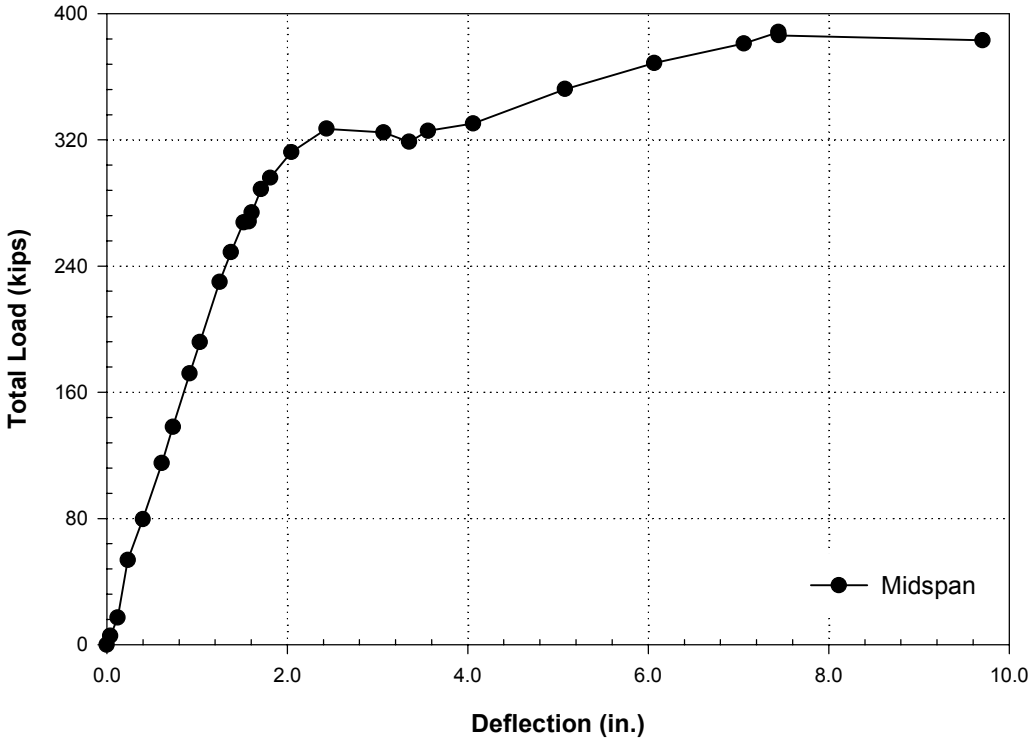

Figure 3.21 IG Total Load vs. Midspan Deflection (FF-2)

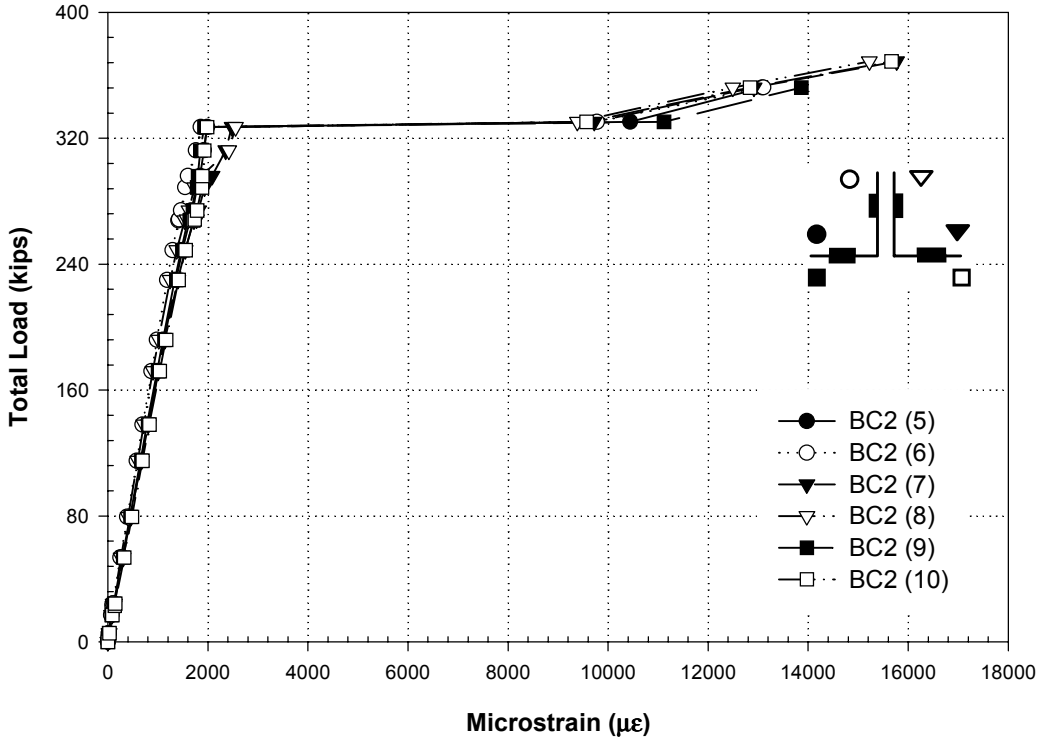

Figure 3.22 IG Total Load vs. Midspan Bottom Chord Strain (FF-2)

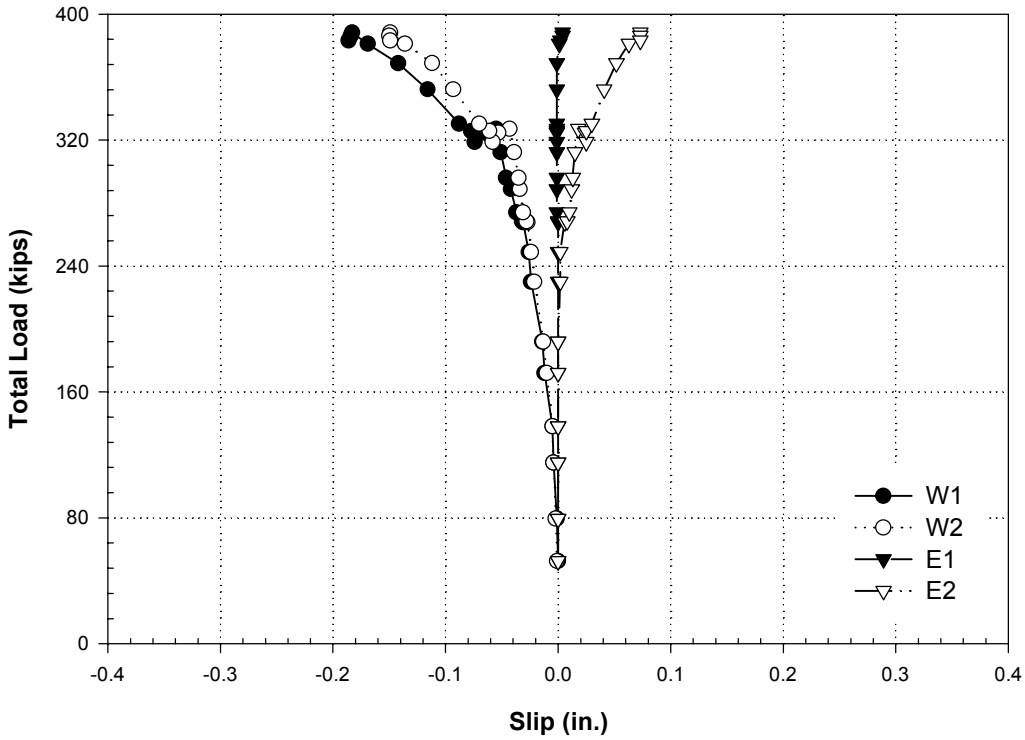

Figure 3.23 IG Total Load vs. Slip (FF-2)

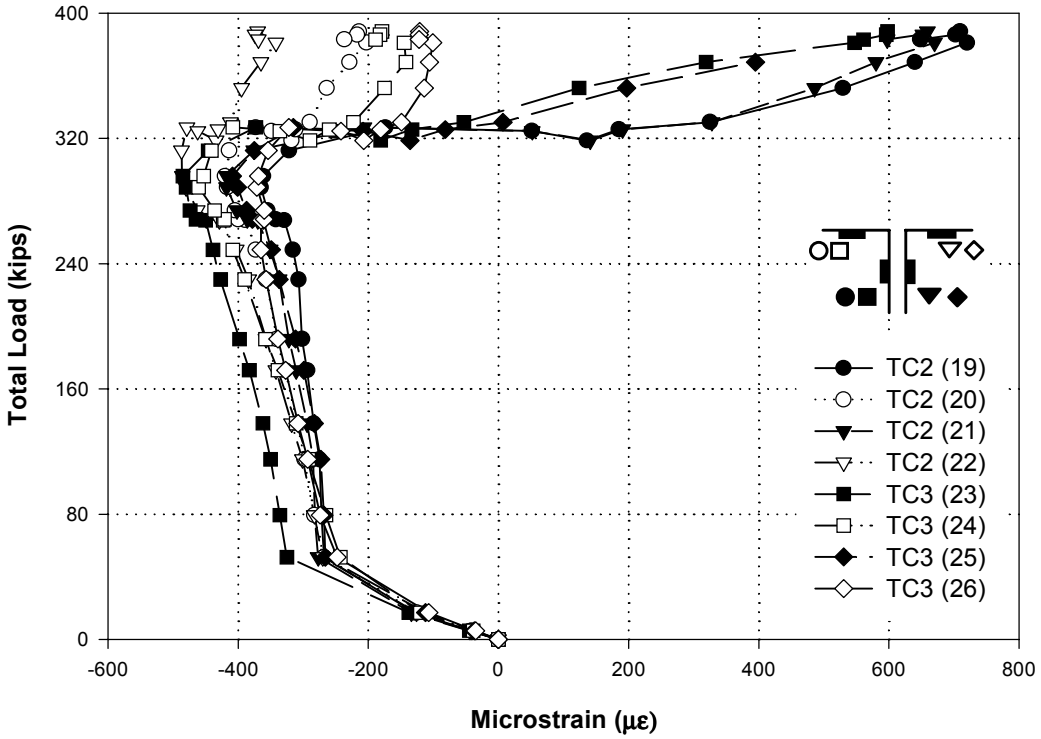

Figure 3.24 IG Total Load vs. Top Chord Strain (FF-2)(E/W 1/3 Pts)

3.3.3 Exterior Girder (EB) (FF-2)

The exterior H-shape (EB) had an experimental ultimate load of 227 kips as indicated on the load vs. midspan deflection plot illustrated in Figure 3.25. The flange strains (1500-2000με) were significantly less than the yield strain of 2441 microstrain but the high level of strain in the webs at the midspan and both third points (> 2000με) indicate that the flange strains were too low. It is unlikely that yielding of the web occurred before the flanges based on equilibrium arguments and on the third point web strains illustrated in Figures 3.28 and 3.29. The east third point showed a similar response to the midspan in terms of total magnitude of strain; however, the west third point did not. The whitewash had flaked off the bottom flange between the third points and had begun to flake off of the web as well. This further indicates that yielding had occurred. The possibilities for error include the calculated yield strain or measured strain gage readings.

Figure 3.30 illustrates that the end slip reached approximately 0.10 to 0.13 in., which indicates that the welded shear studs remained intact at ultimate load. No strain reversal was indicated in Figure 3.26, which would also indicate that the shear studs had not failed.

The H-shape failed by bottom flange yielding and crushing of the concrete slab at a total load of 154 kips and 227 kips, respectively. Loading was terminated at a load of 227 kips, at which point the concrete at midspan crushed over the full width of the floor and no more load was being carried.

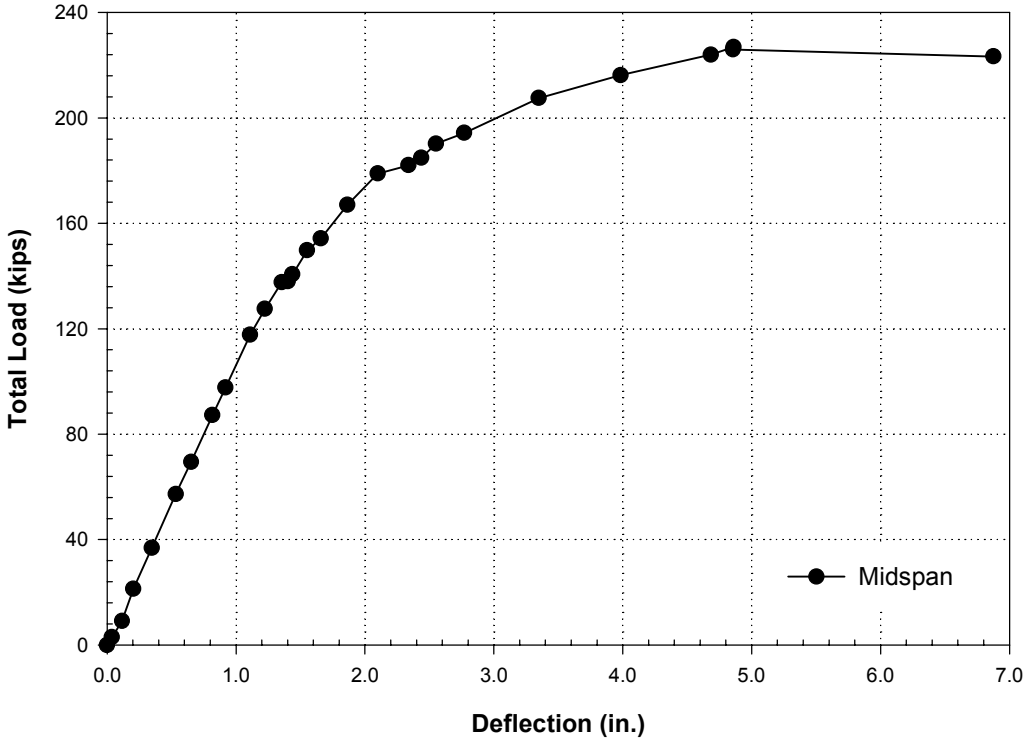

Figure 3.25 EB Total Load vs. Midspan Deflection (FF-2)

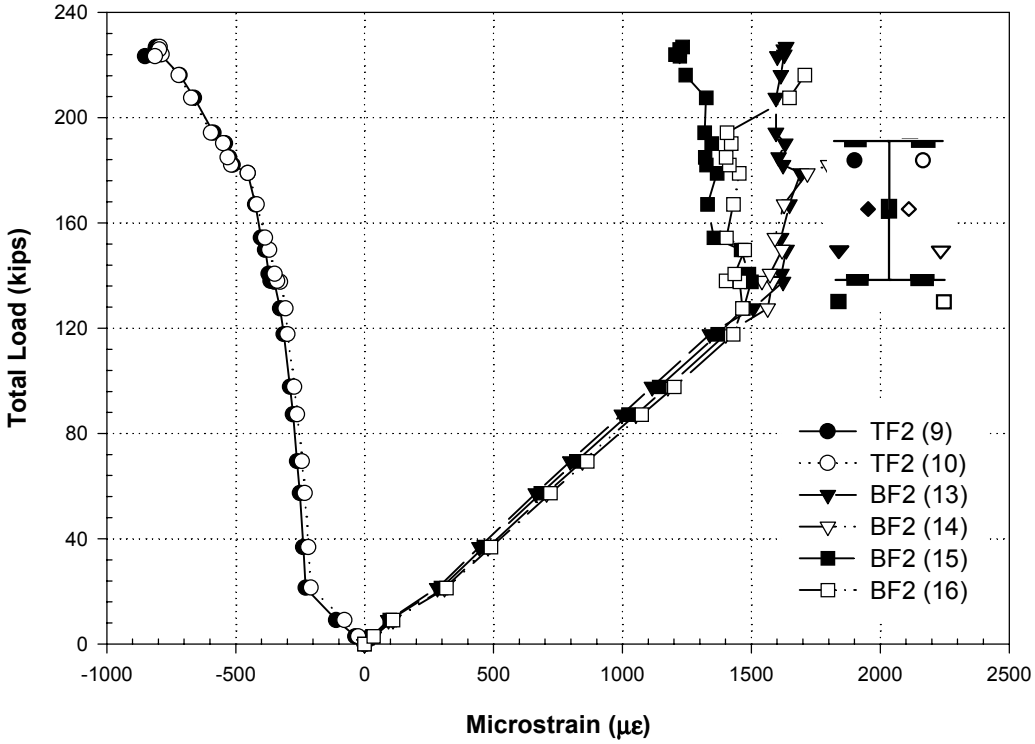

Figure 3.26 EB Total Load vs. Midspan Flange Strains (TF/BF) (FF-2)

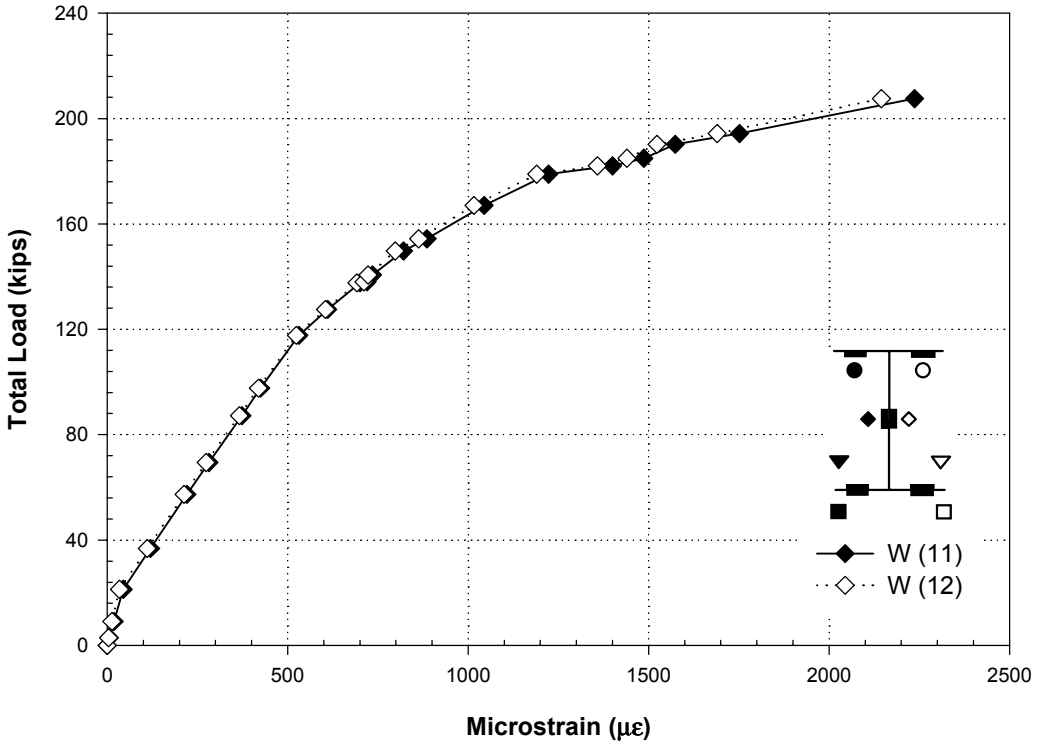

Figure 3.27 EB Total Load vs. Midspan Web Strains (W) (FF-2)

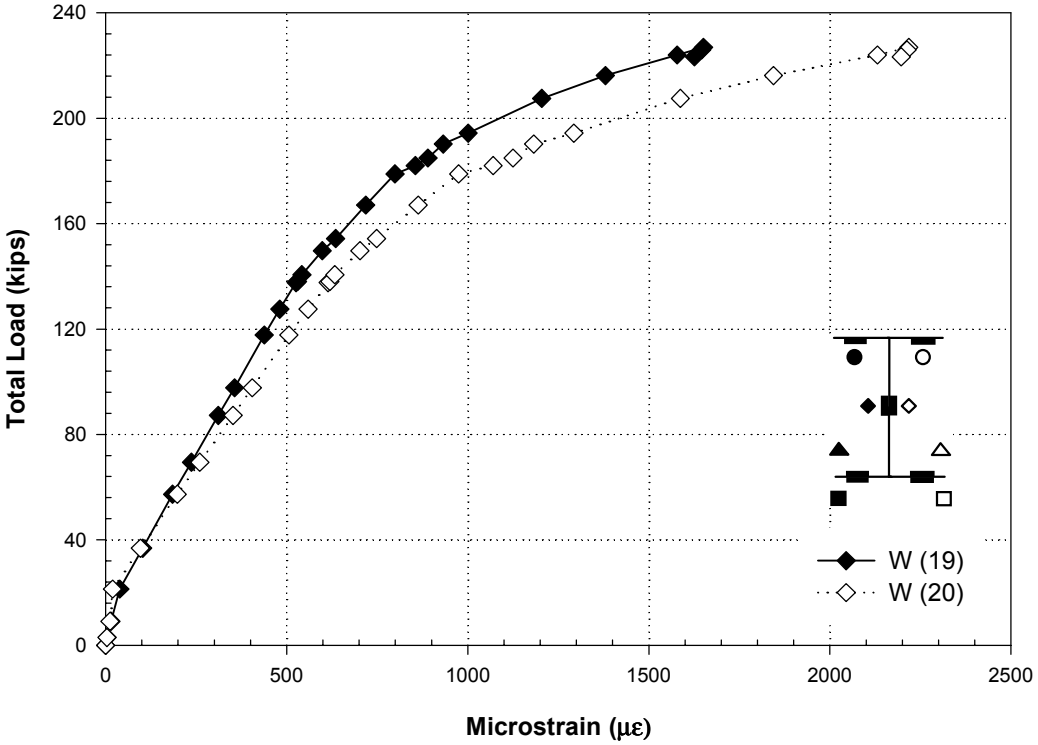

Figure 3.28 EB Total Load vs. W Third Point Web Strains (W) (FF-2)

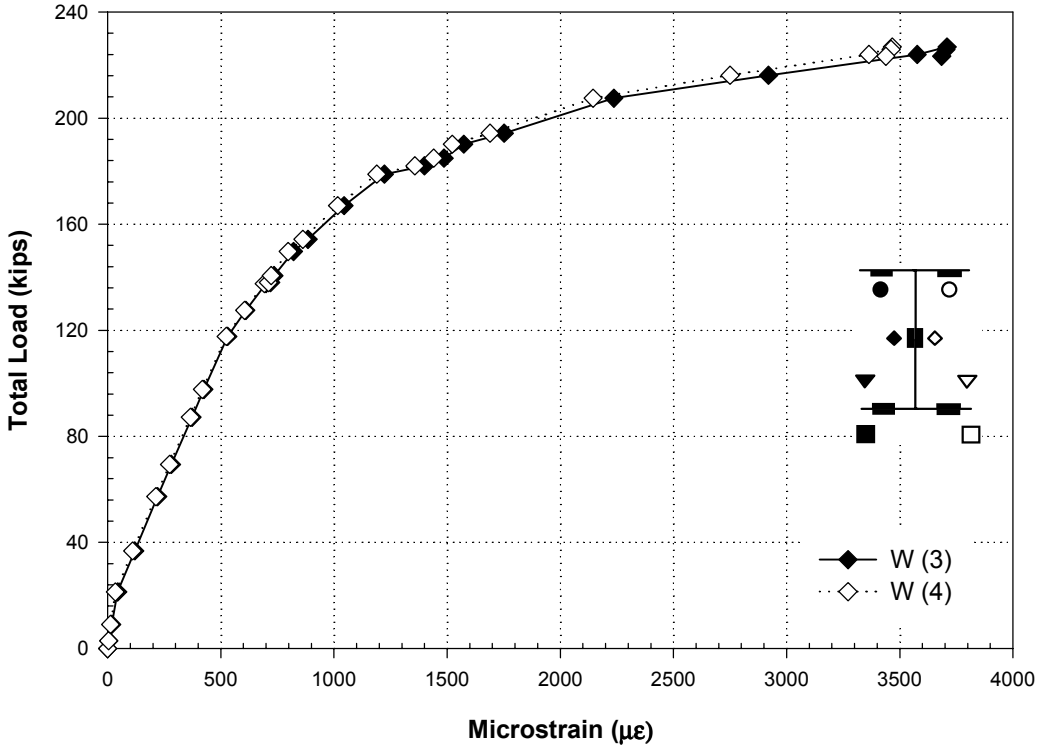

Figure 3.29 EB Total Load vs. E Third Point Web Strains (W) (FF-2)

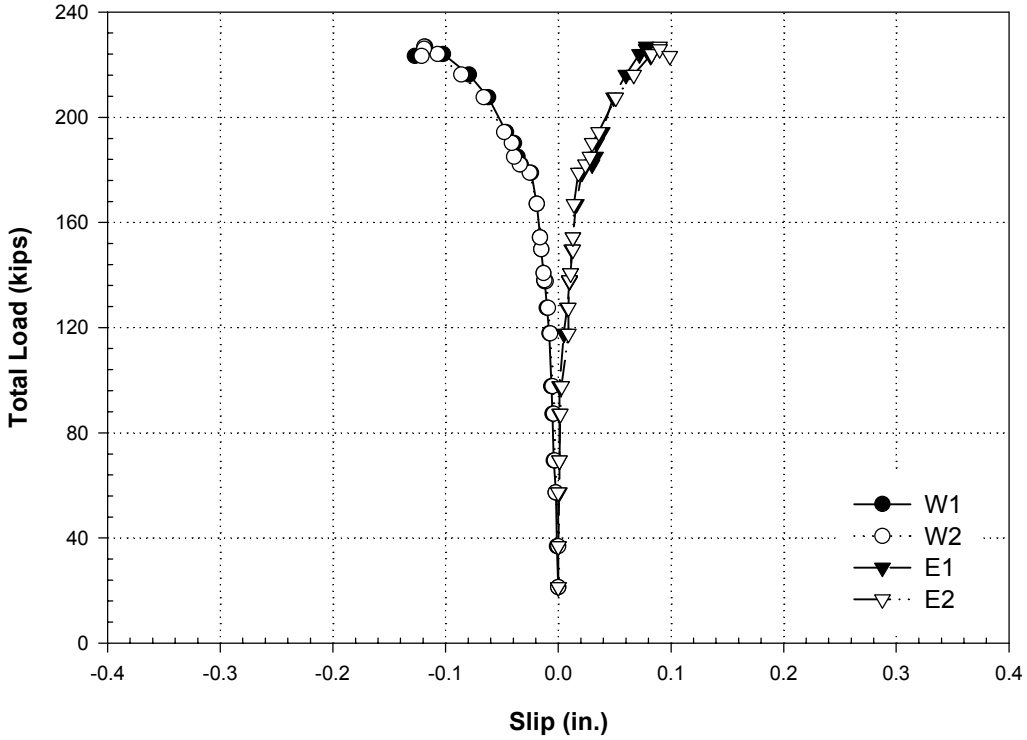

Figure 3.30 EB Total Load vs. Slip (FF-2)

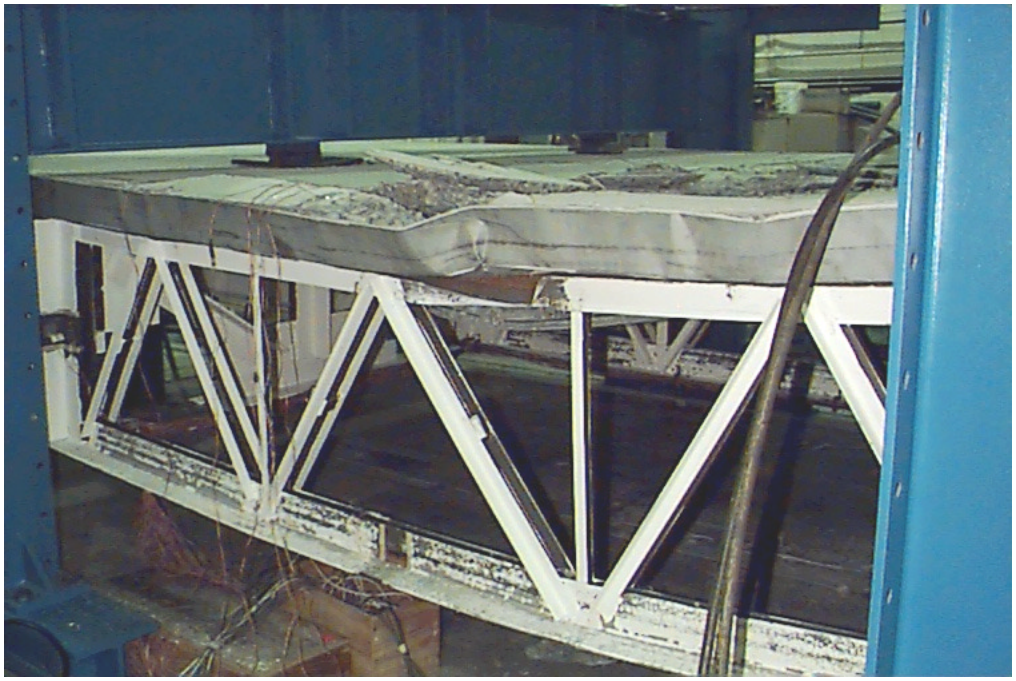

Figure 3.31 Buckling of EG Top Chord and Bottom Chord Yielding Between Third Points (FF-2)

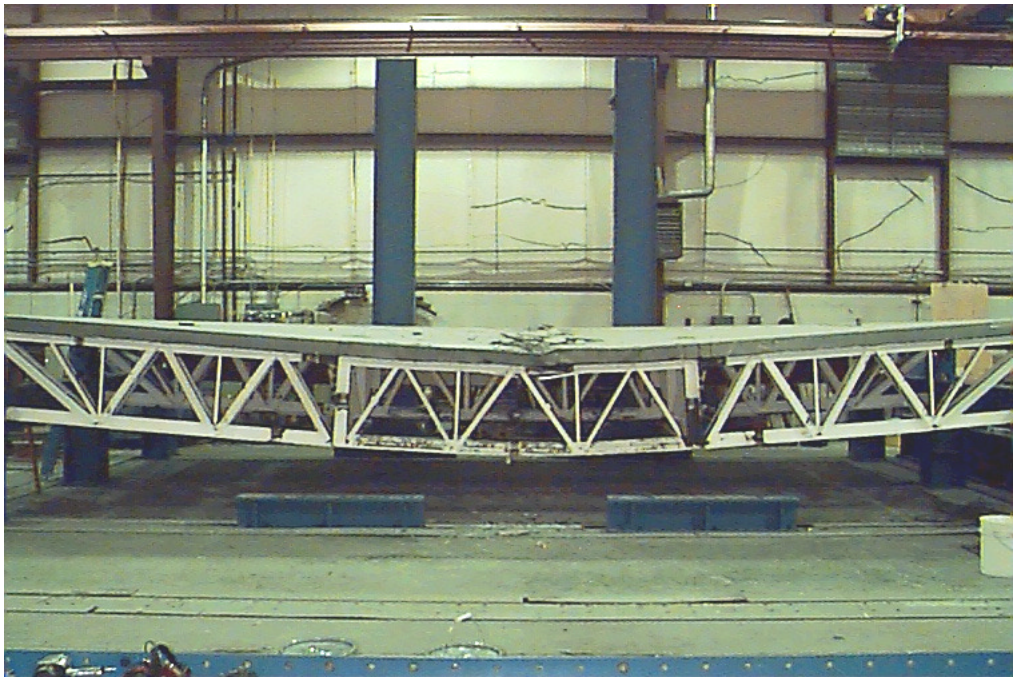

Figure 3.32 Final Deflected Shape Showing Bottom Chord Yielding and Crushing of the Concrete Slab (FF-2)

3.4 Haunch Joist girder Test (H-1)

Showalter (1999) also reported on the behavior of the haunch joist girder (H-1). The overall design of the joist girder was governed by midspan bottom chord yielding with a percentage of top chord contributing tensile forces.

3.4.1 Exterior Joist girder (EGL) (H-1)

The exterior joist girder (EGL) had an experimental ultimate load of 177 kips and the load vs. midspan deflection plot is illustrated in Figure 3.33. The yield strain for the bottom chord was 1907 microstrain, which was exceeded by measured strain readings indicating that the bottom chord had yielded as illustrated in Figure 3.34.

Measured end slip for this member is not included here due to problems with the data. The top chord strains illustrated in Figure 3.35 show strain reversal indicative of bottom chord yielding, however, the characteristic tensile to compressive strain reversal near the ultimate load is not present. Based on this, it can reasonably be concluded that the shear connection remained intact.

The joist girder failed by yielding of the bottom chord, beginning at the east third point, at a total load of 163.0 kips. Slab failures were not reported for EGL.

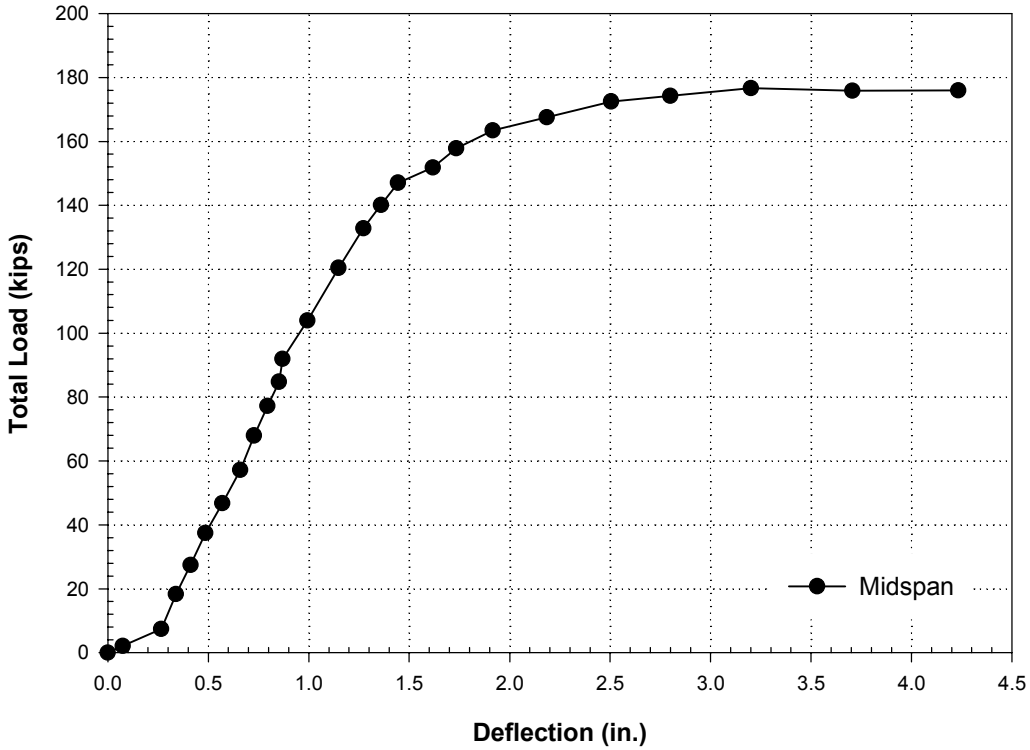

Figure 3.33 EGL Total Load vs. Midspan Deflection (H-1)

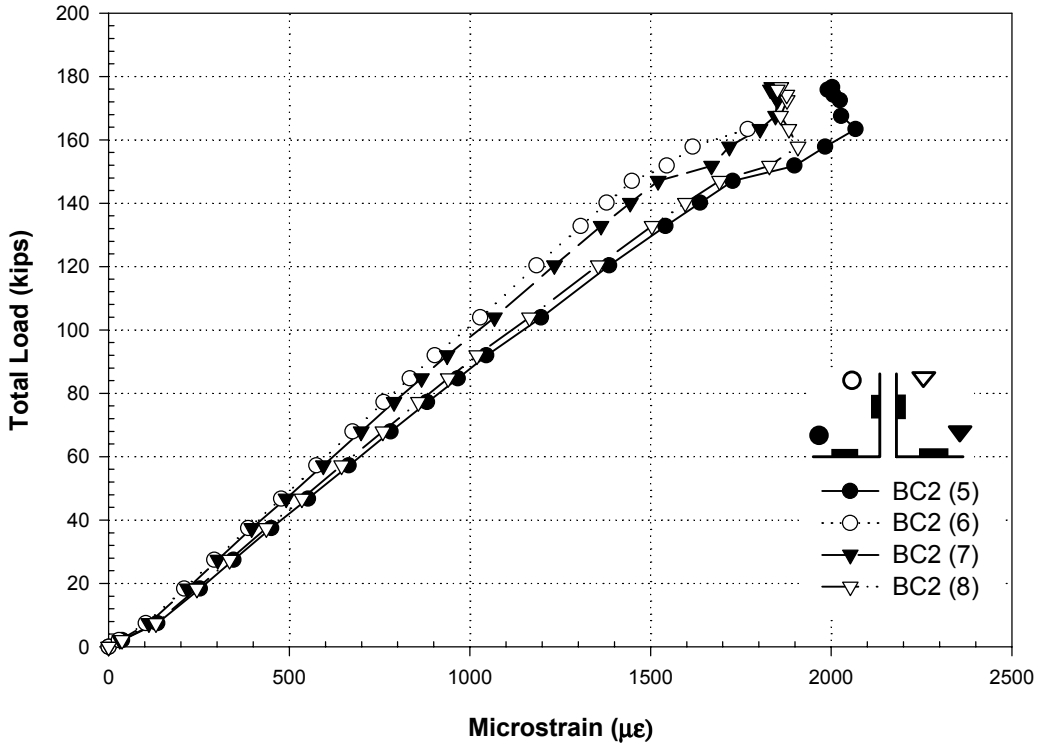

Figure 3.34 EGL Total Load vs. Midspan Bottom Chord Strain (H-1)

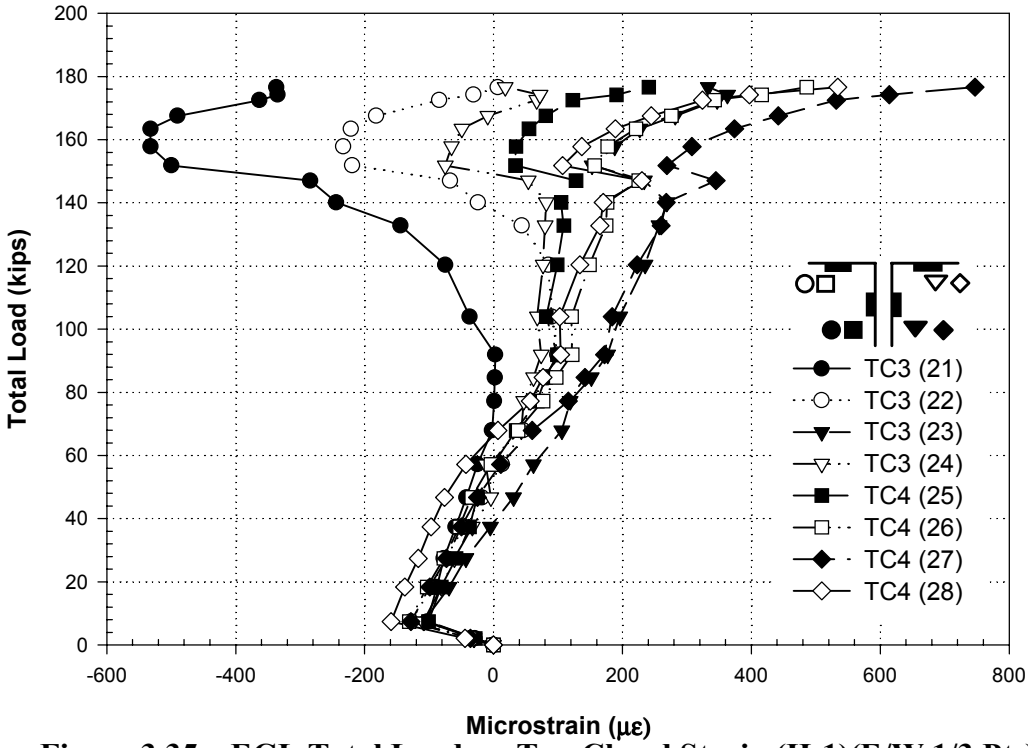

Figure 3.35 EGL Total Load vs. Top Chord Strain (H-1)(E/W 1/3 Pts)

3.4.2 Interior Joist girder (IG) (H-1)

The interior joist girder (IG) had an experimental ultimate load of 409 kips and the load vs. midspan deflection plot is illustrated in Figure 3.36. This girder also showed an increase in load above the plateau at a load of approximately 340 kips. This can be attributed to the top chord picking up a portion of the load as the bottom chord yielding progressed. The yield strain for the bottom chord was 1841 microstrain and the measured strain gage readings show that the average bottom chord strain was approximately at the yield strain.

Figure 3.38 shows that the end slip approached 0.30 in. near the end of testing. The load vs. end slip plot shows a gap in the data points that corresponds to an unloading and reloading of the joist girder at lower loads. These data points have been removed for clarity but the full plot can be seen in the project reports. Top chord strains illustrated in Figure 3.39 show the start of a strain reversal with the tendency towards tensile strains followed by a vertical rise in the plot corresponding to an increase in load without a corresponding increase in strain.

Overall failure of the interior joist girder was attributed to bottom chord yielding which began at the east third point at a total load of 404 kips.

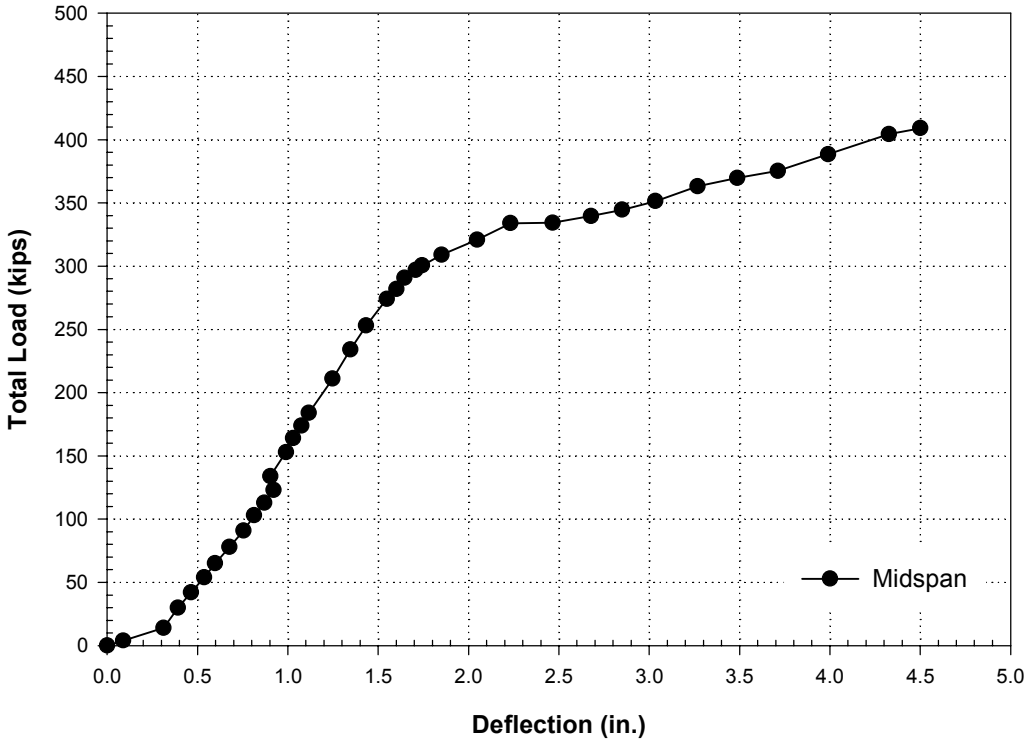

Figure 3.36 IG Total Load vs. Midspan Deflection (H-1)

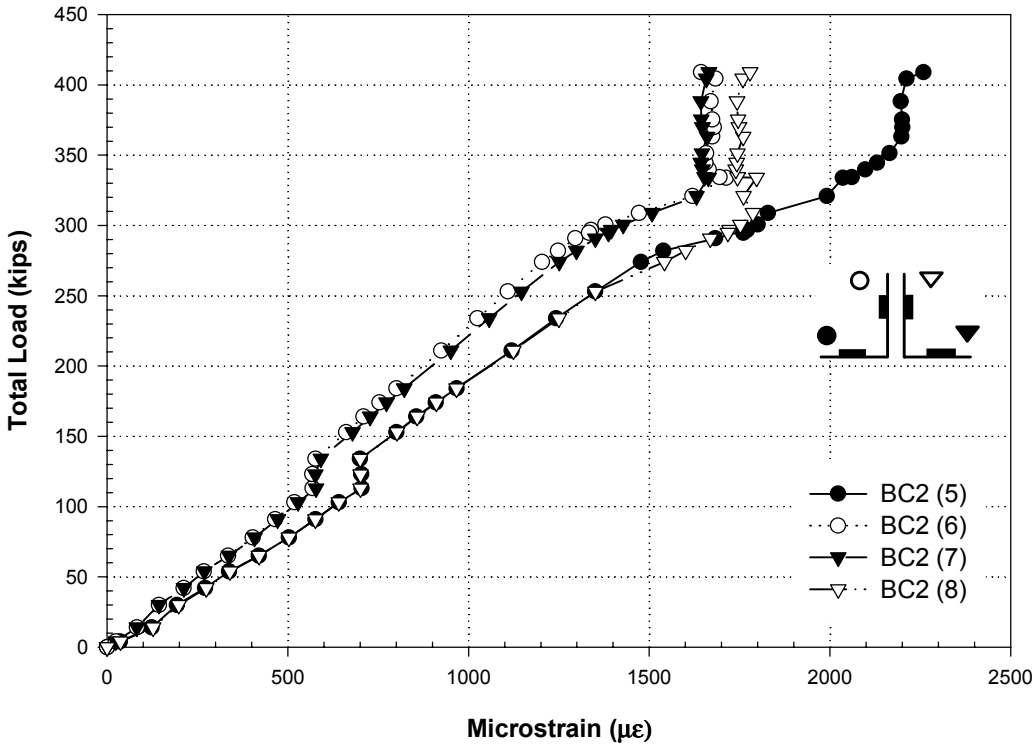

Figure 3.37 IG Total Load vs. Midspan Bottom Chord Strain (H-1)

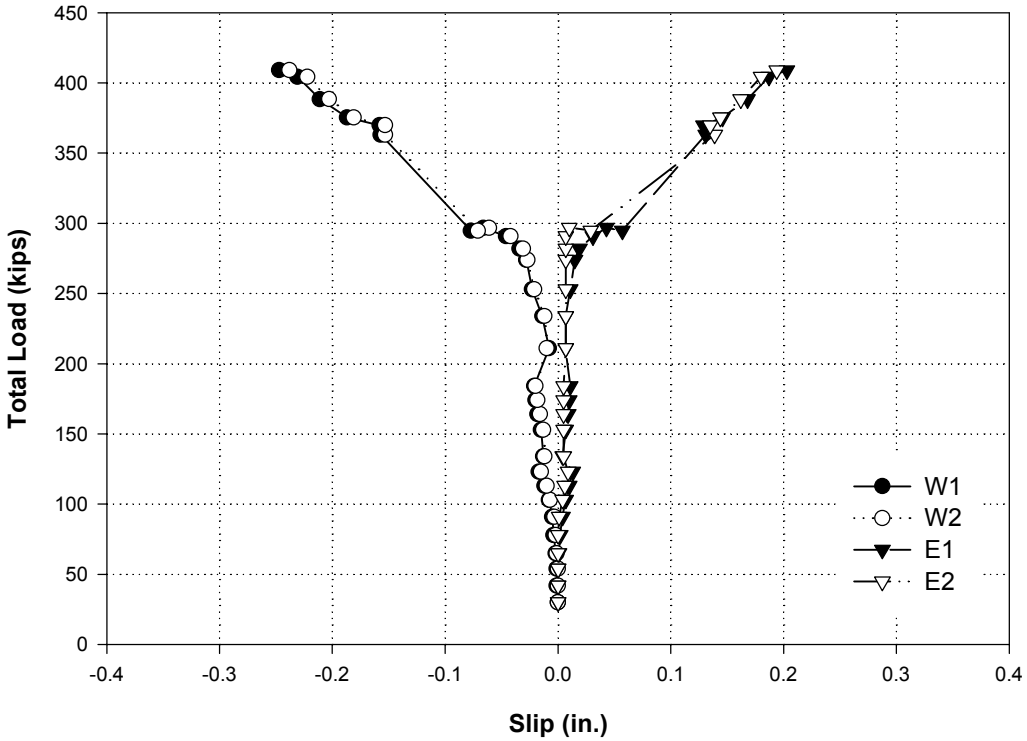

Figure 3.38 IG Total Load vs. Slip (H-1)

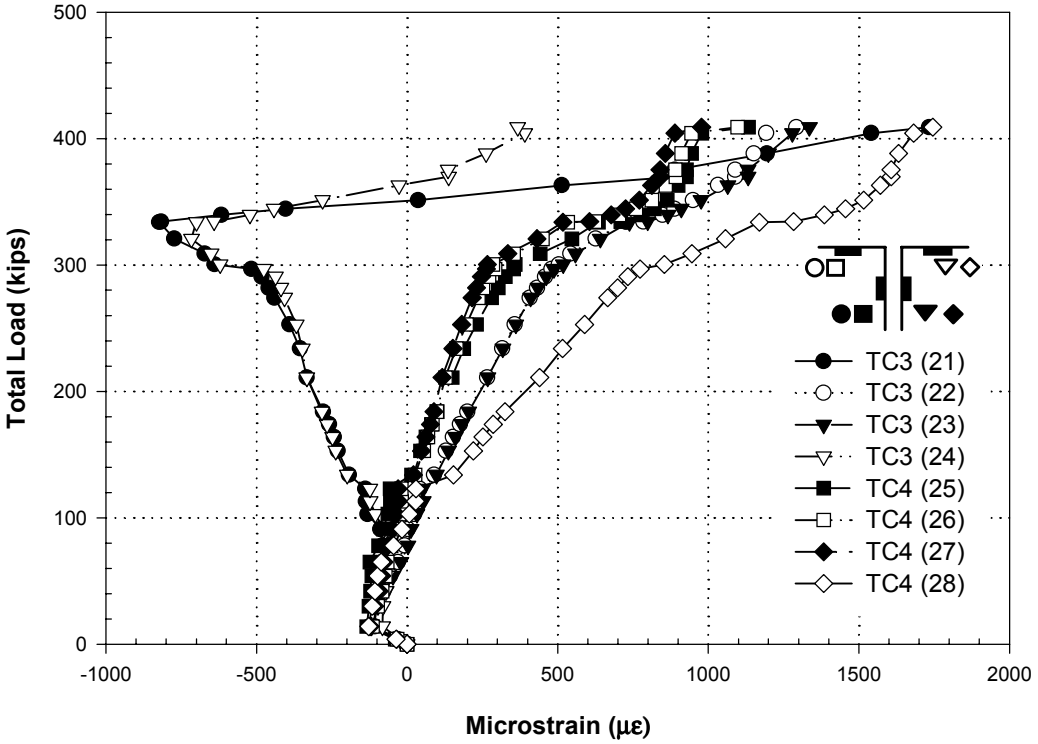

Figure 3.39 IG Total Load vs. Top Chord Strain (H-1)(E/W 1/3 Pts)

3.4.3 Exterior H-Shape (EB) (H-1)

The H-shape (EB) had an experimental ultimate load of 137 kips as indicated by the load vs. midspan deflection plot illustrated in Figure 3.40. No distinct plateau can be seen on the load vs. deflection plot while the load vs. midspan bottom flange strain illustrated in Figure 3.41 shows measured strains in excess of the yield strain of 1658 microstrain. The top flange strains and web strains were below the yield strain as illustrated by Figures 3.41 and 3.42. Problems existed with the H-shape as indicated by the early non-linear behavior of the load vs. deflection plot and the premature failure of the section.

Figure 3.43 shows minimal slip on the order of 0.05 in. at the west end and up to 0.15 in. on the east end indicating that the welded shear studs remained intact. The load vs. top flange strain plot illustrated in Figure 3.41 also verifies that the shear connection was maintained because it does not show any strain reversals. The plot did show the possible beginning of strain reversal, but it could be characterized as the very beginning of shear connection failure.

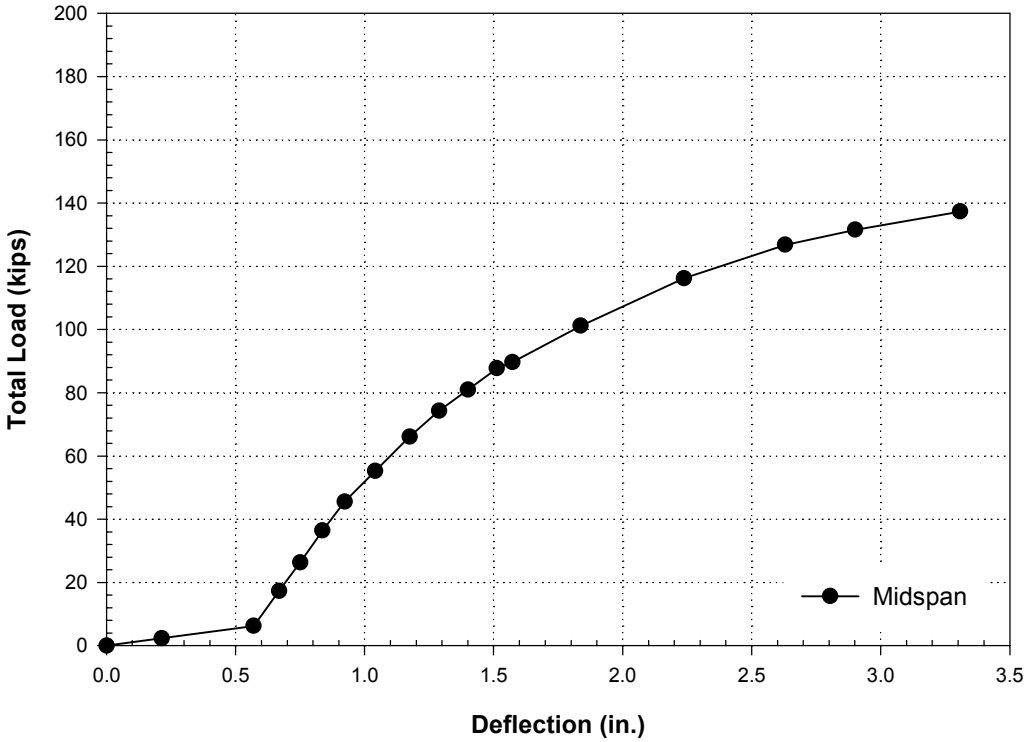

Figure 3.40 EB Total Load vs. Midspan Deflection (H-1)

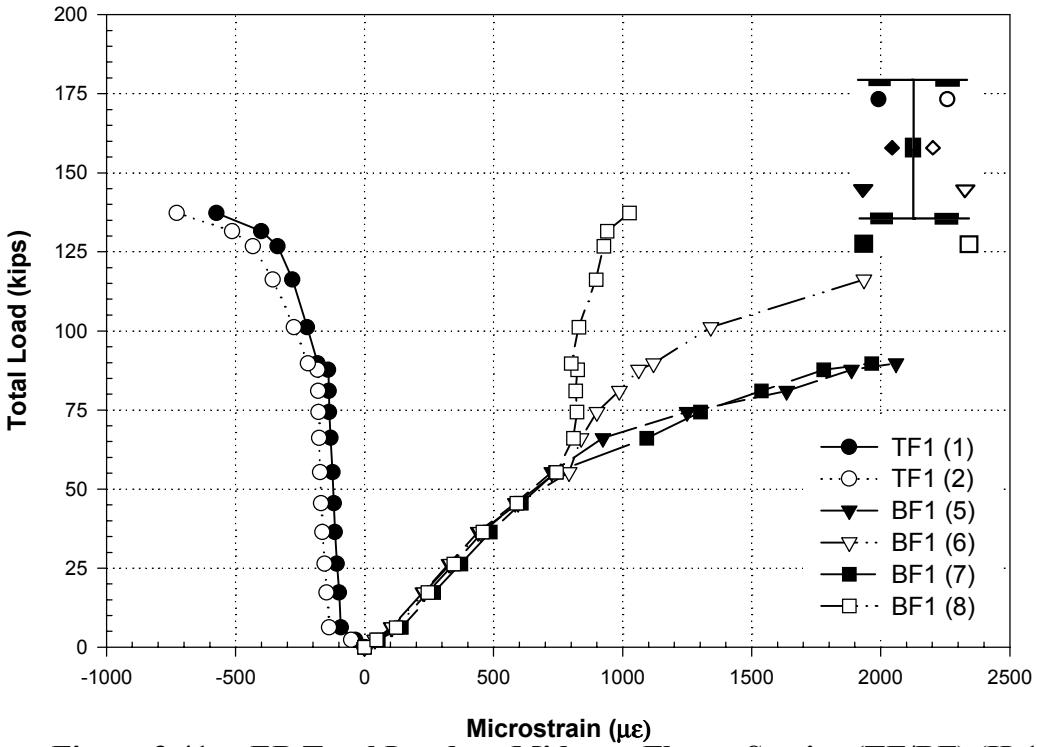

Figure 3.41 EB Total Load vs. Midspan Flange Strains (TF/BF) (H-1)

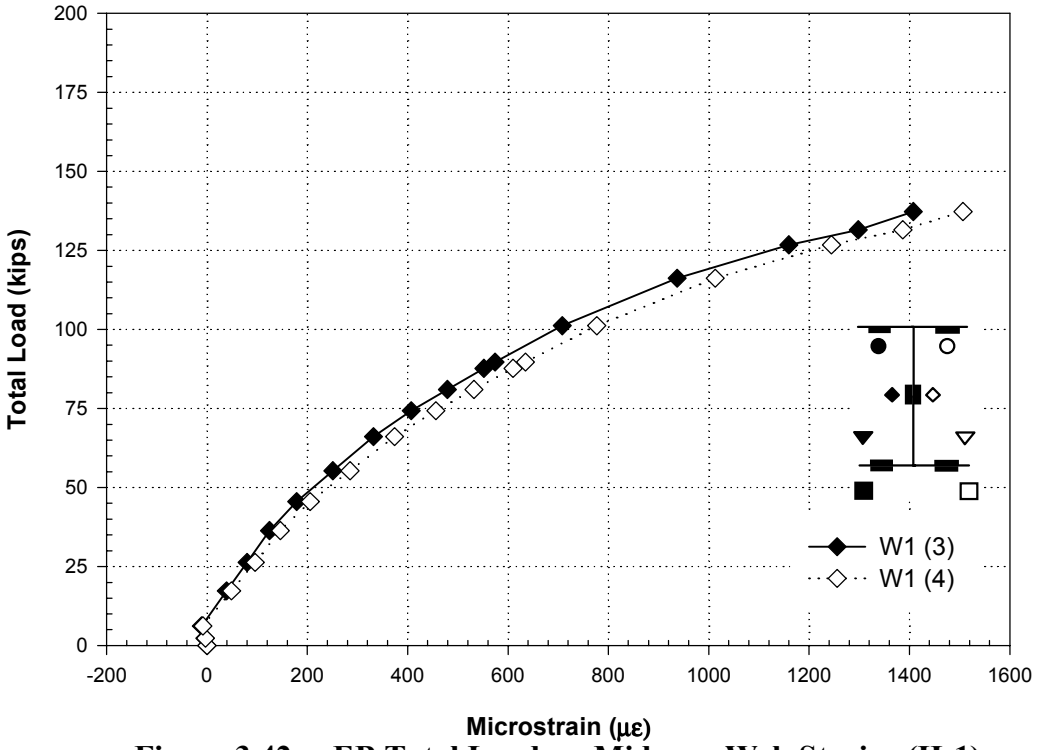

Figure 3.42 EB Total Load vs. Midspan Web Strains (H-1)

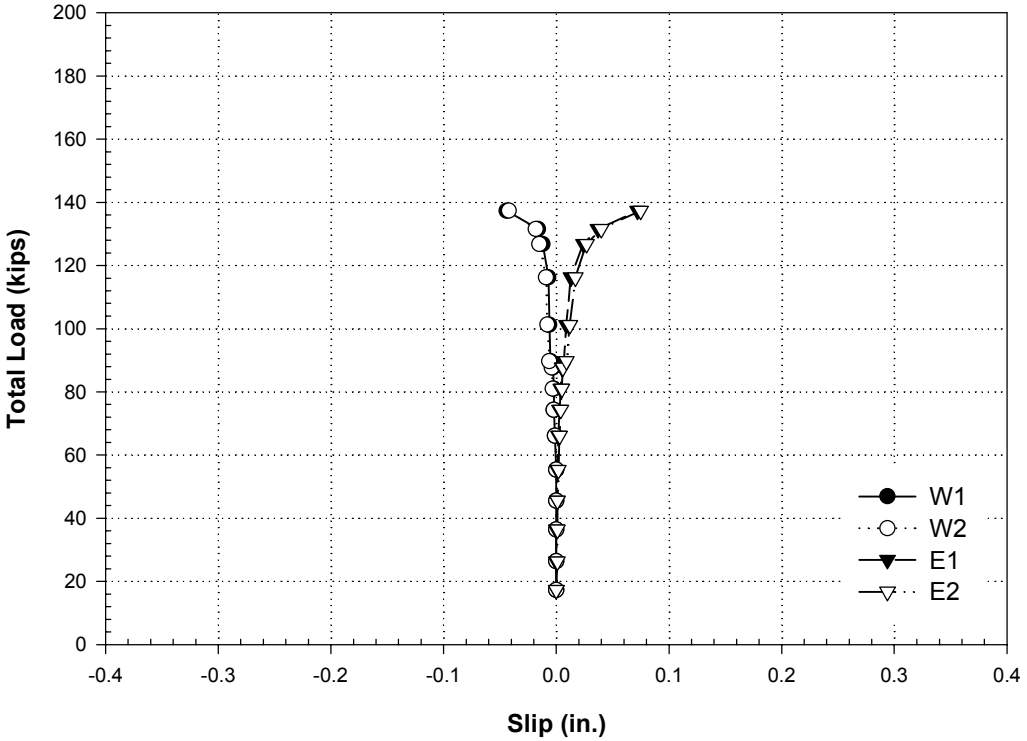

Figure 3.43 EB Total Load vs. Slip (H-1)

3.5 Haunch Joist girder Test (H-2)

3.5.1 Exterior Joist girder (EG) (H-2)

The exterior joist girder (EG) had an experimental ultimate load of 189 kips and the load vs. midspan deflection plot is illustrated in Figure 3.44. The yield strain for the bottom chord was 2096 microstrain, which was greater than the measured bottom chord strains, which indicates that yielding had not occurred. Flaking of whitewash between third points did indicate bottom chord yielding so it is likely that some error is present in either the measured bottom chord strains or the calculated yield strain.

Figure 3.46 shows that the end slip reached approximately 0.10 to 0.12 in., which indicates that the welded shear studs did not fail at ultimate load. This is verified by the load vs. top chord strain illustrated in Figure 3.47, which shows no significant strain reversal from tension to compression.

The joist girder failed by bottom chord yielding and longitudinal splitting in the slab. Loading was terminated at a load of 186 kips at which point no more load was being carried.

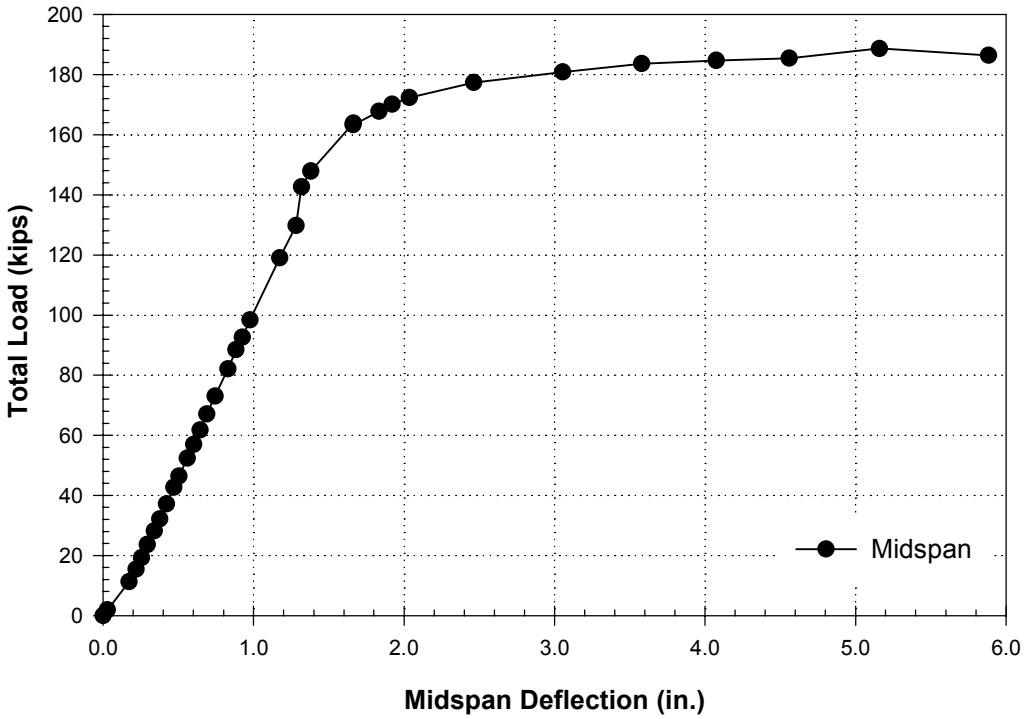

Figure 3.44 EG Total Load vs. Midspan Deflection (H-2)

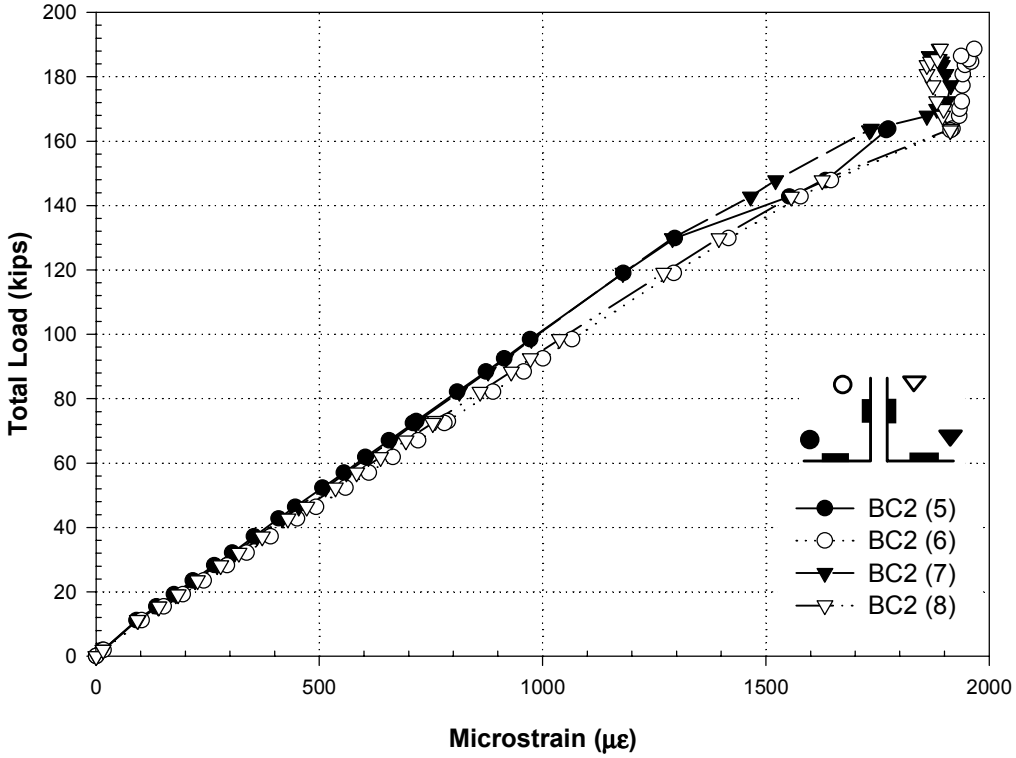

Figure 3.45 EG Total Load vs Bottom Chord Strain (H-2)

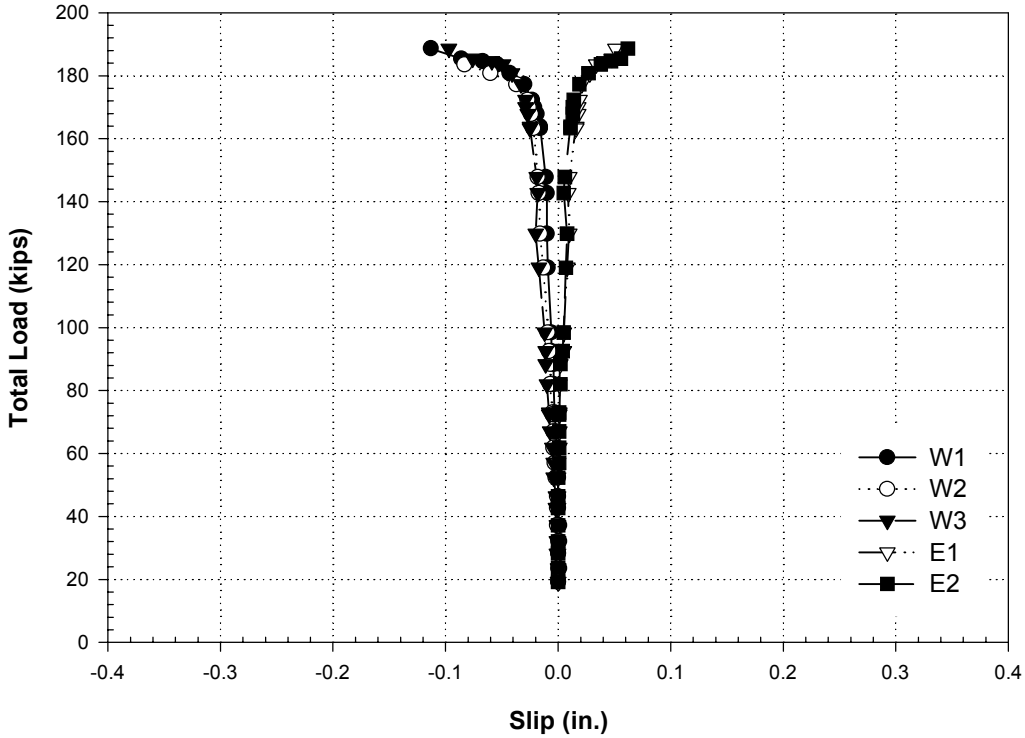

Figure 3.46 EG Total Load vs. Slip (H-2)

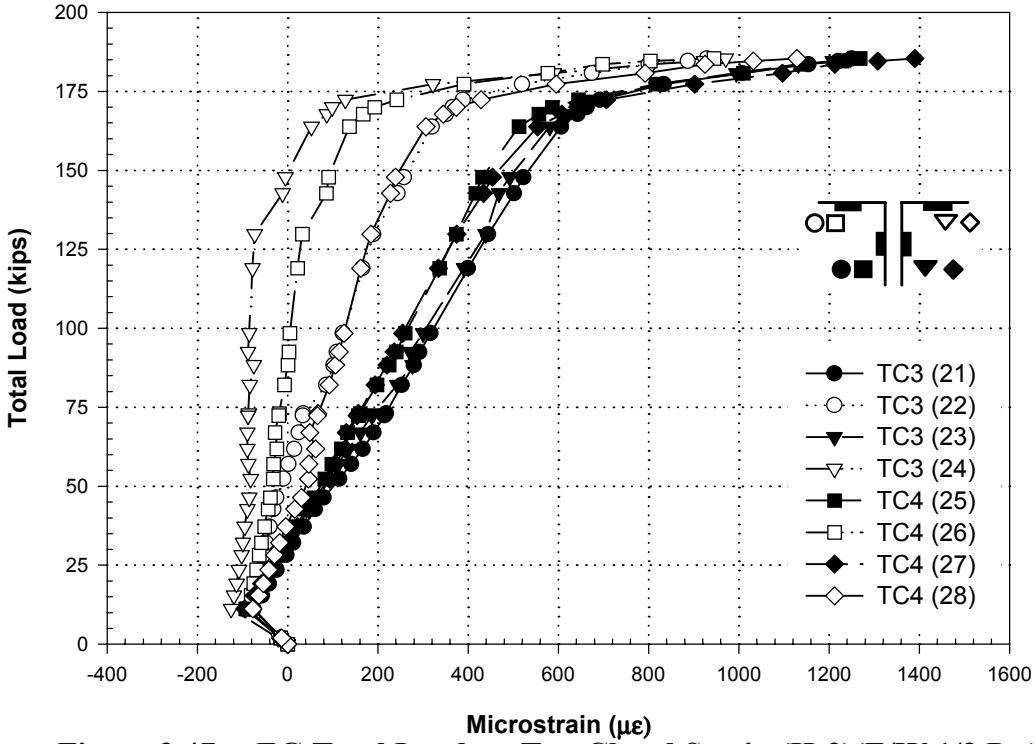

Figure 3.47 EG Total Load vs. Top Chord Strain (H-2)(E/W 1/3 Pts)

3.5.2 Interior Joist girder (IG) (H-2)

The interior joist girder (IG) had an experimental ultimate load of 364 kips and the load vs. midspan deflection plot is illustrated in Figure 3.48. The yield strain for the bottom chord was 1886 microstrain, which was slightly higher than the measured strain. Whitewash flaking was also observed at ultimate load. It can be seen in Figure 3.51 that the top chord strain began to increase rapidly at a load of approximately 325 kips. This corresponds to a slight increase in load above the plateau on the load vs. deflection plot indicating that the top chord was picking up some load.

Figure 3.50 shows that the end slip reached approximately 0.25 to 0.3 in., which indicates that the welded shear studs were approaching failure at ultimate load. This is verified by the load vs. top chord strain illustrated in Figure 3.51, which shows a significant strain reversal at a total load of 350 kips.

The joist girder failed by bottom chord yielding, loss of shear connection and longitudinal splitting. Loading was terminated at 306 kips, at which point no more load was being carried.

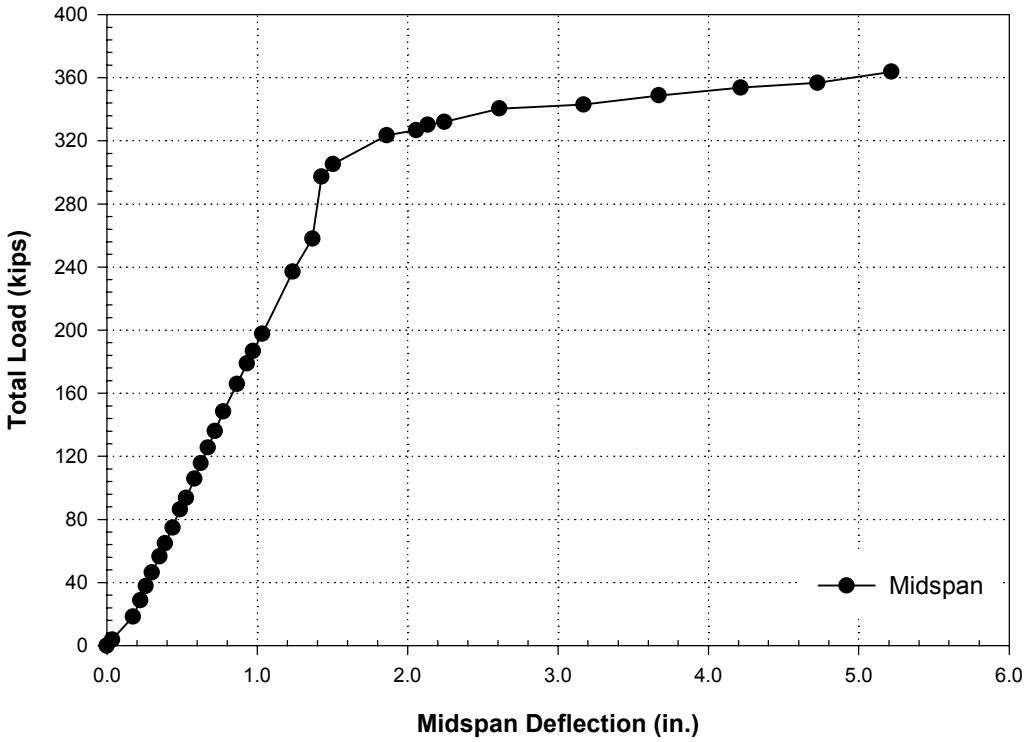

Figure 3.48 IG Total Load vs. Midspan Deflection (H-2)

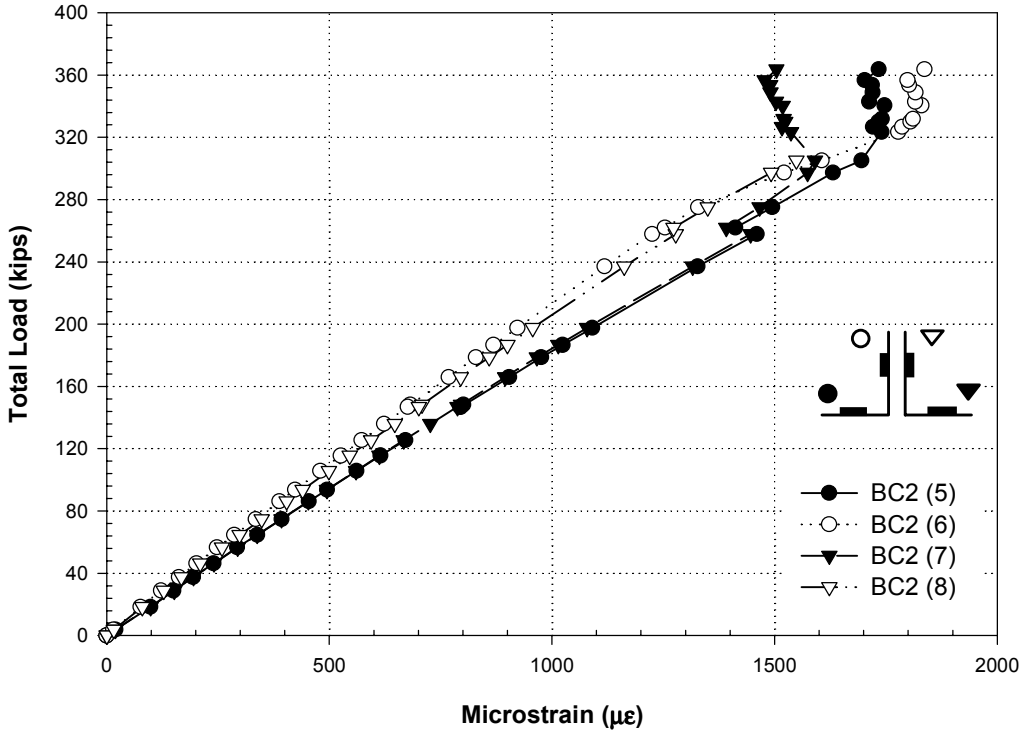

Figure 3.49 IG Total Load vs Midspan Bottom Chord Strain (H-2)

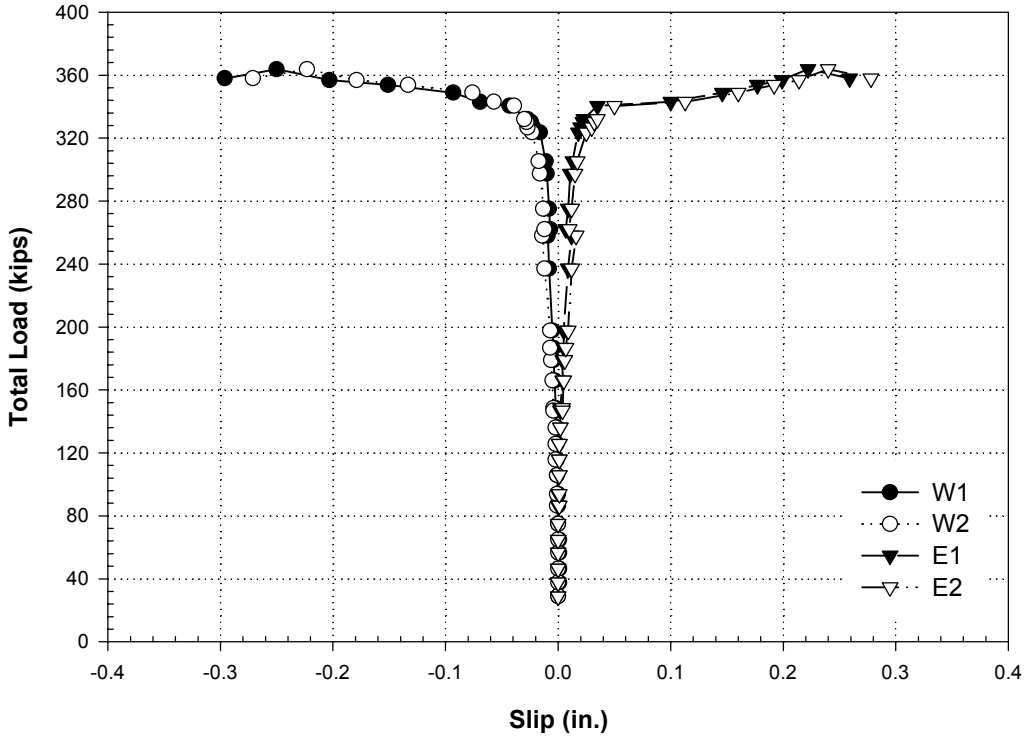

Figure 3.50 IG Total Load vs. Slip (H-2)

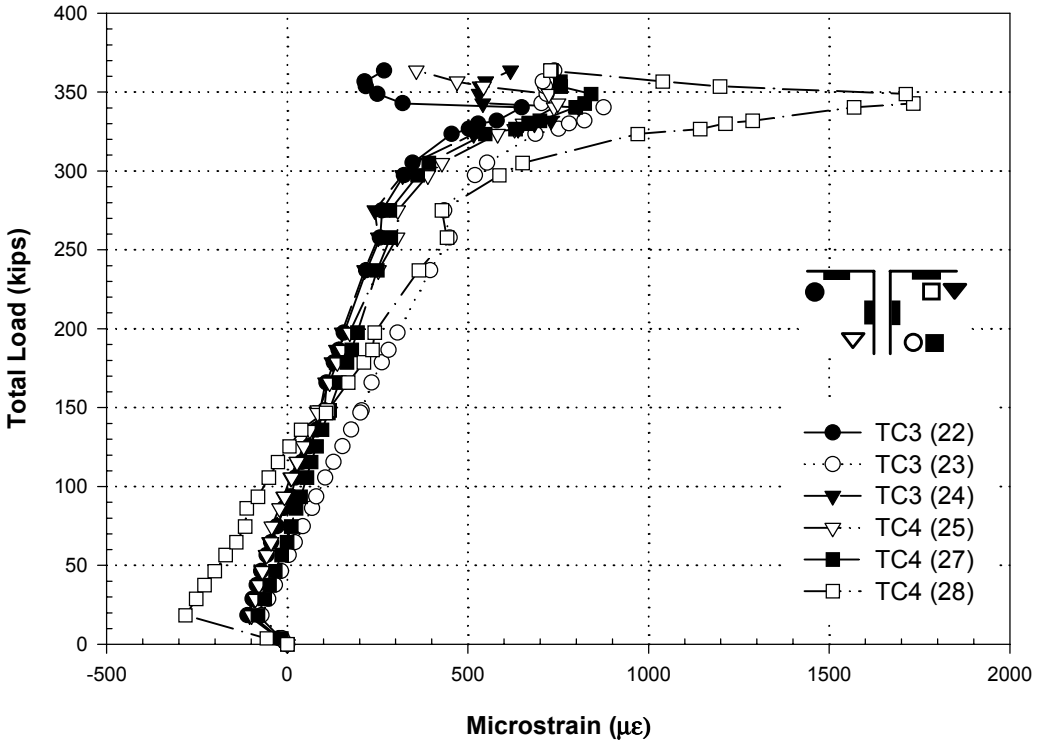

Figure 3.51 IG Total Load vs. Top Chord Strain (H-2)(E/W 1/3 Pts)

3.5.3 Exterior Girder (EB) (H-2)

The H-shape (EB) had an experimental ultimate load of 229 kips and the load vs. midspan deflection plot is illustrated in Figure 3.52. A distinct plateau can be seen on the load vs. deflection plot, while the load vs. bottom flange strain plot illustrated in Figure 3.53 shows strain values at ultimate load well beyond first yield. The yield strain for the bottom chord was 2372 microstrain, which verifies yielding had occurred. Additionally, flaking of whitewash on the bottom flange and web also occurred.

Figure 3.55 shows that the end slip reached approximately 0.1 to 0.2 in. which indicates that the welded shear studs did not fail at ultimate load. The load vs. top flange strain illustrated in Figure 3.53, which did not show any strain reversal, verifies this.

The H-shape failed by bottom flange yielding and longitudinal splitting in the concrete. Loading was terminated at a total load of 229 kips, at which point no more load was being carried. It should be noted, that strain gage measurements are absent for a total load above 130 kips.

It is important to note that problems occurred with the instrumentation and the data acquisition systems that didn't allow accurate measurements to be recorded beyond what is shown in the plots

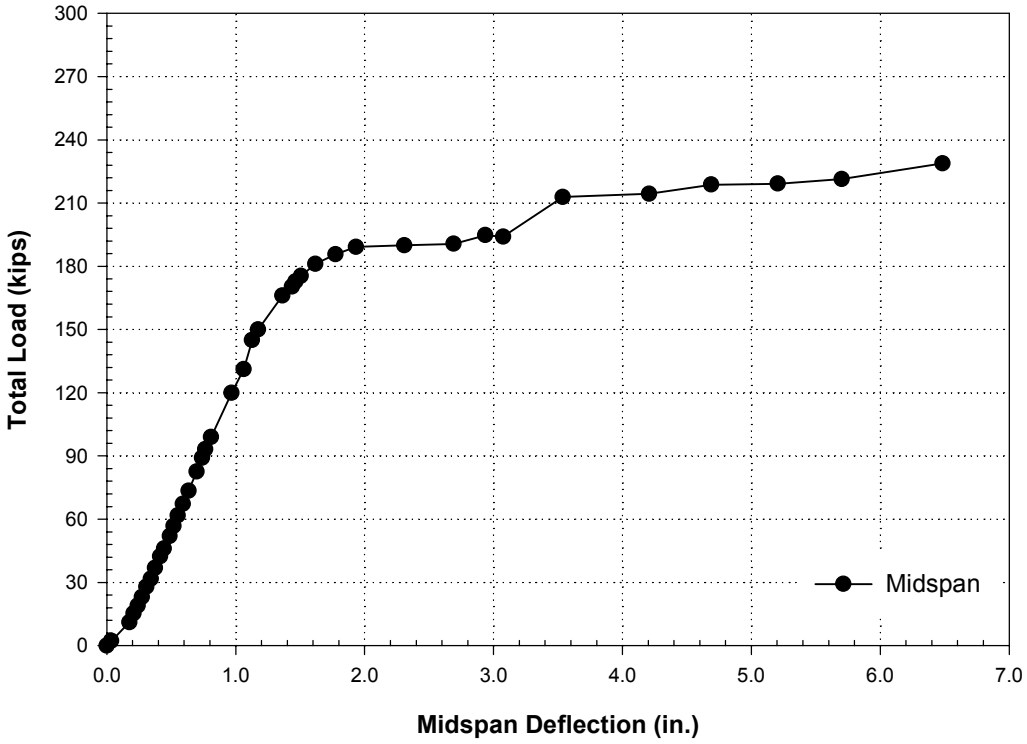

Figure 3.52 EB Total Load vs. Midspan Deflection (H-2)

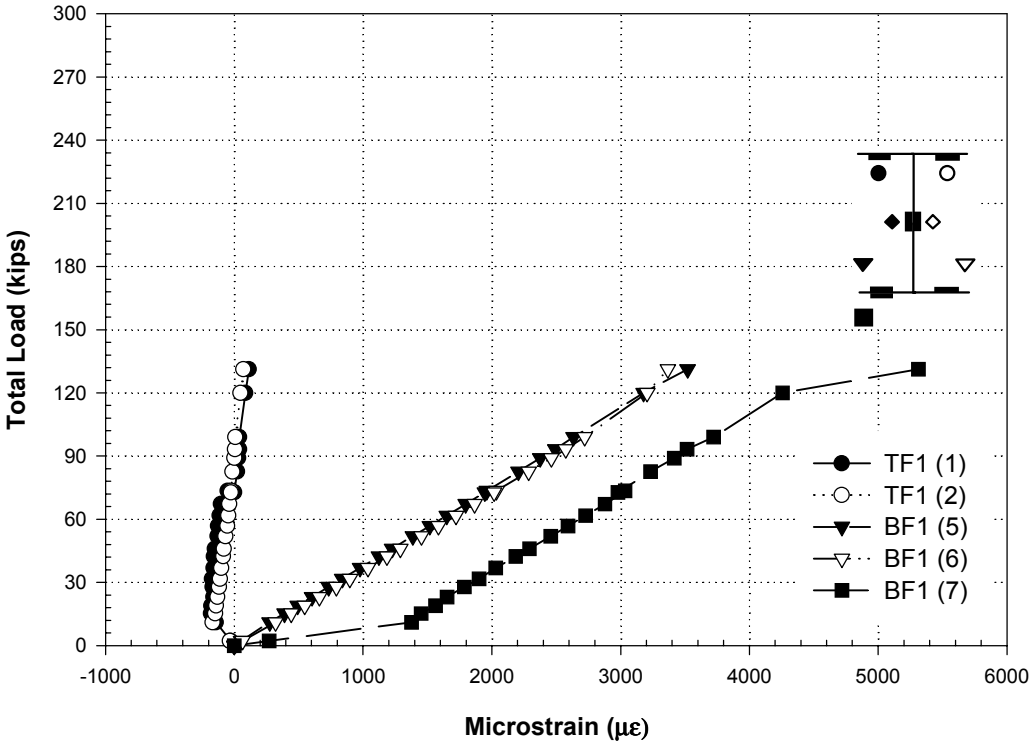

Figure 3.53 EB Total Load vs. Midspan Flange Strains (H-2)

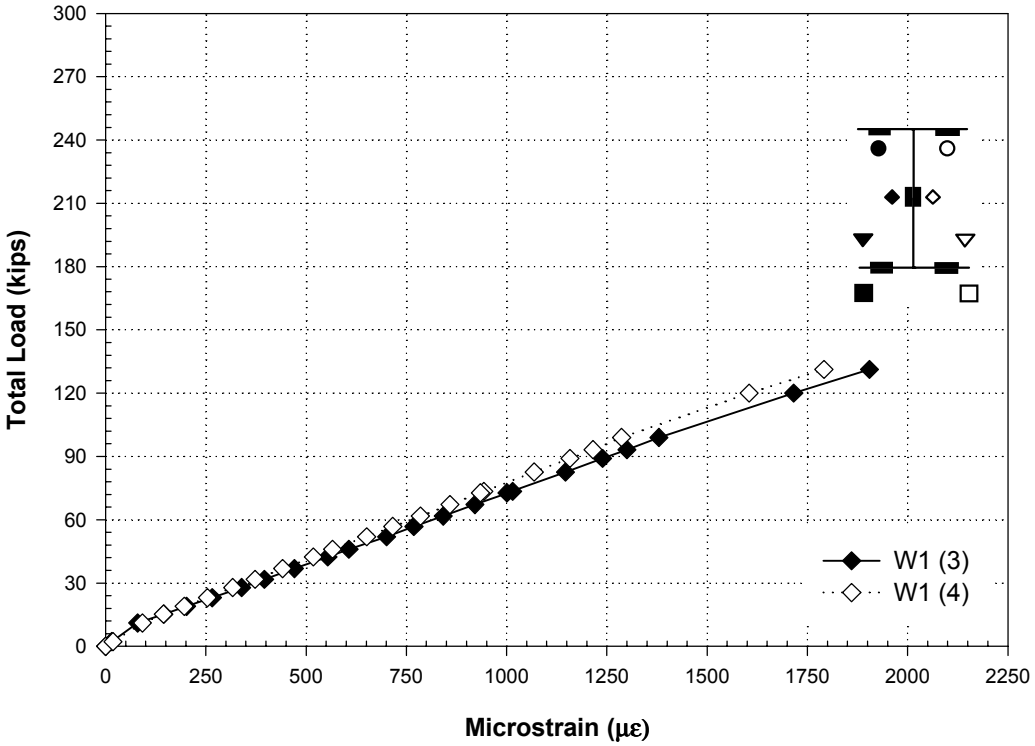

Figure 3.54 EB Total Load vs. Midspan Web Strains (H-2)

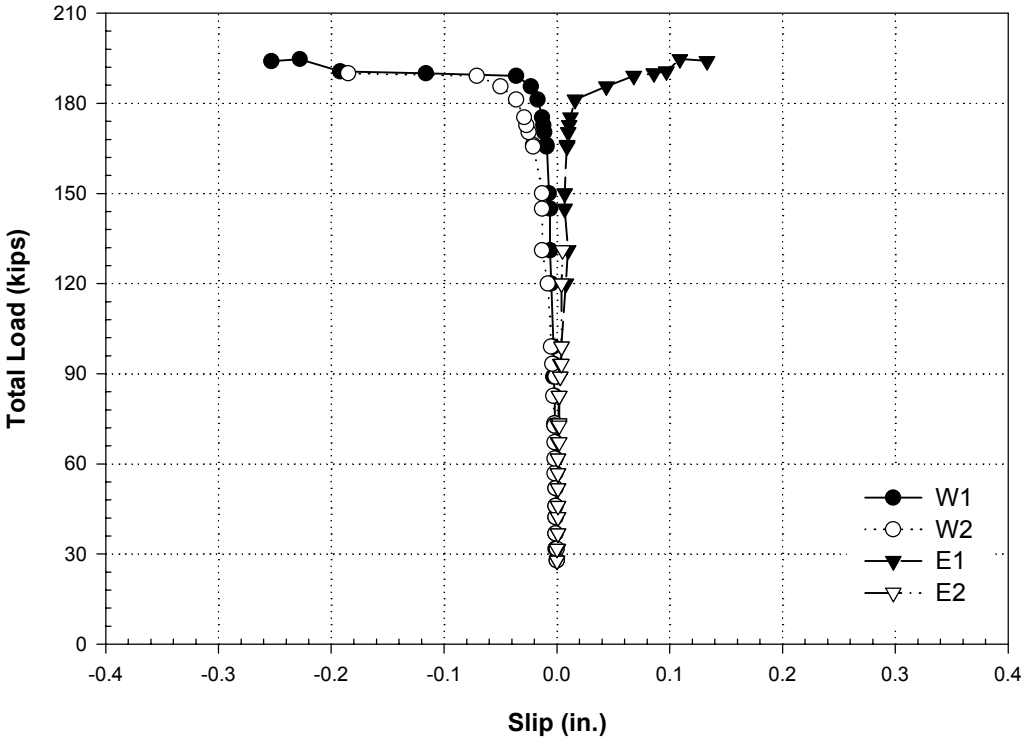

Figure 3.55 EB Total Load vs. Slip (H-2)

3.6 Slab Cracking

Cracking of the concrete slab occurred in all of the tests to varying degrees. Herringbone cracks formed first as a result of shear deformation. In general, the range of loading for the formation of these cracks was between the design load (P_{dn}^{exp}) and the experimental ultimate load (P_u^{exp}) with the exception of IG from FF-1 which had a crack form at a total load of 30 kips.

Some degree of longitudinal splitting occurred in the slab over all of the members in test H-2 and over the exterior H-shape in test H-1, which indicates that insufficient reinforcement was available to prevent this type of cracking. The exterior H-shape for FF-2 showed no longitudinal cracking during the full test range, and it also showed no herringbone cracks characteristic of shear deformation as illustrated in Figures 3.56 and 3.60. One crack did originate from the northwest corner but it only propagated about 2 ft at about a 30-degree angle to the north slab edge as illustrated in Figure 3.56. The floor system (FF-2) did show two longitudinal cracks at the west end but they were midway between the interior joist girder and the slab edges. This is not indicative of a splitting failure, as it occurred away from the critical shear plane near the edge of the effective width, where the total shear is minimal.

The subsequent figures illustrate the degree and type of slab cracking that occurred in tests FF-2 and H-2. Observations relating to cracking for FF-1 and H-1 can be found in the project reports by Kigudde et al. (1996) and in Showalter (1999).

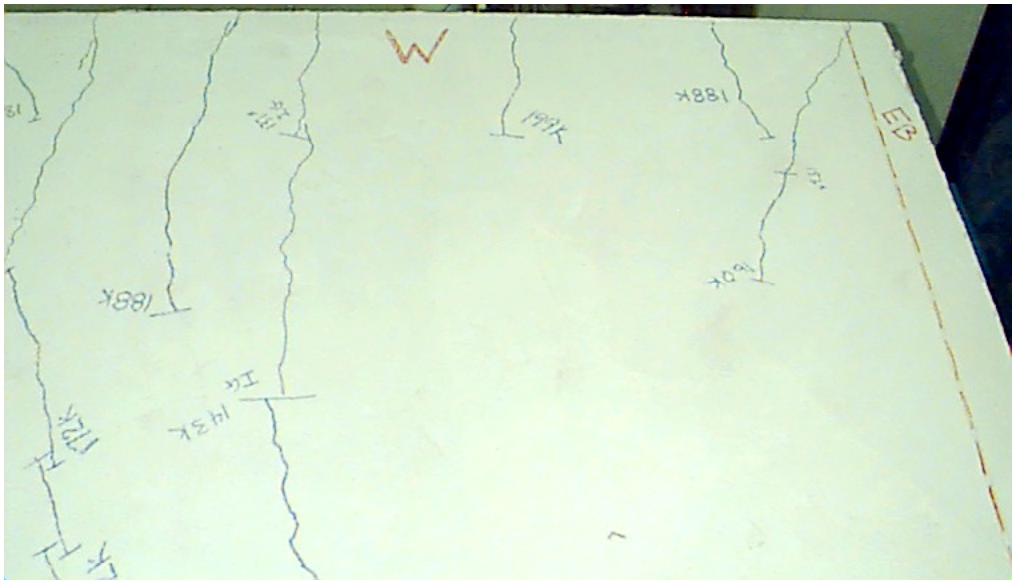

Figure 3.56 West End Slab Cracking Over EB (FF-2)

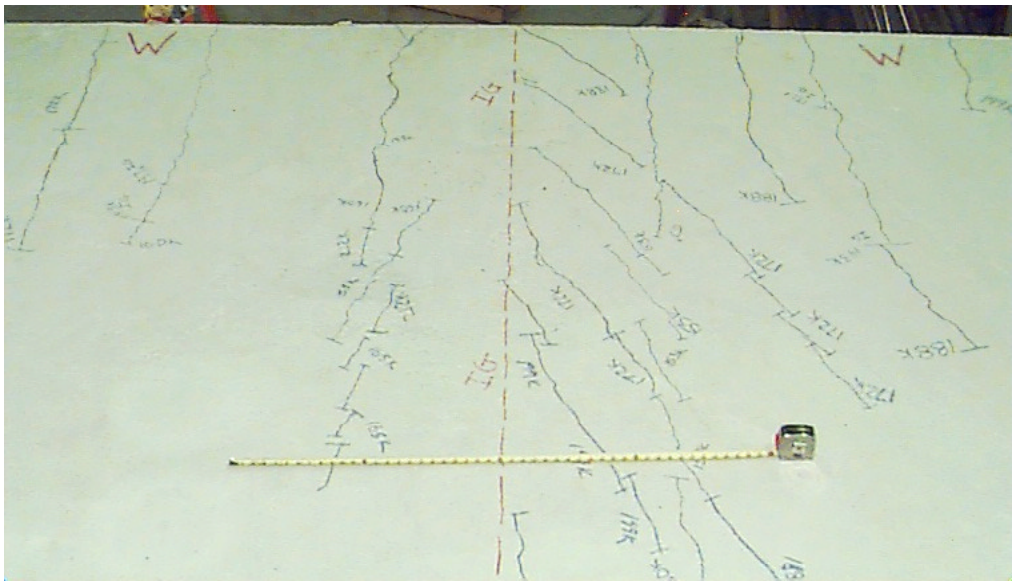

Figure 3.57 West End Slab Cracking Over IG (FF-2)

Figure 3.56 illustrates longitudinal shear cracks occuring between the girders which is not at the location of the critical shear plane near the girder. Note the two cracks over EB which were the only ones to form. Figure 3.57 illustrates both herringbone cracks oriented 45 degrees to the girder centerline and longitudinal shear cracks beginning to form at the end of the span.

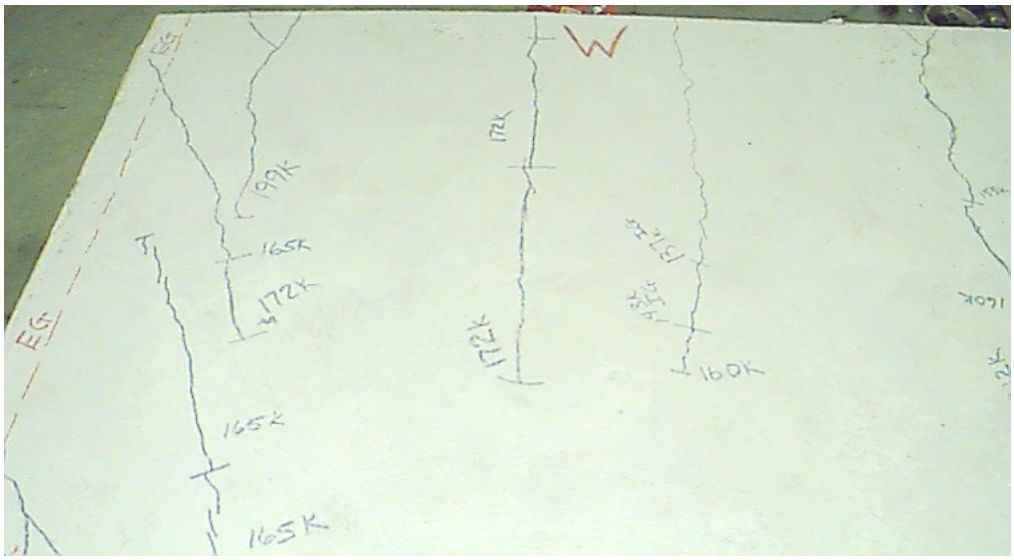

Figure 3.58 West End Slab Cracking Over EG (FF-2)

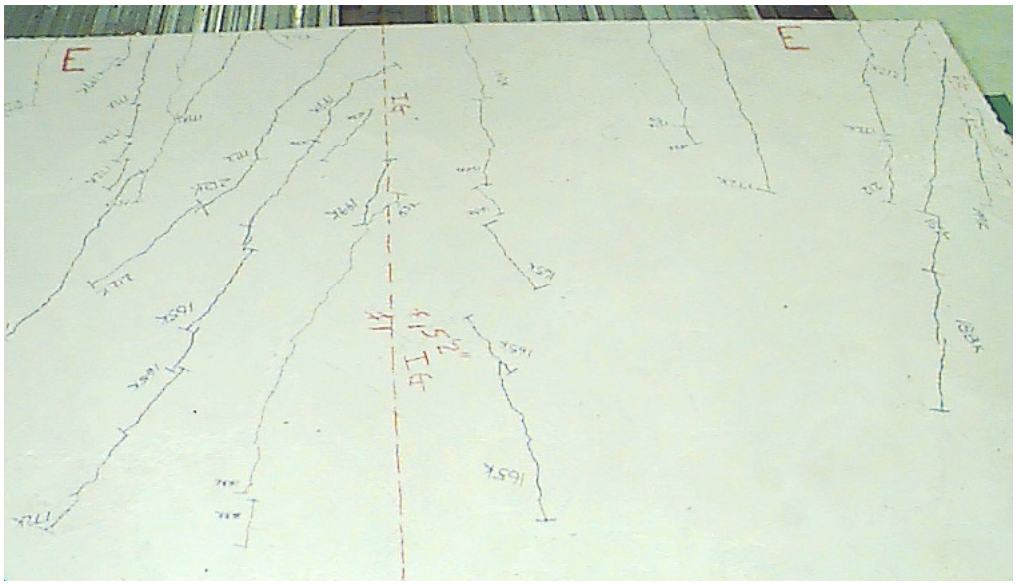

Figure 3.59 East End Slab Cracking Over EG/IG (FF-2)

Figure 3.58 also illustrates longitudinal shear cracks occurring between the girders and over EG. Herringbone cracks can also be seen. Figure 3.59 illustrates both herringbone cracks oriented 45 degrees to the girder centerline and longitudinal shear cracks beginning to form at the end of the span to the right (or south) of the girder centerline.

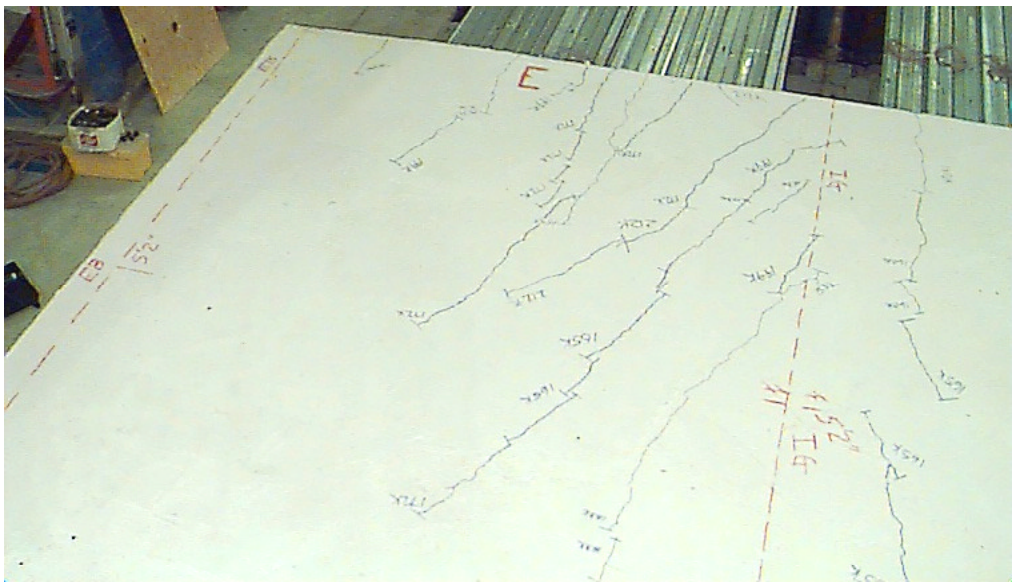

Figure 3.60 East End Slab Cracking Over IG/EB (FF-2)

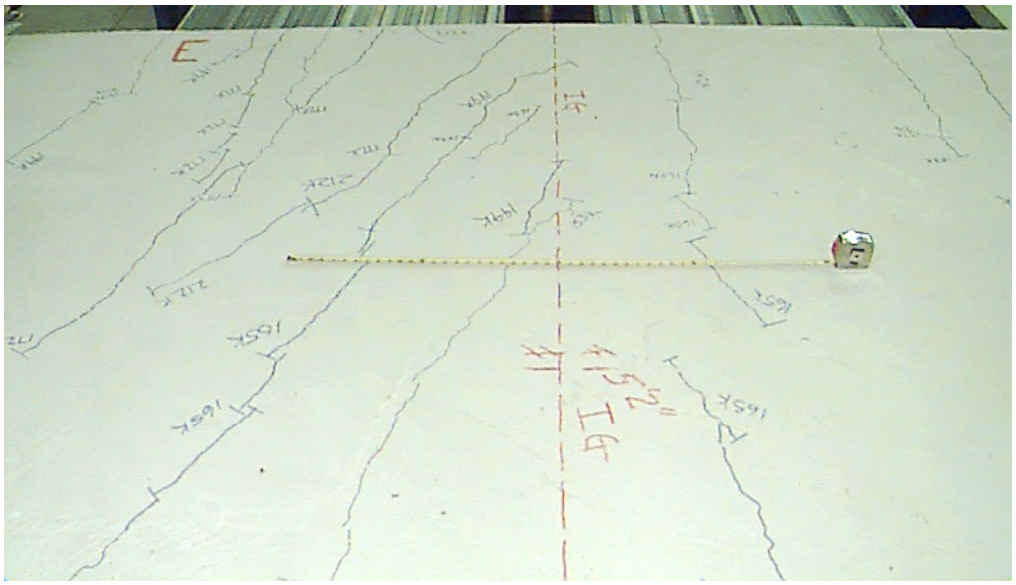

Figure 3.61 East End Slab Cracking Over IG (FF-2)

Figure 3.60 also illustrates longitudinal shear cracks over IG. Herringbone cracks can also be seen. As at the west end, cracks are absent over EB. Figure 3.61 illustrates both herringbone cracks oriented 45 degrees to the girder centerline and longitudinal shear cracks beginning to form at the end of the span to the right (or south) of the girder centerline.

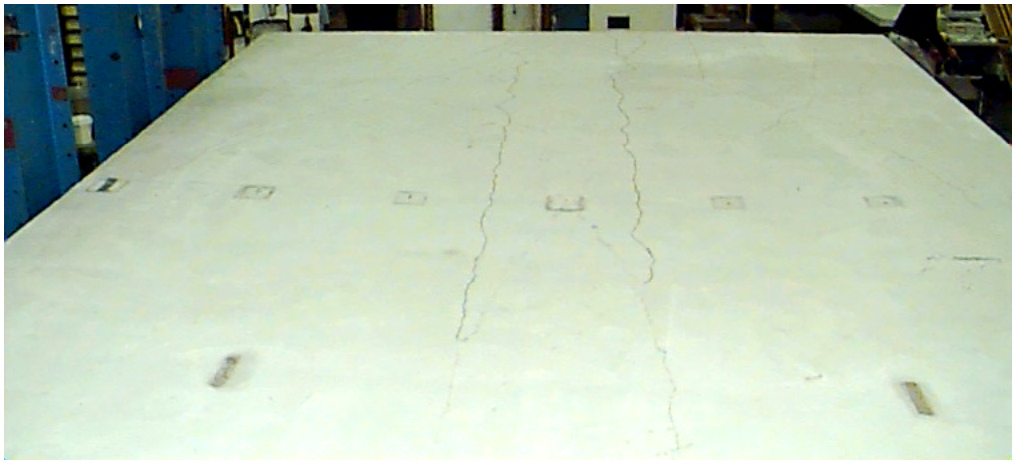

Figure 3.62 East End Slab Cracking Over IG (H-2)

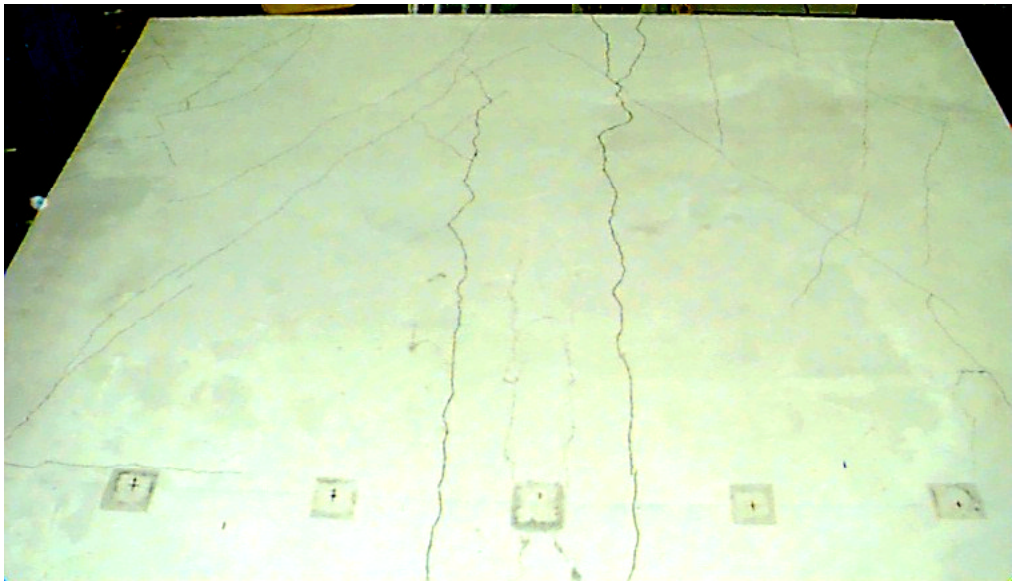

Figure 3.63 East End Slab Cracking (H-2)

Figure 3.62 also illustrates longitudinal shear cracks occurring over IG over the length of the shear span. Figure 3.63 illustrates both herringbone cracks oriented 45 degrees to the girder centerline beginning at the end of the slab and progressing toward the exterior girders and longitudinal shear cracks parallet to the interior girder centerline.

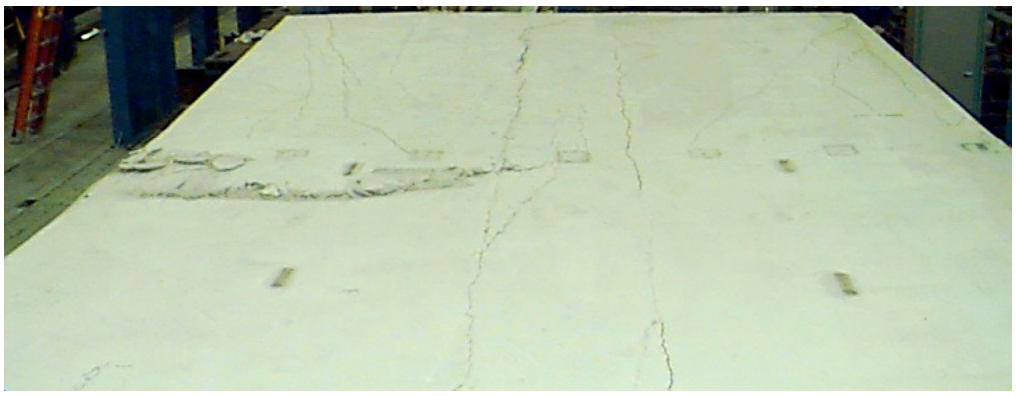

Figure 3.64 West End Slab Cracking (H-2)

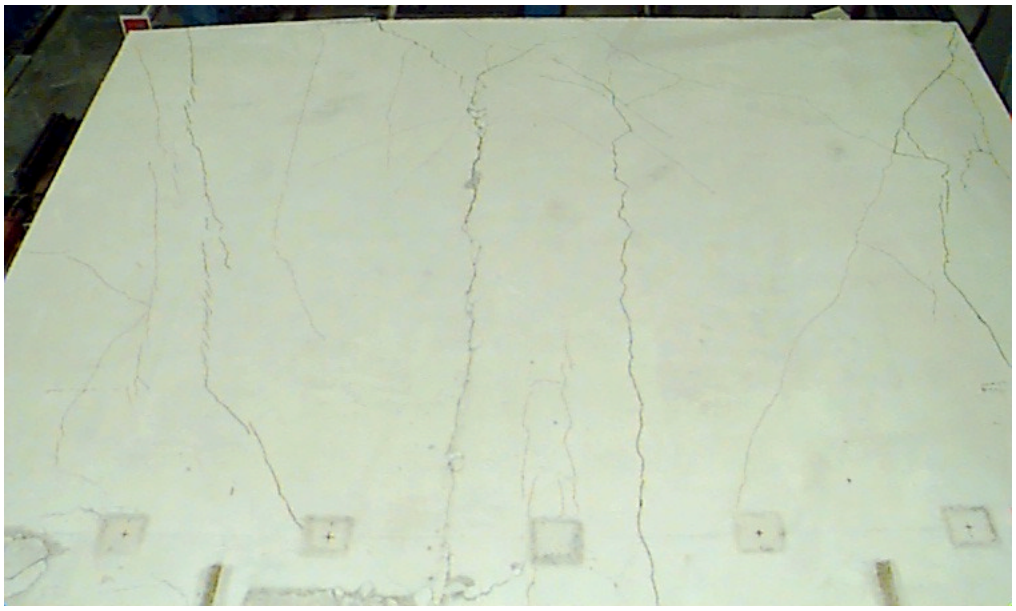

Figure 3.65 West End Slab Cracking (H-2)

Figure 3.64 illustrates longitudinal shear cracks occurring in the entire shear span over EG. Figure 3.65 illustrates both herringbone cracks oriented 45 degrees to the girder centerline and longitudinal shear cracks. It appears that a combination of longitudinal cracks and herringbone cracks also formed as the angle of two of the cracks over the exterior girders are at an angle less than 45 degrees to the girder centerline.

CHAPTER 4
ANALYTICAL METHODS AND DISCUSSION

4.1 General

The benchmark for whether a structural system is adequate for an application is based primarily on the ultimate strength of the system in relation to an applied load or moment. The associated design procedures must therefore adequately account for the ultimate strength in order to represent the behavior of the structural system. In this study, the main strength parameter considered was the ultimate moment that an individual composite member can sustain. The experimental ultimate flexural strength was determined at midspan using principles of statics as illustrated in Figure 4.1.

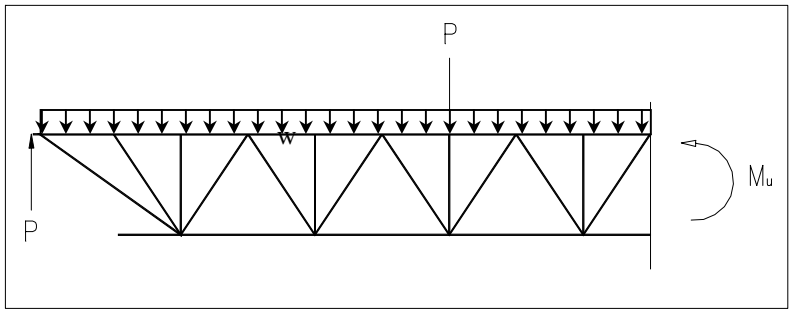

Figure 4.1 Applied Loads

The theoretical and experimental effective moment of inertia was also determined and is presented as a means of fully defining the behavior of these structural systems. Results and discussion for moment of inertia of each girder are presented in Appendix C.

The calculated ultimate moment based on actual material properties was determined from the measured yield stress of the steel elements and the measured compressive strength of the concrete slab by way of cylinder tests. This moment is calculated based on force equilibrium within each of the structural elements contributing to overall bending strength and is set forth in the proposed ASCE specification and commentary on composite joists (Task Committee, 1996). The strength calculations assumes that the bottom chord has fully yielded. The nominal ultimate moment for these tests was calculated based on the nominal material properties of F_y = 50 ksi for the steel section and f'_c = 4 ksi for the concrete. The nominal design moment is equivalent to 60%

of the nominal ultimate moment and is defined as the moment at the maximum service load condition. It should be noted that the design of the H-shape in FF-2, H-1, and H-2 was based on matching the flexural strength of the H-shape with the calculated flexural strength of the exterior joist girder by adjusting the number of shear connectors. The predicted flexural strength based on the AISC specification (1993) of the in-place composite H-shape was calculated with actual and nominal material properties.

The flexural models assume that the flexural strength is limited by $\sum Q_n$, which is defined as the minimum of the yield strength of the bottom chord or steel in tension ($T = \sum A_s F_y$), failure of the welded shear studs (nQ_n), or crushing of the concrete ($C = 0.85\ f'_c\ A_c$). If the effective slab width is large enough, it is not likely that slab crushing will control the design. If longitudinal cracks develop, however, the extreme shear forces at a critical shear plane near the line of shear connectors cannot be transferred effectively into the entire effective slab width. This presents a fourth limit state of longitudinal cracking that needs to be investigated and accounted for.

The required longitudinal shear strength and the available longitudinal shear strength must be determined so that appropriate transverse reinforcement can be provided if necessary. Subsequent sections will present methods for determining the longitudinal shear strengths as well as how they apply to the overall limit states design of composite girders. A complete design example is presented in Appendix A, which includes calculations for exterior and interior joist girders and also for an exterior H-shape.

4.2 Flexural Models

The flexural models for the flush-framed framing configuration and the haunch framing configuration are illustrated in Figures 4.2 and 4.3, respectively. In the flush-framed case, it has been identified and verified in the literature (Lauer et al. 1994) that the top chord can be ignored in strength calculations without sacrificing accuracy. This is valid on the basis that the centroid of the top chord is located approximately at the neutral axis. With this assumption, the model shows that the bottom chord yield strength (T) is balanced by a concrete slab force (C). The joist is generally designed assuming a balanced condition (Lauer et al.1994) whereby the total load carried by the shear connectors is approximately equal to $T = A_s F_y$ for the bottom chord alone. In the case of

the haunch configuration, the additional slab thickness changes the location of the neutral axis; therefore, the top chord should not be ignored in strength calculations. The top chord is typically not sufficiently stressed to reach its full yield strength and due to this, a percentage of the top chord yield stress is assumed for calculation purposes. In this case, a value of 25% of A_sF_y is assumed to contribute to overall strength.

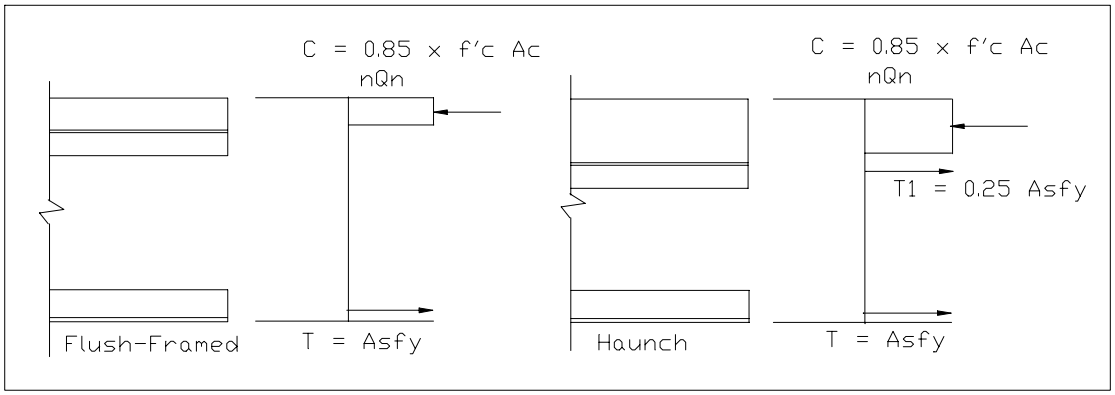

Figure 4.2 Adapted Flexural Models- Joist Girders

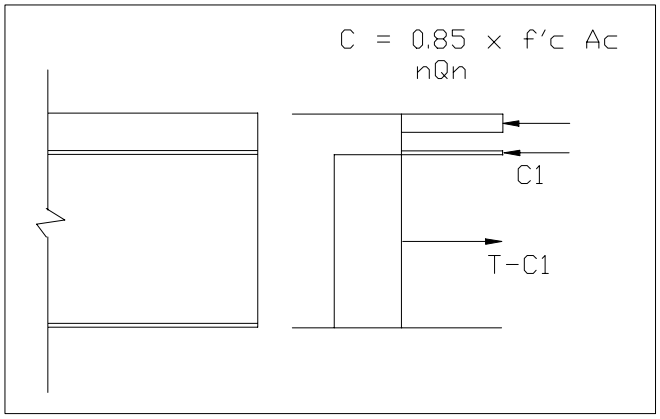

Figure 4.3 Adapted Flexural Model- H-shapes

The H-shapes were partially composite which means that the ratio of $\sum Q_n$ to A_sF_y was less than one. This also means that a portion of the steel girder must be in compression and is illustrated in Figure 4.3. Depending on the magnitude of $\sum Q_n$, the compressive force in the H-shape will in general be resisted by a portion of the steel in the top flange, or by the top flange and a portion of the web.

The effective width of the concrete slab is determined based on AISC (1993) provisions. The effective width is the minimum of the span length divided by eight, one-

half the center to center spacing of adjacent beam/girder (or joist/ joist girder), or the distance to the edge of the slab.

$$effective\ width\ on\ either\ side\ of\ member = \min \begin{vmatrix} \frac{L}{8} \\ 1/2\ center-to-center\ spacing \\ edge\ of\ slab \end{vmatrix}$$

4.3 Flexural Strength

A summary and comparison of experimental and predicted ultimate moments are presented in Table 4.1. The measured experimental moments and the calculated moments are reported in the top portion of the table and comparisons are made in the bottom portion of the tables by way of ratios of experimental values to calculated values. Four terms are presented that define the types of loads considered. The terms are designated with *M* representing the total moment the composite member can sustain including dead load, due to self-weight and slab, and applied load.

The superscript *exp* indicates experimental values while the superscript *calc* represents calculated values. The subscript *u* represents the ultimate moment that was achieved in the experimental case or the predicted ultimate moment based on measured material properties. The subscript *n* indicates the calculated moment based on nominal material properties (F_y = 50 ksi, f'_c = 4 ksi). The subscript *dn* indicates the design moment, which, as indicated earlier, represents 60% of the calculated ultimate moment based on nominal material properties.

The comparison ratios can be viewed as a measure of whether the analytical method over predicts or under predicts the ultimate flexural strength. The experimental values are expressed in the numerator; therefore a number less than 1 indicates that the ultimate strength was over predicted (unconservative). Conversely, a number greater than 1 indicates that the ultimate flexural strength was under predicted (conservative). The ratio used to determine if the flexural models are valid is M_u^{exp} / M_u^{calc}, which compares the experimental ultimate moment with the calculated ultimate moment based on actual material properties.

In general, Table 4.1 shows flexural strength ratios (M_u^{exp}/ M_u^{calc}) for each composite member that are near or exceed 1.0, which indicates that the analytical

procedure in general under predicts the experimental flexural strength. The ratios for the H-shapes, however, show that the analytical method over predicts the flexural strength. Three of the composite members, EB in FF-2, EB H-1, and EB in H-2, had strength ratios that were significantly less than 1.0 indicating that the analytical procedure under predicted the flexural strength. In H-1 and H-2, the degree that the strength ratio under predicted the actual behavior of the exterior H-shapes was particularly significant. In both cases, the amount of transverse reinforcement was minimal with only wire mesh in H-1 and 0.442 in^2 per shear plane and wire mesh in H-2. Additionally, the behavior described in Sec. 3.1.1 may be contributing the low strength.

Table 4.1 Comparison of Experimental and Calculated Flexural Strength

Moment	FF-1			FF-2		
	EGL	IG	EGR	EG	IG	EB
M_u^{exp} (kip-ft)	870	1705	870	1075	1940	1135
M_u^{calc} (kip-ft)	833	1585	833	989	1813	1322
M_n^{calc} (kip-ft)	789	1585	789	790	1595	955
M_{dn}^{calc} (kip-ft)	473	951	473	474	957	573
M_u^{exp}/ M_u^{calc}	1.04	1.08	1.04	1.09	1.07	0.86
M_u^{exp}/ M_n^{calc}	1.10	1.08	1.10	1.36	1.22	1.19
Moment	H-1			H-2		
	EGL	IG	EB	EG	IG	EB
M_u^{exp} (kip-ft)	885	2045	685	945	1820	1145
M_u^{calc} (kip-ft)	910	1765	872	1000	1820	1489
M_n^{calc} (kip-ft)	820	1645	895	820	1650	1180
M_{dn}^{calc} (kip-ft)	492	987	537	492	990	708
M_u^{exp}/ M_u^{calc}	0.97	1.16	0.79	0.95	1.00	0.77
M_u^{exp}/ M_n^{calc}	1.08	1.24	0.77	1.15	1.10	0.97

M_u^{exp} : experimental ultimate moment

M_u^{calc} : calculated ultimate moment with actual material properties

M_n^{calc} : calculated ultimate moment with nominal material properties (F_y = 50 ksi, f'_c = 4 ksi)

M_{dn}^{calc}: calculated design moment base on nominal material properties (60% M_n^{calc})

In FF-2, the strength ratio was 0.86, which indicates that the analytical method was unconservative, however, the testing was terminated after a slab failure occurred at the midspan. The slab failure was unexpected and was likely due to localized punching failure at the load points between the exterior and interior joist girder. It can be concluded that had the slab failure not occurred, EB would have likely carried additional load, which would have increased the strength ratio.

The flexural strength based on nominal material properties is conservative for all the composite members except for the exterior H-shapes for H-1 and H-2. This is due to the assumption that nominal material properties are defined by f'_c = 4 ksi and F_y = 50 ksi. In all cases, the compressive strength of the concrete exceeded the nominal strength and the yield strength for all steel members exceeded 50 ksi except for EB in H-1. It should be noted that the yield strength for the exterior H-shapes in FF-2 and H-2 were approximately 70 ksi, which could present problems in the final design of composite girders.

It is important to note that all the calculations for the strength of the individual shear connector were reduced by a factor of 0.75. Based on preliminary investigations at Virginia Tech, the AISC (1993) provision for the upper limit of the shear stud strength is unconservative and it should be reduced by around 25%. Equation 4.1 (AISC 1993) was therefore limited by $0.75A_{sc}F_u$. Thus, an upper limit of $0.75A_{sc}F_u$ was used for all calculations presented in Table 4.1. Stud reduction factors (SRF) will still apply for 2 in. steel deck when the width of the rib (w_r) is less than or equal to 3 in. (AISC 1993).

$$Q_n = 0.5A_{sc}\sqrt{f'_c E_c} \le 0.75A_{sc}F_u \qquad \text{[Eq. 4.1]}$$

The original strength design of the composite girders did not consider this reduction except for the second flush-framed test (FF-2) where a 20% reduction was used. The strength calculations, therefore, show that the shear studs control the strength for the three joist girders in FF-1 and EG in FF-2, rather than bottom chord yielding. For the haunch tests (H-1 and H-2), the original design considered the full plastic strength of the top and bottom chords. This in turn increased the total number of shear studs to the point that the 25% reduction in shear connector strength did not change the calculated flexural strength when only considering the top chord tension component to be 25% of

A_sF_y. If the strength reduction presented herein was utilized in the original design, the total number of studs would have been increased to ensure that the limiting case for $\sum Q_n$ would have been bottom chord yielding.

4.4 Longitudinal Shear Models

The analytical longitudinal shear models for the exterior and interior joist girders and H-shapes are shown in Figures 4.3 and 4.4. The joist girder and H-shape models assume that the proportioning of the elements (chord sizes, number of shear studs) will be based on existing design procedures for strength (ASCE 1996). The determination of the total shear at the critical shear planes will then be based on those elements.

This is because the shear that is developed is dependent on $\sum Q_n$, which is dependent on the elements in the composite members. The total compressive force ($C+\sum C_1$) in the slab is proportioned to simplify the calculation of the applied longitudinal shear and the longitudinal shear strength at the critical shear plane. The dispersal of shear forces into the slab, or shear lag, is assumed to have a linear distribution with the maximum shear occurring directly over the steel section of the composite member and decreasing linearly to zero at the extreme edges of the effective width.

As stated previously, T and $C+\sum C_1$ are determined on the same basis as determining the ultimate strength of the composite joist girders, which considers A_sF_y of the bottom chord, $0.85f'_cA_c$, and nQ_n. In this case, $\sum Q_n$ is generally equal to A_sF_y for the bottom chord based on the flexural strength model, which assumes the strength of composite joists is governed by bottom chord yielding. As with the strength calculation, the top chord is neglected for the same reasons as explained in section 4.2. The same exception applies to the haunched case where 25% A_sF_y of the top chord is considered.

The H-shape models also assume that the proportioning of the elements (member size, number of shear studs) is based on existing design procedures for strength. In these particular tests the proportioning was based on matching the flexural strength of the exterior joist girder. This was achieved by limiting the number of shear studs that were on the H-shape, hence making it partially composite. The total compressive force ($C+\sum C_1$) in the slab was proportioned in the same manner as for the joist girders, again to

simplify the calculation of the respective required longitudinal shear strength and available longitudinal shear strength.

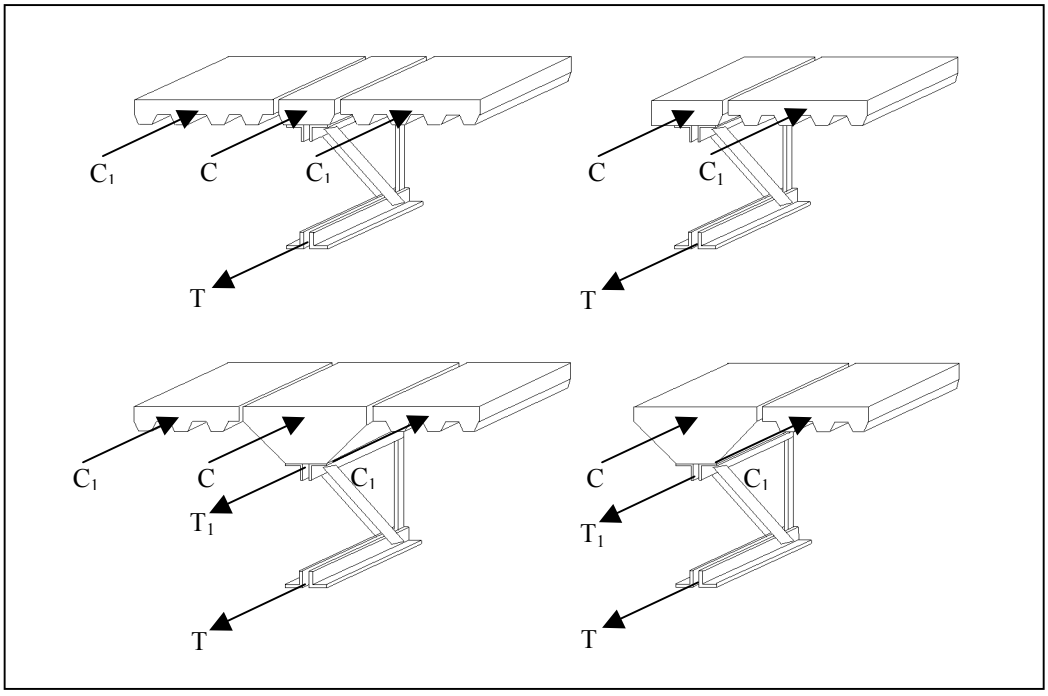

Figure 4.4 Joist Girder Longitudinal Shear Model (After Chien and Ritchie 1984)

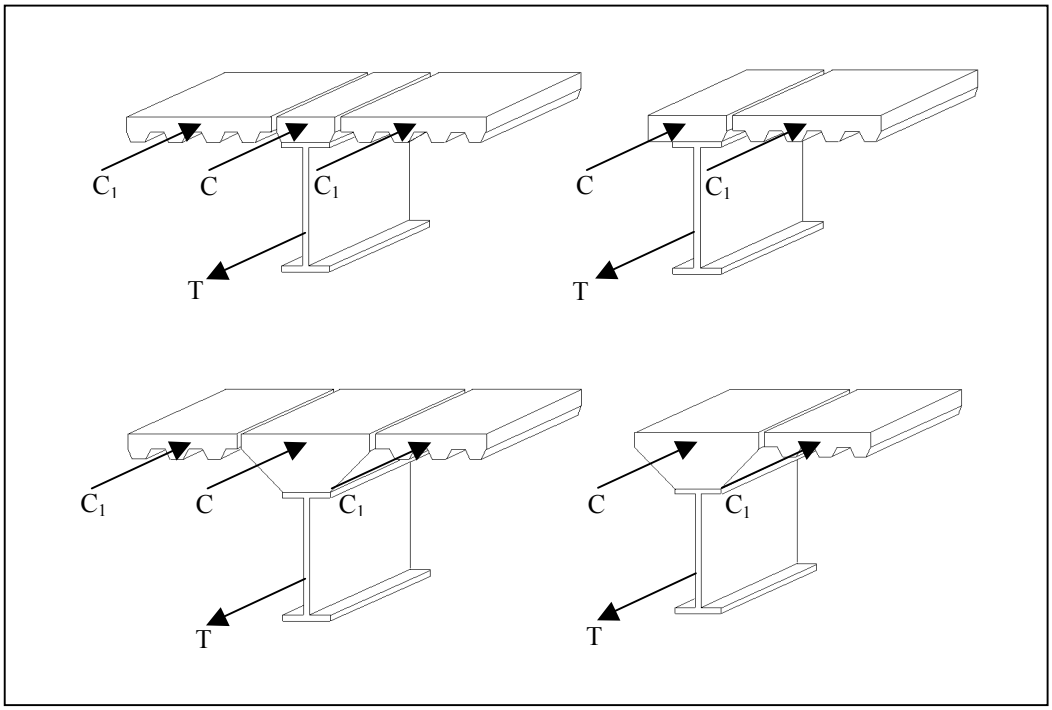

Figure 4.5 H-shape Longitudinal Shear Model (After Chien and Ritchie 1984)

4.5 Longitudinal Shear

The required longitudinal shear strength (V_u) and the longitudinal shear strength (V_r) are the parameters that determine whether or not the composite member will be able to adequately distribute the shear forces into the slab. Two approaches were found for determining the required longitudinal shear strength and are presented in a subsequent section. Various equations from research conducted in the United States, Canada, Australia, and Western Europe (Hofbeck et. al (1969); Chien and Ritchie (1984); Oehlers and Bradford (1995); Johnson (1970)) were found in the literature on composite construction. An additional equation was adapted from the ACI provision that applies to longitudinal shear in reinforced concrete. The equations vary slightly in terms of the relative contribution of each component of the longitudinal shear strength, but the components are the same in all of the approaches. Because of these similarities, not all of the approaches (equations) are presented in this study.

With two methods for calculating the required longitudinal shear strength and two methods for calculating the available longitudinal shear strength, there are four combinations that could be considered. The four methods are evaluated subsequently and a recommendation is made based on this evaluation.

4.5.1 Required Longitudinal Shear Strength

To determine the required longitudinal shear strength at the critical shear planes, the compressive force in the concrete between shear planes must be accounted for and removed from the total compressive force. This is necessary to calculate the remaining amount of force that must be transferred across the shear plane as longitudinal shear. The effective width is defined by the letter b and the portion of the slab between the shear planes or between the slab edge and the shear plane is defined by the letter b'. The area of concrete between shear planes is designated A_{cs}. This model is illustrated in Figure 4.5. It should be noted, that when concrete outside the shear planes is being referred to in this thesis, it includes both the concrete outside either shear plane for an interior girder, or the concrete outside the single shear plane and the edge of the slab for the spandrel girders.

Two methods have been identified to determine the required longitudinal shear strength at the critical shear planes. Method 1 assumes a constant thickness for the slab over the effective width. The constant thickness assumption allows the use of ratios of the total slab width outside critical shear planes to the entire effective

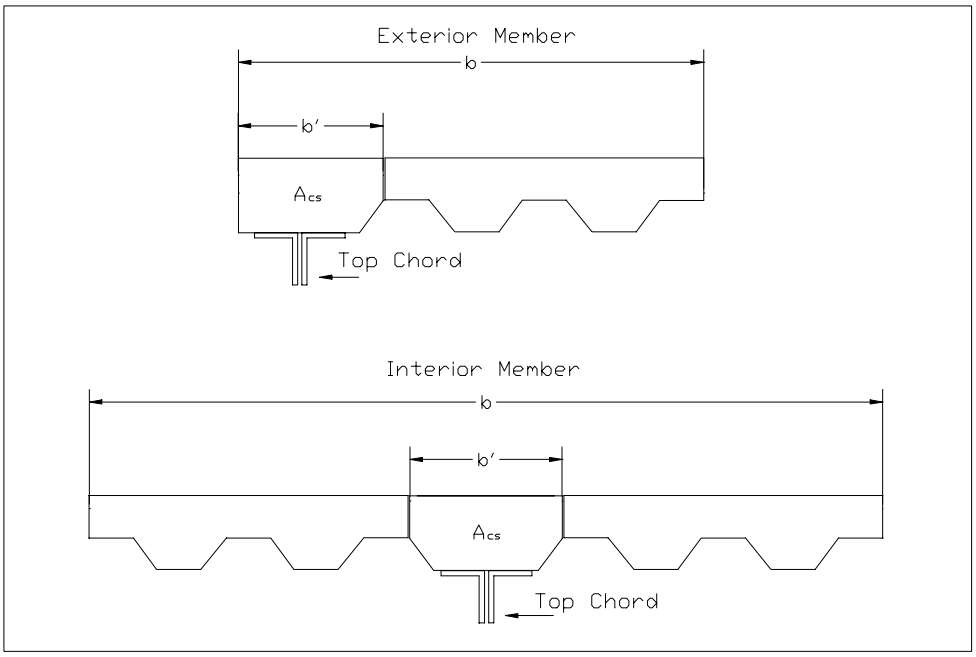

Figure 4.6 Critical Longitudinal Shear Planes

width. The total compressive force in the slab is then multiplied by this ratio to determine a net compressive force on the concrete outside the shear plane, which is assumed to be equal to the required longitudinal shear strength (V_u^T) at the critical shear plane(s).

$$V_u^T = \left(\frac{b-b'}{b}\right)\Sigma Qn \qquad \text{[Eq. 4.2]}$$

The exterior members have one shear plane so the required longitudinal shear strength is equal to the total required longitudinal shear strength and is represented by Equation 4.3. The interior members have two shear planes, which each carry half of the total required longitudinal shear illustrated by Equation 4.4.

$$V_u = \left(\frac{b-b'}{b}\right)\Sigma Qn \qquad \text{[Eq. 4.3]}$$

$$V_u = \frac{1}{2}\left(\frac{b-b'}{b}\right)\Sigma Qn \qquad \text{[Eq. 4.4]}$$

Method 2 assumes the entire portion of the concrete (A_{cs}) between the shear planes resists a portion of the calculated value for $\sum Q_n$. The net compressive force that needs to be transferred ($\sum Q_n - 0.85\ f'_c\ A_{cs}$) is then assumed to be the longitudinal shear force that must be transferred at the critical shear plane(s). Equations 4.5 and 4.6 illustrate the relationships for the required longitudinal shear strength for the spandrel and interior girders, respectively.

$$V_u = \Sigma Qn - 0.85 f'_c\ A_{cs} \qquad \text{[Eq. 4.5]}$$

$$V_u = \frac{1}{2}(\Sigma Qn - 0.85 f'_c\ A_{cs}) \qquad \text{[Eq. 4.6]}$$

In the flush-framed tests, Method 2 predicts that the area of concrete between shear planes was not sufficient to carry full value of $\sum Q_n$. This means that the shear forces developed at the critical shear plane have to be transferred to the rest of the slab outside those planes to reach the ultimate flexural strength ($\sum Q_n - 0.85\ f'_c\ A_{cs} > 0$; $V_u > 0$). In the case of the haunch tests, the area of concrete between the shear planes was sufficient to allow the full value of $\sum Q_n$ to be carried by the haunch ($\sum Q_n - 0.85\ f'_c\ A_{cs} \leq 0$; $V_u = 0$). This means the flexural strength is not reduced if the area of concrete outside the shear planes was not available.

4.5.2 Longitudinal Shear Strength

Methods for calculating the longitudinal shear strength have been developed by various researchers with one of two assumptions: (1) the slab is initially cracked or (2) uncracked longitudinally. The work of Mattock and his colleagues (Hofbeck et al. 1969; Mattock et al. 1976) is the most frequently cited with regard to longitudinal shear in cracked and uncracked concrete elements. The model proposed here was presented by Oehlers and Bradford and has its basis in Mattock's original work. There are differences

in the treatment of the concrete and steel reinforcement and those differences will be discussed in a subsequent section.

The calculated longitudinal shear strength assumes that the slab is initially cracked and the components resisting the applied longitudinal shear are active friction, dowel action, and aggregate interlock. These components are illustrated in Figure 4.6.

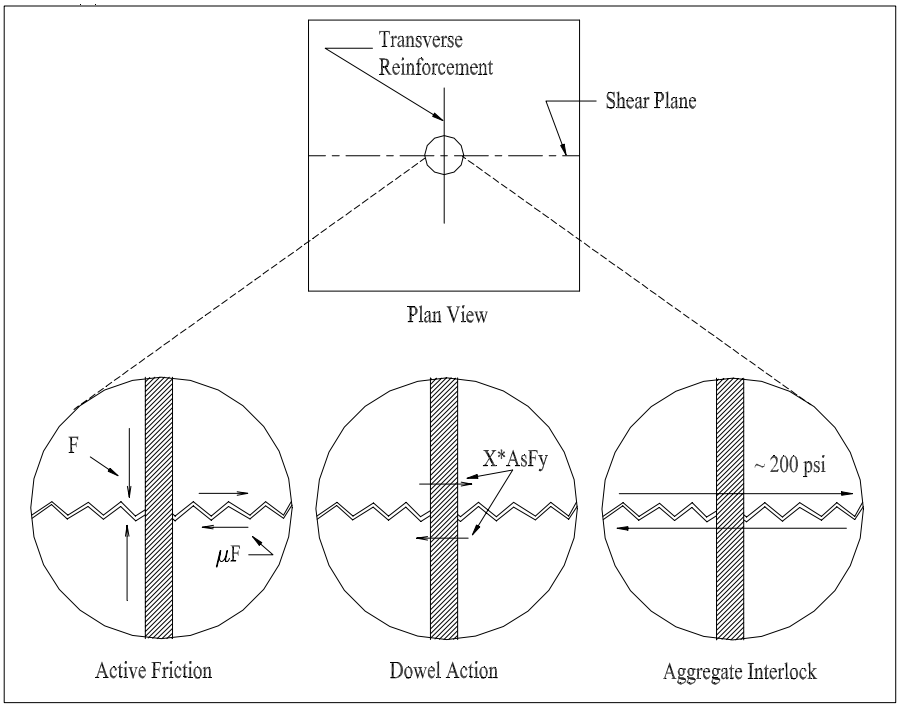

Figure 4.7 Components of Longitudinal Shear Strength

Active friction is provided by a normal force in the slab acting transverse to the steel girder and is applied by an external force. In theory, this can only be achieved by a method such as slab prestressing. It can be argued that an external restraint perpendicular to the girders could provide some active resistance by not allowing the longitudinal cracks to widen excessively. Another mechanism that could apply this normal force is the strut and tie model presented in Chapter 1, which is based on the idea that as herringbone cracks form in the slab concrete, struts are formed at 45-degree angles to the longitudinal shear planes. Because of the presence of transverse reinforcement, the struts are "tied" together and induce tension into the reinforcement. Since the reinforcement crosses the shear planes, a compressive normal force is introduced at the shear plane, thereby increasing the frictional force that needs to be overcome. It could be argued that determining the exact stress condition with such a rigorous method that includes

combined shear and tension in the transverse reinforcement is unnecessary for design purposes. It is convenient to use a slightly more conservative method, which only includes the dowel action of the transverse reinforcement and the aggregate interlock. The method is conservative because it requires additional reinforcement to transfer the shear when, in fact, some active friction may be present that is being ignored.

Relationships that were found in the literature include those presented by Johnson (1970), Oehlers and Bradford (1995), and the Commentary on BS5950 Part 3 Section 3.1 (Lawson 1990). Section 11.7.3 of the ACI code (ACI 318-99) also presents an equation for the amount of shear resistance at a crack boundary based on the shear friction method. For simplicity, all the terms in the different equations that represent the same parameter have been given the same label. The nominal tensile strength for the transverse reinforcement is given by $A_s f_{yr}$ and A_{cv} is the area of concrete in the longitudinal shear plane between the concentrated load points and the end of the slab. Equations 4.7 and 4.8 are presented by ACI (1999) and Oehlers and Bradford (1995), respectively. As indicated previously, the equations are based on the fundamental research by Hofbeck et al. (1969) and Mattock et al (1976).

$$V_r = 0.8 A_s f_{yr} + K_1 A_{cv} \qquad \text{(lb, in)} \qquad \text{[Eq. 4.7]}$$
$$K_1 = 400\,psi$$

$$V_r = 0.8 A_s f_{yr} + 200 A_{cv} \qquad \text{(lbs, in}^2\text{)} \qquad \text{[Eq. 4.8]}$$

$$V_r = \left[3.4 * \left(\frac{E_c}{E_s} \right)^{0.40} * \left(\frac{f'_c}{F_y} \right)^{0.35} \right] A_s f_{yr} + 200 A_{cv} \qquad \text{[Eq. 4.9]}$$

It is important to identify the individual components in Equations 4.7 and 4.8 because different assumptions are made in those equations. In Equation 4.7, the term 0.8 $A_s F_y$ represents what is defined as a friction term with 0.8 as the coefficient of friction. This assumes that as the protrusions of concrete slide past one another, they begin to separate and induce a tensile stress in the transverse reinforcement up to the yield stress.

The available "friction" force then is the normal force (A_sF_y) multiplied by the coefficient of friction (0.8). The second term for normal weight concrete, K_1A_{cv} = 400 A_{cv} represents the combined effect of the shear resistance of the concrete protrusions at the interface and the dowel action of the transverse reinforcement (ACI 1999).

Equation 4.8 also has the term $0.8A_sF_y$, but this term represents the available dowel strength across the shear plane (Oehlers and Bradford 1995). The coefficient of 0.8 is assumed to be representative of the term in brackets in Equation 4.9. The second term of 200 psi times the area of concrete A_{cv} in the shear plane represents the shear strength of the individual concrete protrusions.

As discussed in previous sections, the total shear strength is assumed to be the summation of three components: dowel strength, active friction, and aggregate interlock (passive friction). In Equation 4.7, the assumption is that the concrete protrusions can slide and separate (active friction) while also resisting direct shear through aggregate interlock of the same protrusions. The initial assumption is that the active friction, or sliding, is sufficient to fully yield the transverse reinforcement. If the transverse reinforcement is fully yielded in tension, then its resistance to direct shear (dowel action) cannot be included. If it is included, then some interaction between the shear and tension must be accounted for in both the active friction term and the dowel action term.

Oehlers and Bradford (1995) concluded that the fracture of the protrusions is of primary importance and that the transverse reinforcement provides only passive friction rather than active friction. That is, the transverse reinforcement only needs to be sufficient enough to prevent wide cracks and any friction that develops should be ignored. The only case where active friction should be considered is when an external applied force is present to provide a normal force at the crack face.

These discrepancies in the equations are not accounted for in this study, but in order to fully understand the behavior at the longitudinal shear planes, these issues need to be investigated further in the future. Despite these discrepancies, the approach that Oehlers and Bradford have presented is the better of the two approaches from a mechanics standpoint and should be used for design.

4.5.3 Proposed Analytical Method for Longitudinal Shear Strength

Method 2 provides a more clearly defined way of determining whether or not the presence of transverse reinforcement is required for strength. If the flexural strength is calculated with only the area of concrete between shear planes, and that strength is equal to or exceeds what was calculated with the entire effective width, then the transverse reinforcement is only needed for serviceability. While some shear transfer may actually be necessary at the critical shear planes, if it cannot be shown that the flexural strength requires part of the concrete compression flange outside the shear planes, then the flexural strength is independent of any reinforcement provided. As explained in section 4.5.2, Oehlers and Bradford's approach should be used to calculate the available shear strength at the critical shear plane.

The girders with the flush-framed configuration all required a portion of the concrete flange outside the shear plane to reach their full strength as illustrated by the values for M_u', defined as the calculated flexural strength considering only the concrete between the shear planes, in Table 4.2.

Table 4.2 Comparison of Flexural Strengths (Method 2)

Flexural Strength		FF-1			FF-2		
		EGL	IG	EGR	EG	IG	EB
M_u'	(k-ft)	397	354	397	734	959	1068
M_u^{calc}	(k-ft)	833	1585	833	989	1813	1322
M_u^{exp}	(k-ft)	870	1705	870	1075	1940	1135
M_u' / M_u^{calc}		0.48	0.22	0.48	0.74	0.53	0.81
M_u' / M_u^{exp}		0.46	0.21	0.46	0.68	0.49	0.94

In FF-1, the flexural strength only considering the concrete between the shear planes is significantly less (~50 – 80%) than the experimental flexural strength. The difference for the second flush-framed test (FF-2) isn't as significant, however, the numbers clearly indicate that concrete outside the shear planes is required to reach the ultimate flexural strength.

In tests H-1 and H-2 (not illustrated), M_u' was greater than or equal to M_u^{calc} for any of the six girders. Based on the proposed methods, the area of concrete outside the critical shear planes, therefore, is not needed for strength. This is not verified by the

experimental results for the H-shapes in H-1 and H-2, which reached an ultimate flexural strength significantly below the predicted flexural strength. Because the H-shapes had minimal transverse reinforcement in the slab (0 in^2 in H-1 and 0.44 in^2 in H-1) and significant longitudinal cracking occurred, it is likely that some additional transverse reinforcement was required at the critical shear plane(s). The results, however, are inconclusive as to whether the flexural strength was not reached because of longitudinal shear.

Table 4.3 summarizes the experimental results and the recommended analytical approach for determining the required longitudinal shear and the available longitudinal shear strength. A comparison of the flexural strength ratios and the longitudinal shear strength ratios shows that the proposed method for calculating longitudinal shear strength works well for the composite joist girders. In the flush-framed tests, it can be seen that the flexural strength ratio is near 1.0 and the longitudinal shear strength ratio shows that the amount of transverse reinforcement is adequate. In four of the six cases, the longitudinal shear strength ratio indicates that the amount of reinforcement could be reduced which means that this approach is conservative.

The haunch tests show that the flexural strength ratio is also near 1.0 for the joist girders and near 0.8 for the H-shapes. The fact that the required longitudinal shear strength is zero indicates that the transverse reinforcement provided was not necessary to reach the ultimate flexural strength.

Table 4.3 Summary of Experimental and Analytical Results

		FF-1			FF-2		
		EGL	IG	EGR	EG	IG	EB
V_u^{exp} (2)	(kips)	126	200	126	57	148	335
V_r (Eq. 4.8)	(kips)	153	191	153	145	163	335
V_u^{exp} / V_r		0.82	1.05	0.82	0.39	0.91	1.00
M_u^{exp} / M_u^{calc}		1.04	1.08	1.04	1.09	1.07	0.86
		H-1			H-2		
		EGL	IG	EB	EG	IG	EB
V_u^{exp} (2)	(kips)	0	0	0	0	0	0
V_r (Eq. 4.8)	(kips)	157	589	88	109	109	109
V_u^{exp} / V_r		0	0	0	0	0	0
M_u^{exp} / M_u^{calc}		0.97	1.16	0.79	0.95	1.00	0.77

For composite joist girders and H-shapes that are flush-framed and joist-girders that have haunches, it can be concluded that if the flexural strength does not change when only the concrete between shear planes is considered then no transverse reinforcement is required. If however, concrete outside the shear plane(s) is required to balance the tensile force in the steel section, then transverse reinforcement is required. The analysis and design for longitudinal shear should then proceed using the approach presented herein.

4.6 Adjusted Flexural Strength

If the available longitudinal shear strength is less than what is required at the critical plane, then the flexural strength is limited by the available shear strength (V_r) rather than $\sum Q_n$ and the flexural strength is reduced accordingly. The methods presented in the previous sections can be used to determine this adjusted flexural strength.

A reduced flexural strength did not apply for any of the flush-framed girders regardless of which method was used to determine the longitudinal shear strength at the critical shear plane. This result was expected because in no case did the calculated flexural strength exceed the experimental flexural strength. The exception to this was the H-shape in FF-2, which was explained in detail in a previous section. In addition, the available longitudinal shear strength generally equaled or exceeded the required longitudinal shear strength at the critical shear plane.

For the haunch tests, the flexural capacity did not change when comparing the flexural strength using the entire effective width to the flexural strength using only the area of concrete between shear planes (or shear plane and edge of slab). The experimental results for the two H-shapes show that they did not reach their predicted flexural strength despite having adequate concrete between the shear planes or between the shear plane and the edge of the slab. As explained previously, the H-shape in H-1 showed problems early in the test that affected its overall performance. This may indicate a limitation of the approaches presented in this report for H-shapes or for composite girders with haunches.

CHAPTER 5
SUMMARY AND CONCLUSIONS

5.1 Summary

The objective of this study was to develop a design procedure for transverse reinforcement in the slabs of composite joist girders and composite H-shapes.

Four tests were conducted on two types of floor systems that had two spandrel or exterior girders in the form of joist girders or hot-rolled shapes, and one interior joist girder. Each member was nominally 30 ft 4 in. long and had 6 ft 9 in. joists framing in at the third points of each of the three girders. The two types of floor systems were flush-framed and haunched. Loadings were typically applied to the joists as point loads that transferred their load to the girders via concentrated end reactions.

The test specimens were constructed and tested at the Structures and Materials Laboratory at the Virginia Polytechnic Institute and State University in Blacksburg, VA. Kigudde et al. (1996) and Showalter (1999) reported the results for two of the tests. Several parameters were recorded for each test that included end reactions for each of the girders, chord, flange, and web strains, midspan and third point or quarter point deflections, concrete strains, and relative end slip deflections.

The results of the experimental testing were compared with predicted values for ultimate load or moment and predicted longitudinal shear strength.

5.1.1 Flush-Framed Tests

The flush-framed tests are defined by the position of the top chords/ flanges of the girders relative to the joists. In this configuration, all the top chords/flanges are at the same elevation with the deck resting on the top chords/flanges. The connections between the joists and joist girders were bolted by way of gusset plates. In the first flush-framed test, failure occurred by buckling of web members and bottom chord yielding. In the second flush-framed test, the failure modes were yielding of the bottom chord/flange and crushing of the concrete slab at the midspan of the floor system. The concrete failure began over the exterior joist girder and propagated across the slab with a final sudden

brittle failure of the concrete. This failure was initiated by localized slab crushing at the load bearing points

5.1.2 Haunch Tests

The haunch tests are defined by the presence of additional concrete formed over each of the girders with the use of forming steel. This effectively increases the moment capacity of the given composite member without increasing the depth of the steel section, and this was achieved by having the joist seat bear on the top chord of the girders and placing the deck on the top chord of the joists. Haunch pans are then put in place and fastened to the joist girders with puddle welds and to the cold-formed steel deck with mechanical fasteners. In the first haunch test, premature failure occurred with the H-shape when the floor was tested as a system. Early non-linear behavior in the load vs. deflection plot and indications of premature yielding and loss of shear connection showed that the H-shape was not behaving as expected. Failure of the joist girders was due mainly to bottom chord yielding and initiation of loss of shear connection. In the second haunch test, the test behaved as expected with failure coming by way of yielding of the bottom chord/flange, loss of shear connection, and longitudinal cracking.

5.2 Conclusions

- The flexural models worked well to predict the ultimate experimental load for the joist girders. The flexural models did not predict the strength well for the exterior H-shapes in H-1 and H-2.
- Two methods of determining the required longitudinal shear strength can be used for design. The first method assumes a constant concrete thickness (based on the depth of the compressive stress block) and the required longitudinal shear strength varies linearly to zero from a maximum at the line of shear connectors to zero at the edge of the effective width. The second method assumes all the concrete between shear planes or between a shear plane and the slab edge resists a portion of $\sum Q_n$ leaving the balance to be transferred across the critical shear plane(s). The constant concrete thickness method is more conservative compared to

the second method, which predicts lower required shear strengths at the critical shear planes.

- Two equations for determining the longitudinal shear strength can be used for design. The first equation is from ACI (1999) and includes active friction, aggregate interlock, and dowel action. The second equation was presented by Oehlers and Bradford (1995) and includes dowel action and aggregate interlock. The ACI equation is less conservative compared with the equation by Oehlers and Bradford based on the fact that it will over predict the longitudinal shear strength by as much as $200*A_{cv}$. Despite the fact that the terms are defined in the equations differently, the net difference for any given case is based on the net difference between $400A_{cv}$ and $200A_{cv}$
- Transverse reinforcement is not required for strength if the flexural strength is unaffected by the absence of concrete outside of the shear planes. The flexural strength is calculated based on the concrete between shear planes or between the shear plane and the edge of the slab. If this flexural strength is less than the calculated ultimate flexural strength with the full effective width, then one of the methods describe above should be used to design the appropriate amount of transverse reinforcement.

5.3 Further Research

On the basis of the experimental and theoretical results from this study, four areas of future research have been identified.

1. The longitudinal shear behavior of composite H-shapes need to be investigated further to better understand whether the analytical methods for flexural strength and longitudinal shear strength are adequate for these members. Testing should include a full-scale floor system with spandrel and interior H-shape girders. Single full-scale girders should also be tested and compared with the results from

the floor system testing to determine if the single girder test is able to accurately model what happens in a complete floor system.

2. An analytical model should be generated and verification analysis should be performed on the existing pool of data for composite joist, joist girder, and hot-rolled shapes. This model should consider the effects of shear connectors, concrete strength, strength of the steel in the girders and transverse reinforcement, and the effects of spacing of the girders to better model the effects of negative transverse moment over the girders. The model should also attempt to include the first phase of crack formation due to shear deformation and the second phase of crack formation due to longitudinal splitting.

3. The effects of dowel action, aggregate interlock, and friction need to be investigated further to determine how their effects apply to the calculation of the longitudinal shear strength in composite joist girders.

4. The 25% strength reduction for the upper limit on shear connector strength as it applies to push-out tests needs to be investigated for composite joists and joist girders to verify the application of this reduction to full-scale composite members.

References

AISC, (1993). "Load and Resistance Factor Design Specification for Structural Steel Buildings", Chicago, IL.

Task Committee on Design Criteria for Composite Structures in Steel and Concrete (1996) "Proposed specification and commentary for composite joists and composite trusses." *Journal of Strucutral Engineering*, ASCE, 122(4), 350-358.

Azmi, M.H. (1972). "Composite open-web trusses with metal cellular floor." Master of Engineering thesis, McMaster University, Hamilton, Ontario, Canada.

ACI, (1999) "Building Code Requirements for Structural Concrete and Commentary (ACI 318-99)", Farmington Hills, MI.

Barnard, P.R., (1965). "Series of tests on simply supported composite beams." *Proceedings of the American Concrete Institute*, 62, 443-455.

Buckner, C.D., DeVille, D.J., and McKee, D.C. (1981). "Shear strength of slabs in composite stub girders." *Journal of the Structural Division*, ASCE, 107 (ST2) 273-279.

Chien, E.Y.L. and Ritchie, J.K. (1984). Design and construction of composite floor systems. *Canadian Institute of Steel Construction*, Willowdale, Ontario, Canada.

Davies, C. (1969). "Tests on half-scale steel-concrete composite beams with welded stud connectors." *The Structural Engineer*, 47(1), 29-40.

El-Ghazzi, M.N., Robinson, H., and Elkholy, A.S. (1976). "Longitudinal shear capacity of the slabs of composite beams." *Canadian Journal of Civil Engineering*, 3(4),514-522.

Elkelish, M.S. and Robinson, H. (1986). "Longitudinal cracking of composite beams with ribbed metal deck." *Canadian Journal of Civil Engineering*, 13(6), 733-740.

Henderson, W.D. (1976). "Effect of stud height on shear connector strength in composite beams with lightweight concrete and three-inch metal deck." M.Sc. thesis, The University of Texas, Austin, TX.

Hofbeck, J.A., Ibrahim, I.O., and Mattock, A.M. (1969). "Shear transfer in reinforced concrete." *Proceedings of the American Concrete Institute,* 66(2),119-128.

Hosain, M.U., Chien, E.Y.L., and Kennedy, D.J.L. (1992). "New canadian provisions related to the design of composite beams." *Composite Construction in Steel and Concrete II. Proceedings of the Engineering Foundation Conference, Potosi, MO*, ASCE, 39-48.

Gibbings, D.R., Easterling, W.S., and Murray, T.M. (1991). "Strength of composite long-span joists." *Report No. CE/VPI-ST 91/02*, Virginia Polytechnic Institute and State University, Blacksburg, VA.

Johnson, R.P. (1970). "Longitudinal shear strength of composite beams." *ACI Journal*, June 1970, 67, 464-466.

Kigudde, M., Rambo-Roddenberry, M., Easterling, W.S., and Murray, T.M. (1996). "Flush-framed composite joist-girder tests" *Report No CE-VPI-ST 96(98)/11*, Virginia Polytechnic Institute and State University, Blacksburg, VA.

Lauer, D.F., Gibbings, D.R.,Easterling, W.S., and Murray, T.M. (1996). "Evaluation of composite short span joists" *Report No CE-VPI-ST 96/06*, Virginia Polytechnic Institute and State University, Blacksburg, VA.

Lawson, R.M. (1990). *Commentary on BS5950, Part 3, Section 3.1*. The Steel Construction Institute, Silwood Park, Ascot, United Kingdom.

Mattock, A.H., Li, W.K., and Wang, T.C. (1976). "Shear transfer in lightweight reinforced concrete." *Prestressed Concrete Institute*, 21(1), 20-39.

Murray, T.M., Allen, D.E., and Ungar, E.E. (1997). *Floor vibrations due to human activity.* Steel Design Guide Series No. 11, AISC, Chicago, IL.

Oehlers, D.J. and Park, S.M. (1992). "Shear connectors in composite beams with longitudinally cracked slabs." *Journal of Structural Engineering*, ASCE, 118 (8), 2004-2022.

Oehlers, D.J. and Park, S.M. (1994). "Shear connection in haunched composite beams with sloping sides." *Journal of Structural Engineering*, 120(7), 2227-2232.

Oehlers, D.J. and Bradford, M.A. (1995). Composite steel and concrete structural members. Kidlington, Oxford, U.K., Tarrytown, N.Y.

Piotter, J.M., Easterling, W.S., and Murray, T.M. (2001). "Longitudinal slab splitting in composite joist-girders" *Report No CE-VPI-ST 01/01*, Virginia Polytechnic Institute and State University, Blacksburg, VA.

Robinson, H. and Wallace, I.W. (1973). "Composite beams with 1-1/2 inch metal deck and partial and full shear connection." *Transactions of the Canadian Society for Civil Engineering*, 16(A-8), I-VIII.

Robinson, H. (1981). "Resistance to longitudinal cracking in composite members." *Report No. 81-1*, McMaster University, Hamilton, Ontario, Canada.

Showalter, S.L. (1999). Investigation of ultimate strength of composite open-web joist-girders. Master of Science thesis, Department of Civil and Environmental Engineering, Virginia Polytechnic Institute and State University, Blacksburg, VA.

Taylor, R., Plum, D.R., and Papazomenos, A.G. (1970). "Investigation on the Use of Deep Haunches in Composite Construction." *Institution of Civil Engineers*, Sept-Dec 1970, pp. 43-54.

APPENDIX A

Transverse Reinforcement Design Example

A.1 General

The design procedure presented here assumes that the composite member has been proportioned for the applied load. This means that the steel sections have been sized for the applied load, the appropriate number of shear studs have been determined, and the collateral design such as web capacities for the joist girders have been completed. This method was employed for the design of the transverse reinforcement for the second flush-framed test, which was effectively a direct experimental verification of this procedure. As such, that design procedure will be presented here.

A.2 Joist girder Transverse Reinforcement (Interior)

Joist Girder: IG (FF-2)

Given:

L_v	= 122 in.	w_{conc}	= 145 pcf	F_y = 50 ksi	F_{yr} = 60 ksi
F_{ymesh}	= 65 ksi	f'_c	= 4 ksi	b = 84 in.	b′ = 19 in.
A_{BC}	= 11.72 in^2	A_{TC}	= 5.72 in^2		

Number of shear studs in shear span:	28
Area of mesh in shear plane:	0.282 in^2
Number of shear planes:	2
$A_{sc}F_u$ per shear stud	28.7 kips/stud

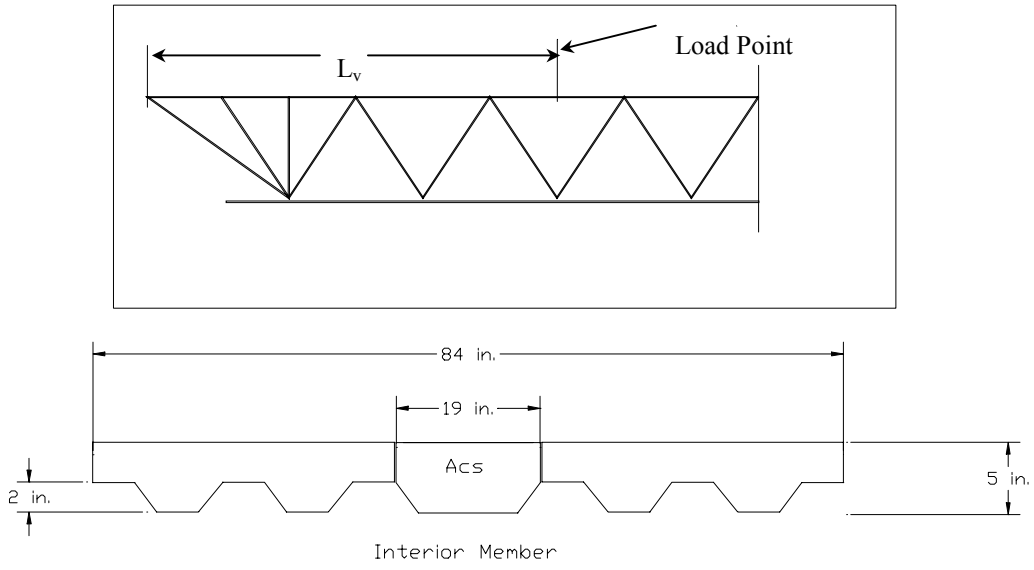

Area of concrete in shear plane, A_{cv}

$A_{cv} = L_v$ (nominal slab thickness – deck depth)

$A_{cv} = 122$ in. (5 in. – 2 in.) = 366 in^2

Area of concrete between shear planes, A_{cs}

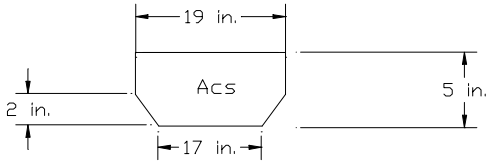

$$A_{cs} = 19\ in.\ x\ (3\ in.) + \left(\frac{19\ in. + 17\ in.}{2}\right) x\ (2\ in.) = 93\ \text{in}^2$$

Determination of Total V_u

$$\Sigma Q_n = \min\begin{pmatrix} A_s F_{y\,BC} = 11.719\ in^2\ x\ 50\ ksi = 586\ kips \\ 0.85 f'_c\ A_c = 0.85\ x\ 4\ ksi\ x\ (84\ in.\ x\ 4\ in.) = 1142\ kips \\ 0.75 n Q_n = 0.75\ x\ 28\ studs\ x\ 28.7\ kips/stud = 603\ kips \end{pmatrix}$$

$\Sigma Q_n = 586$ kips

Determination of Total V_u that has to be transferred at shear plane (Method 2)

$$V_u = \Sigma Q_n - 0.85 f'_c\ A_{cs} = 586\ kips - 0.85\ x\ 4\ ksi\ x\ 93\ in^2 = 270\ \text{kips}$$

V_u per shear plane = 270 / 2 = 135 kips

Determination of V_r

$$V_r = 0.8\ x\ A_s F_{yr} + 200 A_{cv} \qquad (\text{lbs, in}^2) \qquad \text{[Eq. 4.8]}$$

$$V_r = 0.8\ x\ 0.282\ in^2\ x\ 65000\ ksi + 200\ psi\ x\ 366\ in^2 = 88000\ lbs \Rightarrow 88\ kips$$

Determination of longitudinal shear to be carried by transverse steel

$V_u - V_r = 135$ kips – 88 kips = 47 kips

Determination of Area of steel required to carry remaining shear

$V_u - V_r = 0.8\ A_s f_{yr}$

$$A_s = \left(\frac{V_u - V_r}{0.8\ x\ F_{yr}} \right) = \left(\frac{47\ kips}{0.8\ x\ 60\ ksi} \right) = 0.98\_in^2$$

A.3 Joist girder Transverse Reinforcement (Exterior)

Joist Girder: EG

Given:

L_v	= 122 in.	w_{conc}	= 145 pcf	F_y	= 50 ksi	F_{yr}	= 60 ksi
F_{ymesh}	= 65 ksi	f'_c	= 4 ksi	b	= 46 in.	b′	= 13.5 in.
A_{BC}	= 5.72 in^2	A_{TC}	= 2.88 in^2				

Number of shear studs in shear span:	17
Area of mesh in shear plane:	0.282 in^2
Number of shear planes:	1
$A_{sc}F_u$ per shear stud	28.7 kips/stud

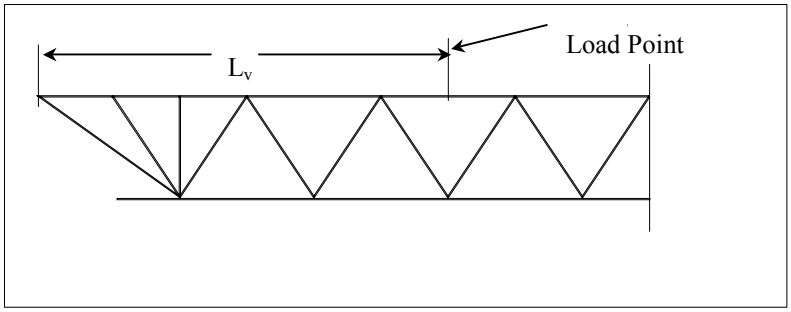

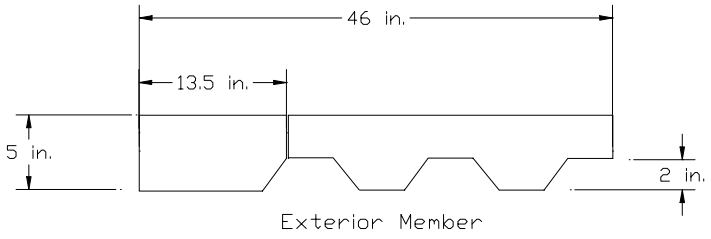

Area of concrete in shear plane, A_{cv}

$A_{cv} = L_v$ (nominal slab thickness – deck depth)

$A_{cv} = 122$ in. (5 in. – 2 in.) = 366 in^2

Area of concrete between shear planes, A_{cs}

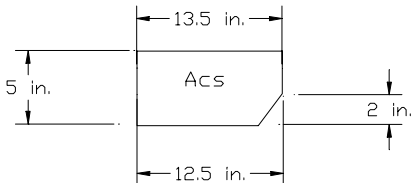

$$A_{cs} = 13.5\ in.\ x\ (3\ in.) + \left(\frac{13.5\ in. + 12.5\ in.}{2}\right) x\ (2\ in.) = 66.5\ \text{in}^2$$

Determination of Total V_u

$$\Sigma Q_n = \min\begin{pmatrix} A_s F_{y\,BC} = 5.719\ in^2\ x\ 50\ ksi = 286\ kips \\ 0.85 f'_c\ A_c = 0.85\ x\ 4\ ksi\ x\ (46\ in.\ x\ 4\ in.) = 626\ kips \\ 0.75 n Q_n = 0.75\ x\ 14\ studs\ x\ 28.7\ kips/stud = 301\ kips \end{pmatrix}$$

$\Sigma Q_n = 286$ kips

Determination of Total V_u that has to be transferred at shear plane (Method 2)

$$V_u = \Sigma Q_n - 0.85 f'_c\ A_{cs} = 286\ kips - 0.85\ x\ 4\ ksi\ x\ 66.5\ in^2 = 59.9 \text{ kips}$$

V_u per shear plane = 59.9 / 1 = 59.9 kips

Determination of V_r

$$V_r = 0.8\ x\ A_s F_{yr} + 200 A_{cv} \qquad (\text{lbs, in}^2)$$

$$V_r = 0.8\ x\ 0.282\ in^2\ x\ 65000\ psi + 200\ psi\ x\ 366\ in^2 = 88000\ lbs \Rightarrow 88\ kips$$

Determination of longitudinal shear to be carried by transverse steel

$V_u - V_r = 59.9 - 88 = -28.1$ kips ➔ No transverse reinforcement required

A.4 H-Shape Transverse Reinforcement

Girder: EB

Given:

L_v = 122 in. w_{conc} = 145 pcf F_y = 50 ksi F_{yr} = 60 ksi
F_{ymesh} = 65 ksi f'_c = 4 ksi b = 46 in. b′ = 13.5 in.
A_G = 16.2 in^2

Number of shear studs in shear span:	31
Area of mesh in shear plane:	0.282 in^2
Number of shear planes:	1
$A_{sc}F_u$ per shear stud	28.7 kips/stud

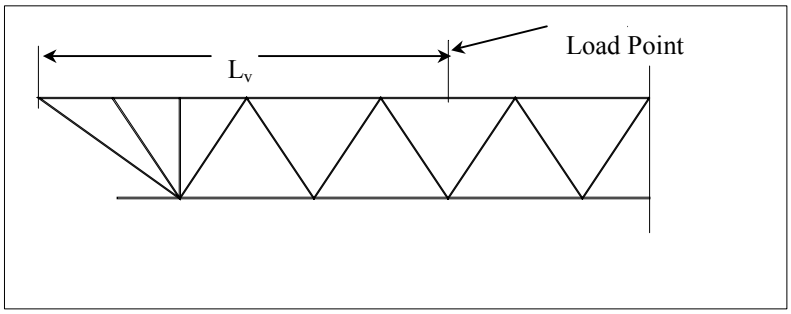

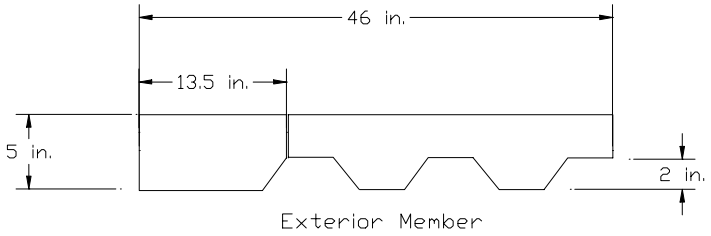

Area of concrete in shear plane, A_{cv}

$A_{cv} = L_v$ (nominal slab thickness – deck depth)
A_{cv} = 122 in. (5 in. – 2 in.) = 366 in^2

Area of concrete between shear planes, A_{cs}

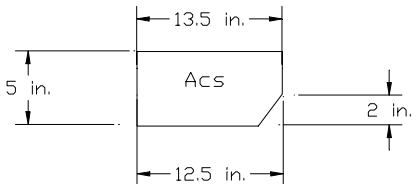

$$A_{cs} = 13.5\ in.\ x\ (3\ in.) + \left(\frac{13.5\ in. + 12.5\ in.}{2}\right) x\ (2\ in.) = 66.5\ \text{in}^2$$

Determination of Total V_u

$$\Sigma Q_n = \min\begin{pmatrix} A_s F_{y\,BC} = 16.20\ in^2\ x\ 50\ ksi = 810\ kips \\ 0.85 f'_c\ A_{cv} = 0.85\ x\ 4\ ksi\ x\ (46\ in.\ x\ 4\ in.) = 626\ kips \\ 0.75 n Q_n = 0.75\ x\ 31\ studs\ x\ 28.7\ kips/stud = 667\ kips \end{pmatrix}$$

ΣQ_n = 626 kips

Determination of Total V_u that has to be transferred at shear plane

$$V_u = \Sigma Q_n - 0.85\ x\ f'_c\ A_{cs} = 626\ kips - 0.85\ x\ 4\ ksi\ x\ 66.5\ in^2 = 400 \text{ kips}$$

V_u per shear plane = 400 / 1 = 400 kips

Determination of V_r

$$V_r = 0.8\ x\ A_s F_{yr} + 200 A_{cv} \qquad (\text{lbs, in}^2) \qquad \text{[Eq. 4.8]}$$

$$V_r = 0.8\ x\ 0.282\ in^2\ x\ 65000\ psi + 200\ x\ 366\ in^2 = 88000\ lbs \Rightarrow 88\ kips$$

Determination of longitudinal shear to be carried by transverse steel

$V_u - V_r$ = 400 – 88 = 312 kips

Determination of area of steel required to carry remaining shear

$V_u - V_r = 0.8\ A_s F_{yr}$

$$A_s = \left(\frac{V_u - V_r}{0.8\ x\ F_{yr}}\right) = \left(\frac{312\ kips}{0.8\ x\ 60\ ksi}\right) = 6.5\ in^2$$

APPENDIX B

Summary of Test Results

COMPOSITE JOIST-GIRDER TEST SUMMARY SHEET

TEST DESIGNATION: EGL TEST DATE: 28-30 November 1995

TEST DESCRIPTION

Joist-Girder:	Span:	30'-0"	Weight:	48.9 plf
	Depth:	30 in.	Spacing:	7 ft
	Top Chord:	2L-3.00x3.00x0.250	Yield Stress:	58.0 ksi
	Bottom Chord:	2L-4.00x4.00x0.375	Yield Stress:	60.2 ksi
Deck:	Type:	2VL	Gage:	18 ga
Slab:	Total Depth:	5 in.	Concrete Strength:	4900 psi
Shear Connector:	Type:	3/4 in. x 4 1/2 in. Welded Headed Shear Studs		
	Quantity:	14 per shear span		
Transverse Rebar:	Quantity:	6 no 4 @ 21" per shear span	Area:	1.18 in^2

THEORETICAL CALCULATIONS

Theoretical Max. Total Load per Joist-Girder: 154 kips

Theoretical Moment of Inertia: 3474 in^4

TEST RESULTS

Maximum Total Load per Joist-Girder: 174 kips

Experimental Moment of Inertia: 2934 in^4

Mode of Failure: Comp. buckling of Web Member W3R

COMPARISON OF EXPERIMENTAL TO THEORETICAL

$$\frac{\text{Maximum Total Load per Joist-Girder}}{\text{Theoretical Max. Total Load per Joist-Girder}} = 1.13$$

Figure B.1 EGL Test Summary (FF-1)

COMPOSITE JOIST-GIRDER TEST SUMMARY SHEET

TEST DESIGNATION: IG TEST DATE: 28-30 November 1995

TEST DESCRIPTION

Joist-Girder:	Span:	30'-0"	Weight:	91.3 plf
	Depth:	30 in.	Spacing:	7 ft
	Top Chord:	2L-4.00x4.00x0.375	Yield Stress:	58.7 ksi
	Bottom Chord:	2L-5.00x5.00x0.625	Yield Stress:	55.0 ksi
Deck:	Type:	2VL	Gage:	18 ga
Slab:	Total Depth:	5 in.	Concrete Strength:	4900 psi
Shear Connector:	Type:	3/4 in. x 4 1/2 in. Welded Headed Shear Studs		
	Quantity:	27 per shear span		
Transverse Rebar:	Quantity:	10 no. 4 bars @ 13" per shear span	Area:	1.96 in^2

THEORETICAL CALCULATIONS

Theoretical Max. Total Load per Joist-Girder: 294 kips

Theoretical Moment of Inertia: 6889 in^4

TEST RESULTS

Maximum Total Load per Joist-Girder: 341 kips

Experimental Moment of Inertia: 5345 in^4

Mode of Failure: Failure of Filler Welds, Web Buckling

COMPARISON OF EXPERIMENTAL TO THEORETICAL

$$\frac{\text{Maximum Total Load per Joist-Girder}}{\text{Theoretical Max. Total Load per Joist-Girder}} = 1.16$$

Figure B.2 IG Test Summary (FF-1)

COMPOSITE JOIST-GIRDER TEST SUMMARY SHEET

TEST DESIGNATION: EGR TEST DATE: 28-30 November 1995

TEST DESCRIPTION

Joist-Girder:	Span:	30'-0"	Weight:	48.9 plf
	Depth:	30 in.	Spacing:	7 ft
	Top Chord:	2L-3.00x3.00x0.250	Yield Stress:	59.5 ksi
	Bottom Chord:	2L-4.00x4.00x0.375	Yield Stress:	60.0 ksi
Deck:	Type:	2VL	Gage:	18 ga
Slab:	Total Depth:	5 in.	Concrete Strength:	4900 psi
Shear Connector:	Type:	3/4 in. x 4 1/2 in. Welded Headed Shear Studs		
	Quantity:	14 per shear span		
Transverse Rebar:	Quantity:	6 no. 4 bars @ 21" per shear span	Area:	1.18 in^2

THEORETICAL CALCULATIONS

Theoretical Max. Total Load per Joist-Girder: 154 kips

Theoretical Moment of Inertia: 3474 in^4

TEST RESULTS

Maximum Total Load per Joist-Girder: 173 kips

Experimental Moment of Inertia: 2888 in^4

Mode of Failure: Comp. Buckling of Web Member W3R

COMPARISON OF EXPERIMENTAL TO THEORETICAL

$$\frac{\text{Maximum Total Load per Joist-Girder}}{\text{Theoretical Max. Total Load per Joist-Girder}} = 1.12$$

Figure B.3 EGR Test Summary (FF-1)

COMPOSITE JOIST-GIRDER TEST SUMMARY SHEET

TEST DESIGNATION: EG TEST DATE: 01 November 2000

TEST DESCRIPTION

Joist-Girder:	Span:	30'-0"	Weight:	52.3 plf
	Depth:	30 in.	Spacing:	7 ft
	Top Chord:	2L-3.00x3.00x0.250	Yield Stress:	--
	Bottom Chord:	2L-4.00x4.00x0.375	Yield Stress:	62.9 ksi
Deck:	Type:	2VL	Gage:	18 ga
Slab:	Total Depth:	5 in.	Concrete Strength:	5200 psi
Shear Connector:	Type:	3/4 in. x 4 1/2 in. Welded Headed Shear Studs		
	Quantity:	17 per shear span		
Transverse Rebar:	Quantity:	3 no. 4 U-bars@ 40" per shear span	Area:	1.18 in^2

THEORETICAL CALCULATIONS

Theoretical Max. Total Load per Joist-Girder: 187 kips

Theoretical Moment of Inertia: 3472 in^4

TEST RESULTS

Maximum Total Load per Joist-Girder: 215 kips

Experimental Moment of Inertia: 2892 in^4

Mode of Failure: BC Yielding, Slab crushing

COMPARISON OF EXPERIMENTAL TO THEORETICAL

$$\frac{\text{Maximum Total Load per Joist-Girder}}{\text{Theoretical Max. Total Load per Joist-Girder}} = 1.15$$

Figure B.4 EG Test Summary (FF-2)

COMPOSITE JOIST-GIRDER TEST SUMMARY SHEET

TEST DESIGNATION: IG TEST DATE: 01 November 2000

TEST DESCRIPTION

Joist-Girder:	Span:	30'-0"	Weight:	99.7 plf
	Depth:	30 in.	Spacing:	7 ft
	Top Chord:	2L-4.00x4.00x0.375	Yield Stress:	--
	Bottom Chord:	2L-5.00x5.00x0.625	Yield Stress:	57.0 ksi
Deck:	Type:	2VL	Gage:	18 ga
Slab:	Total Depth:	5 in.	Concrete Strength:	5200 psi
Shear Connector:	Type:	3/4 in. x 4 1/2 in. Welded Headed Shear Studs		
	Quantity:	34 per shear span		
Transverse Rebar:	Quantity:	4 no. 4 bars @ 12"	Area:	1.57 in^2
		4 no. 4 bars @ 20" per shear span		

THEORETICAL CALCULATIONS

Theoretical Max. Total Load per Joist-Girder: 364 kips

Theoretical Moment of Inertia: 6818 in^4

TEST RESULTS

Maximum Total Load per Joist-Girder: 388 kips

Experimental Moment of Inertia: 4960 in^4

Mode of Failure: BC Yielding, Slab crushing

COMPARISON OF EXPERIMENTAL TO THEORETICAL

$$\frac{\text{Maximum Total Load per Joist-Girder}}{\text{Theoretical Max. Total Load per Joist-Girder}} = 1.07$$

Figure B.5 IG Test Summary (FF-2)

COMPOSITE H-SHAPE TEST SUMMARY SHEET

TEST DESIGNATION: EB TEST DATE: 01 November 2000

TEST DESCRIPTION

Joist-Girder:	Span:	30'-0"	Weight:	55.0 plf
	Depth:	23.6 in.	Spacing:	7 ft
	As	16.2 in^2	Yield Stress:	70.8 ksi
Deck:	Type:	2VL	Gage:	18 ga
Slab:	Total Depth:	5 in.	Concrete Strength:	5200 psi
Shear Connector:	Type:	3/4 in. x 4 1/2 in. Welded Headed Shear Studs		
	Quantity:	31 per shear span		
Transverse Rebar:	Quantity:	26 no. 4 @ 4.5" per shear span	Area:	5.10 in^2

THEORETICAL CALCULATIONS

Theoretical Max. Total Load per H-Shape: 260 kips

Theoretical Moment of Inertia: 3453 in^4

TEST RESULTS

Maximum Total Load per H-Shape: 227 kips

Experimental Moment of Inertia: 2985 in^4

Mode of Failure: Flange Yielding, Crushing of the Concrete

COMPARISON OF EXPERIMENTAL TO THEORETICAL

$$\frac{\text{Maximum Total Load per H-Shape}}{\text{Theoretical Max. Total Load per H-Shape}} = 0.87$$

Figure B.6 EB Test Summary (FF-2)

COMPOSITE JOIST-GIRDER TEST SUMMARY SHEET

TEST DESIGNATION: EGL TEST DATE: 17-19 December 1996

TEST DESCRIPTION

Joist-Girder:	Span:	30'-0"	Weight:	46.1 plf
	Depth:	25 in.	Spacing:	6 ft 9 in.
	Top Chord:	2L-3.00x3.00x0.250	Yield Stress:	58.0 ksi
	Bottom Chord:	2L-4.00x4.00x0.375	Yield Stress:	55.3 ksi
Deck:	Type:	2VL	Gage:	18 ga
Slab:	Total Depth:	5 in.	Concrete Strength:	4500 psi
Shear Connector:	Type:	3/4 in. x 8 in. Welded Headed Shear Studs		
	Quantity:	26 per shear span		
Transverse Rebar:	Quantity:	7 no. 3 U-bars per shear span	Area:	1.55 in^2

THEORETICAL CALCULATIONS

Theoretical Max. Total Load per Joist-Girder: 182 kips

Theoretical Moment of Inertia: 3543 in^4

TEST RESULTS

Maximum Total Load per Joist-Girder: 177 kips

Experimental Moment of Inertia: 3539 in^4

Mode of Failure: Bottom Chord Yielding

COMPARISON OF EXPERIMENTAL TO THEORETICAL

$$\frac{\text{Maximum Total Load per Joist-Girder}}{\text{Theoretical Max. Total Load per Joist-Girder}} = 0.97$$

Figure B.7 EGL Test Summary (H-1)

COMPOSITE JOIST-GIRDER TEST SUMMARY SHEET

TEST DESIGNATION: IG TEST DATE: 17-19 December 1996

TEST DESCRIPTION

Joist-Girder:	Span:	30'-0"	Weight:	89.2 plf
	Depth:	25 in.	Spacing:	6 ft 9 in.
	Top Chord:	2L-4.00x4.00x0.375	Yield Stress:	55.7 ksi
	Bottom Chord:	2L-5.00x5.00x0.625	Yield Stress:	53.4 ksi
Deck:	Type:	2VL	Gage:	18 ga
Slab:	Total Depth:	5 in.	Concrete Strength:	4500 psi
Shear Connector:	Type:	3/4 in. x 8 in. Welded Headed Shear Studs		
	Quantity:	52 per shear span		
Transverse Rebar:	Quantity:	11 no. 4 @ 12"	Area:	10.4 in^2
		27 no. 5 @4.5" per shear span		

THEORETICAL CALCULATIONS

Theoretical Max. Total Load per Joist-Girder: 353 kips

Theoretical Moment of Inertia: 6833 in^4

TEST RESULTS

Maximum Total Load per Joist-Girder: 409 kips

Experimental Moment of Inertia: 6231 in^4

Mode of Failure: Bottom Chord Yielding at East Third Point

COMPARISON OF EXPERIMENTAL TO THEORETICAL

$$\frac{\text{Maximum Total Load per Joist-Girder}}{\text{Theoretical Max. Total Load per Joist-Girder}} = 1.16$$

Figure B.8 IG Test Summary (H-1)

COMPOSITE H-SHAPE TEST SUMMARY SHEET

TEST DESIGNATION: EB TEST DATE: 17-19 December 1996

TEST DESCRIPTION

Joist-Girder:	Span:	30'-0"	Weight:	55.0 plf
	Depth:	23.6 in.	Spacing:	6 ft 9 in.
	As	16.2 in^2	Yield Stress:	48.1 ksi
Deck:	Type:	2VL	Gage:	18 ga
Slab:	Total Depth:	5 in.	Concrete Strength:	4500 psi
Shear Connector:	Type:	3/4 in. x 4 1/2 in. Welded Headed Shear Studs		
	Quantity:	17 per shear span		
Transverse Rebar:	Quantity:	None	Area:	0 in^2

THEORETICAL CALCULATIONS

Theoretical Max. Total Load per H-Shape: 174 kips

Theoretical Moment of Inertia: 3503 in^4

TEST RESULTS

Maximum Total Load per H-Shape: 137 kips

Experimental Moment of Inertia: 2661 in^4

Mode of Failure: Yielding of Bottom Flange, Nonlinear Behav.

COMPARISON OF EXPERIMENTAL TO THEORETICAL

$$\frac{\text{Maximum Total Load per H-Shape}}{\text{Theoretical Max. Total Load per H-Shape}} = 0.79$$

Figure B.9 EB Test Summary (H-1)

COMPOSITE JOIST-GIRDER TEST SUMMARY SHEET

TEST DESIGNATION: EG TEST DATE: 20-21 October 1999

TEST DESCRIPTION

Joist-Girder:	Span:	30'-0"	Weight:	46.0 plf
	Depth:	25 in.	Spacing:	6 ft 9 in.
	Top Chord:	2L-3.00x3.00x0.250	Yield Stress:	--
	Bottom Chord:	2L-4.00x4.00x0.375	Yield Stress:	60.8 ksi
Deck:	Type:	2VL	Gage:	18 ga
Slab:	Total Depth:	5 in.	Concrete Strength:	5300 psi
Shear Connector:	Type:	3/4 in. x 9 3/16 in. Welded Headed Shear Studs		
	Quantity:	20 per shear span		
Transverse Rebar:	Quantity:	4 no. 3 @ 28" per shear span	Area:	0.44 in^2

THEORETICAL CALCULATIONS

Theoretical Max. Total Load per Joist-Girder: 200 kips

Theoretical Moment of Inertia: 3523 in^4

TEST RESULTS

Maximum Total Load per Joist-Girder: 189 kips

Experimental Moment of Inertia: 3104 in^4

Mode of Failure: Bottom Chord Yielding

COMPARISON OF EXPERIMENTAL TO THEORETICAL

$$\frac{\text{Maximum Total Load per Joist-Girder}}{\text{Theoretical Max. Total Load per Joist-Girder}} = 0.95$$

Figure B.10 EG Test Summary (H-2)

COMPOSITE JOIST-GIRDER TEST SUMMARY SHEET

TEST DESIGNATION: IG TEST DATE: 20-21 October 1999

TEST DESCRIPTION

Joist-Girder:	Span:	30'-0"	Weight:	89.2 plf
	Depth:	25 in.	Spacing:	6 ft 9 in.
	Top Chord:	2L-4.00x4.00x0.375	Yield Stress:	--
	Bottom Chord:	2L-5.00x5.00x0.625	Yield Stress:	54.7 ksi
Deck:	Type:	2VL	Gage:	18 ga
Slab:	Total Depth:	5 in.	Concrete Strength:	5300 psi
Shear Connector:	Type:	3/4 in. x 9 3/16 in. Welded Headed Shear Studs		
	Quantity:	40 per shear span		
Transverse Rebar:	Quantity:	4 no. 3 @ 28" per shear span	Area:	0.44 in^2

THEORETICAL CALCULATIONS

Theoretical Max. Total Load per Joist-Girder: 364 kips

Theoretical Moment of Inertia: 6790 in^4

TEST RESULTS

Maximum Total Load per Joist-Girder: 364 kips

Experimental Moment of Inertia: 5819 in^4

Mode of Failure: Bottom Chord Yielding

COMPARISON OF EXPERIMENTAL TO THEORETICAL

$$\frac{\text{Maximum Total Load per Joist-Girder}}{\text{Theoretical Max. Total Load per Joist-Girder}} = 1.00$$

Figure B.11 IG Test Summary (H-2)

COMPOSITE H-SHAPE TEST SUMMARY SHEET

TEST DESIGNATION: EB TEST DATE: 20-21 October 1999

TEST DESCRIPTION

Joist-Girder:	Span:	30'-0"	Weight:	55.0 plf
	Depth:	25 in.	Spacing:	6 ft 9 in.
	As	16.2 in^2	Yield Stress:	55.7 ksi
Deck:	Type:	2VL	Gage:	18 ga
Slab:	Total Depth:	5 in.	Concrete Strength:	5300 psi
Shear Connector:	Type:	3/4 in. x 9 3/16 in. Welded Headed Shear Studs		
	Quantity:	6 per shear span		
Transverse Rebar:	Quantity:	4 no. 3 @ 28" per shear span	Area:	0.44 in^2

THEORETICAL CALCULATIONS

Theoretical Max. Total Load per H-Shape: 293 kips

Theoretical Moment of Inertia: 5243 in^4

TEST RESULTS

Total Load per H-Shape at First Yield: 150 kips

Maximum Total Load per H-Shape: 229 kips

Experimental Moment of Inertia: 3976 in^4

Mode of Failure: Bottom Flange Yielding

COMPARISON OF EXPERIMENTAL TO THEORETICAL

$$\frac{\text{Maximum Total Load per H-Shape}}{\text{Theoretical Max. Total Load per H-Shape}} = 0.78$$

Figure B.12 EB Test Summary (H-2)

APPENDIX C

Girder Stiffness

C.1 Theoretical Moment of Inertia

Theoretical stiffness is based on the effective moment of inertia that can be predicted from the composite joist, joist girder, or H-shape. This effective moment of inertia can be calculated based on the slope of the linear portion of the load vs. deflection curve and is used to predict deflections based on service load conditions.

The theoretical effective moment of inertia was calculated using equations developed for open-web composite joists and joist girders. In general, the equations take into account to some degree the contributions from the slab and the steel joist with associated material transformations for calculation purposes. The equations also account for slip and web effects by means of reduction factors. The procedure for calculating the effective moment of inertia consists of calculating the moment of inertia for the steel element, calculating the transformed moment of inertia for the concrete slab, and then applying prediction equations. The H-shape moment of inertia was calculated considering only material properties and transformed section properties.

The first equation was presented in the AISC Steel Design Guide Series (no. 11) for Floor Vibrations (Murray et al. 1997).

$$I_{eff} = \frac{1}{\frac{\gamma}{I_{chords}} + \frac{1}{I_{comp}}} \qquad \text{[Eq. C.1]}$$

$$\gamma = \frac{1}{C_r} - 1, \qquad C_r = 0.90\,[1 - e^{-0.28(L/D)}]^{2.8} \quad \text{for } 6 \le (L/D) \le 24$$

Where:

I_{eff}: effective transformed moment of inertia taking shear deformation into account

I_{comp}: fully composite moment of inertia

I_{chords}: moment of inertia of the joist chords only

L: nominal span

D: depth of bare joist or joist girder

The second equation was presented by Viest et al. (1997) in *Composite Construction Design for Buildings.*

$$I_{eff} = I_s^{'} + 0.77(I_t^{'} - I_s^{'}) \qquad \text{[Eq. C.2]}$$

Where:

I_{eff} : effective moment of inertia

$I_s^{'}$: moment of inertia of the steel section (I_s) divided by 1.1 to account for flexibility of web

$I_t^{'}$: moment of inertia of the transformed concrete slab

The third equation was presented by Gibbings et al.(1990).

$$I_{eff} = \frac{I_{comp} - 0.15 I_s}{1 + 0.15} \qquad \text{[Eq. C.3]}$$

Where:

I_{eff} : effective moment of inertia

I_{comp}: fully composite moment of inertia

I_s: moment of inertia of the steel joist

The results of the predicted effective moments of inertia are presented in Table C.1.

Table C.1 Theoretical Moment of Inertia

Test	Member	I_{eff}^1 in^4	I_{eff}^2 in^4	I_{eff}^3 in^4
FF-1	EGL	2758	3606	3474
	IG	5406	7135	6889
	EGR	2758	3606	3474
FF-2	EG	2757	3605	3472
	IG	5373	7067	6818
H-1	EGL	2683	3570	3543
	IG	5156	6882	6833
H-2	EG	2674	3551	3523
	IG	5138	6840	6790

Table C.2 shows the theoretical moment of inertia for the H-shapes in tests FF-2, H-1, and H-2. These values were calculated using transformed section properties and an example calculation is presented in Appendix D.1.

Table C.2 Theoretical Moment of Inertia

FF-2	EB	3453	in^4
H-1	EB	3503	in^4
H-2	EB	5243	in^4

C.2 Experimental Moment of Inertia

The experimental effective moment of inertia was back calculated from the experimental load vs. displacement data. This was done by isolating the linear-elastic portion of the load vs. deflection plot and performing a linear least squares fit. Each load vs. deflection plot was treated this way and the slopes (m) of each line were used in calculating the effective experimental moment of inertia.

The theoretical and experimental moment of inertia is predicated on the theory that the deflection equation for a simply supported member is valid and therefore represents the behavior of the joist girder or H-shape. The equation for predicting the midspan deflection with concentrated loads at the third points is as follows:

$$\Delta_{MS} = \frac{Pa}{24EI}\left(3l^2 - 4a^2\right) \qquad \text{[Eq. C.4]}$$

Where:

P: applied load at each of two symmetrically placed load points (kips)

a : distance form end of member to location of load (in.)

l : nominal span length (in.)

E : modulus of elasticity (ksi)

I : moment of inertia (in^4)

Taking a = (10 x 12) = 120 in. and l = (30 x 12) = 360 in. with E = 29000 ksi, the equation can be reduced to:

$$\Delta_{MS} = \frac{57.103P}{I} \qquad \text{[Eq. C.5]}$$

This equation assumes that the only loads acting on the member are the point loads and as such, the calculations must be made without the dead load due to the slab, the joists, and the joist girders or H-shape. Additionally P in this equation is defined as the total load divided by 2. The slope (m) obtained from the best fit line is equal to P/Δ_{MS} and I_{exp} is equal to 57.103/2 or 28.552 times the slope (m). Table C.3 shows the experimental moment of inertia for the four tests considered in this study.

Table C.3 Experimental Moment of Inertia

Test	Member	m	R^2	I_{exp} in^4
FF-1	EG3	102.77	0.9955	2934
	IG	187.23	0.9994	5345
	EG4	101.16	0.9993	2888
FF-2	EG	101.28	0.9984	2892
	IG	173.73	0.9992	4960
	EB	104.54	0.9985	2985
H-1	EG	123.95	0.9809	3539
	IG	218.26	0.9864	6231
	EB	93.22	0.9834	2661
H-2	EG	108.72	0.9998	3104
	IG	203.82	0.9985	5819
	EB	139.26	0.9993	3976

Table C.4 shows the comparison of the experimental moment of inertia with the three analytical methods predicting the moment of inertia. In terms of the best predictor of the experimental stiffness for the joist girders, Equation C.1 had the best overall results when compared to the experimental stiffness for the flush-framed girder tests. Equations C.2 and C.3, however, were better predictors of the experimental moment of inertia for the first haunch test that Equation C.1. In the second haunch test, all three equations did not predict the experimental moment of inertia accurately. Equation C.1 underpredicted the experimental values and Equations C.2 and C.3 over predicted the experimental moment of inertia. In terms of the H-shapes, the stiffness was overpredicted by the analytical method for both the haunched and flushed-framed configurations

Table C.5 shows the calculated R^2 values obtained from a linear regression where the experimental stiffness was entered as the y-variable and the calculated stiffness was entered as the x-variable. The regression statistics show that there is very little difference statistically between the three methods, however, the limited number of data points may explain this.

Table C.4 Comparison of Experimental to Predicted Moment of Inertia

Test	Member	I_{exp} / I_{eff}^{1}	I_{exp} / I_{eff}^{2}	I_{exp} / I_{eff}^{3}
FF-1	EGL	1.06	0.81	0.84
	IG	0.99	0.75	0.78
	EGR	1.05	0.80	0.83
FF-2	EG	1.05	0.80	0.83
	IG	0.92	0.70	0.73
	EB	0.86	0.86	0.86
H-1	EGL	1.32	0.99	1.00
	IG	1.21	0.91	0.91
	EB	0.76	0.76	0.76
H-2	EG	1.16	0.87	0.88
	IG	1.13	0.85	0.86
	EB	0.76	0.76	0.76

FF-2	EB	0.86
H-1	EB	0.76
H-2	EB	0.76

Table C.5 Regression Statistics

Regression Statistics			
	[C.1]	[C.2]	[C.3]
Multiple R	0.94	0.95	0.96
R Square	0.89	0.90	0.92
Adjusted R Square	0.87	0.88	0.91
Standard Error	501	473	414
Observations	9	9	9

APPENDIX D

Sample Calculations

D.1 Composite Moment of Inertia of Haunched Joist Girder

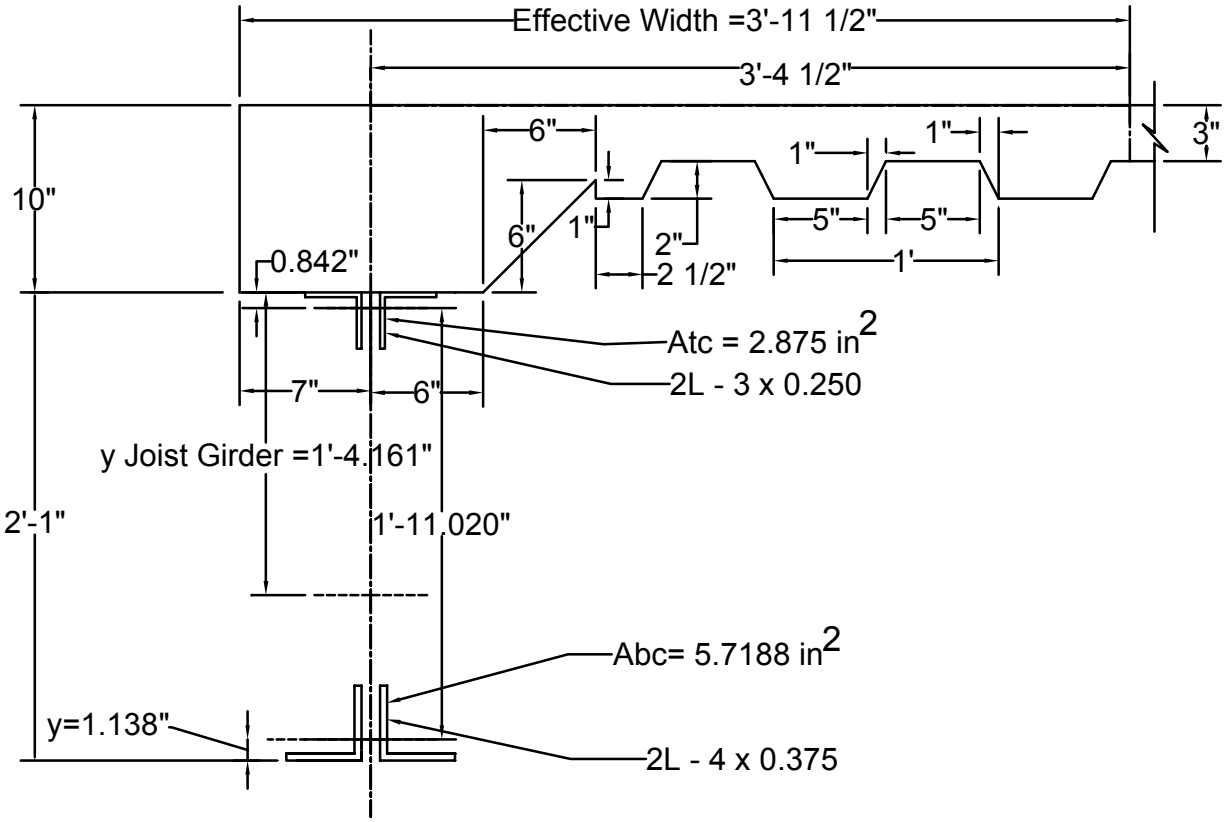

1) Calculate Joist Girder Noncomposite Moment of Inertia

Joist Girder Non-Composite Moment of Inertia					
A_{TC}	2.875	in^2	y_{TC}	0.842	in
A_{BC}	5.719	in^2	y_{BC}	1.138	in
I_{TC}	2.488	in^4	d	25.000	in
I_{BC}	8.718	in^4	d_e	23.020	
y_{JG}	16.161	in	$I_{NC,JG}$	1025.04	in^4

$$y_{Joist\ Girder} = \frac{A_{TC}y_{TC} + A_{BC}(d_{Joist\ Girder} - y_{BC})}{A_{TC} + A_{BC}} = \frac{2.875\,(0.842) + 5.7188\,(25 - 1.138)}{2.875 + 5.7188} = 16.2\ \text{in}$$

$$I_{Joist\ Girder\ \ Noncomposite} = I_{TC} + I_{BC} + \frac{A_{TC}A_{BC}d_e^{\ 2}}{A_{TC} + A_{BC}}$$

Where:

$d_{Joist\ Girder}$ = Depth of steel joist girder = 25 in

I_{TC} = Moment of Inertia for both top chord angles = 1.244 in^4 x 2 angles = 2.488 in^4

I_{BC} = Moment of Inertia for both bottom chord angles = 4.359 in^4 x 2 angles = 8.718 in^4

y_{TC} = Location for centroid of top chord = 0.842 in

y_{BC} = Location for centroid of bottom chord = 1.138 in

d_e = Joist girder effective depth = 25 in - 0.842 in - 1.138 in = 23.020 in

A_{TC} = Area of both top chord angles = 1.438 in^2 x 2 angles = 2.875 in^2

A_{BC} = Area of both bottom chord angles = 2.859 in^2 x 2 angles = 5.7188 in^2

$$I_{Joist\ Girder\ Noncomposite} = 2.488\,in^4 + 8.718\,in^4 + \frac{(2.875\,in^2)(5.7188\,in^2)(23.020\,in)^2}{(2.875\,in^2 + 5.7188\,in^2)} = 1{,}025\,in^4$$

2) <u>Calculate Transformed Moment of Inertia for Concrete Slab</u>

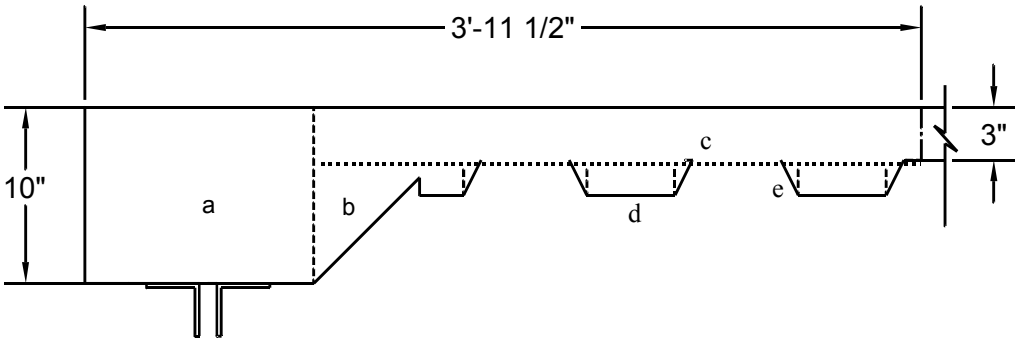

$$n = \frac{E_s}{E_C}$$

$$E_c = 33w^{1.5}\sqrt{f_c'} = 33\,(145\ pcf)^{1.5}\sqrt{4000} = 3{,}644\ ksi$$

$$n = \frac{29{,}000\ ksi}{3{,}644.1\ ksi} = 7.96$$

Element	Element Area in^2	Element Area/n in^2	No. pieces	Total Area in^2	Total $Area_{tr}$ in^2	y to top of slab in	A_{tr} x y_{top} in^3	h in	A_{tr} x h^2 in^4	I_o in^4	Total I_o / n in^4
a	130.0	16.34	1	130	16.34	5	81.7	1.29	27	1083	136
b	24.5	3.08	1	24.5	3.08	6	18.5	2.29	16	67	8
c	103.5	13.01	1	103.5	13.01	1.5	19.5	-2.21	64	26	3
d	10.0	1.26	2	20	2.51	4	10.1	0.29	0	3	1
e	1.0	0.13	4	4	0.50	3.67	1.8	-0.04	0	0	0
Total	268.0	33.68		282	35.44		131.56		107.06		148.71
y_{tr}	3.71	in	I_{tr}	255.78	in^4						

3) Calculate Combined Transformed Moment of Inertia for Slab and Girder

Element	Element Area in^2	$y_{top\ of\ slab}$ in	Area x y_{top} in^3	h in	Area x h^2 in^4	I_o in^4
Joist Girder	8.59	26.16	224.82	18.07	2805	1025
Slab	35.44	3.71	131.56	-4.38	680	256
Total	44.03		356.38		3485	1281
$y_{centroid}$	8.09	in	$I_{composite}$	4766	in^4	

D.2 Predicted Strength of Composite Joist Girder

Material Properties:

f'c = 5200 psi

F_{yBC} = 62987 psi EG

= 57034 psi IG

= 70774 psi EB

Dead Load Determination:

IG	Joist girder Weight	= 99.7 lb/ft
EG	Joist girder Weight	= 52.3 lb/ft
EB	H-Shape Girder Weight	= 55.0 lb/ft

joist dead load

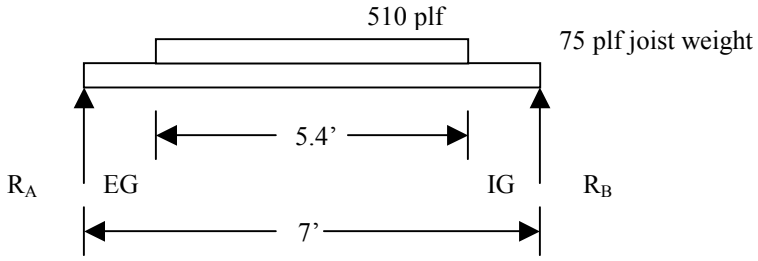

wt of deck plus 5 in concrete deck = 51 psf x 10' (trib width) = 510 plf
$R_A = R_B =$ ½(6.67*75) + ½(510*5.4) = 1.627 kips

concrete weight over joist girder

IG $A_c = 89\ in^2$ EG $A_c = 64.5\ in^2$ EB $A_c = 64.5\ in^2$

IG Conc.Wt. = 89 x 12 x $(1/12^3)$ x 145 = 89.6 plf

EG,EB Conc. Wt. = 64.5 x 12 x $(1/12^3)$ x 145 = 64.9 plf

Interior Joist girder

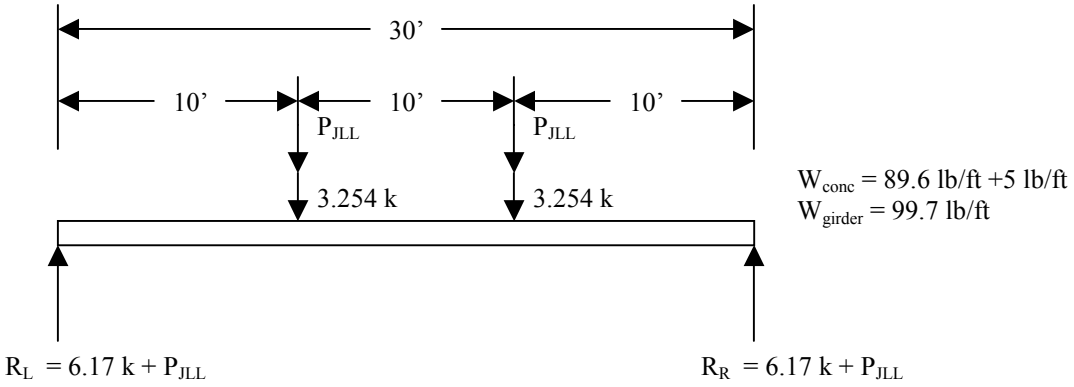

d_{joist} = 30 in. BC Area = 11.718 in.^{2}

y_{BC} = 1.479 in.

T_{BC}^{A} = 11.718*(57.034) = 668 kips

A_c^{Tot} = 344 in.^{2} C_{max} = 0.85*5200*344 = 1521 kips

Area req’d to balance BC@57 ksi = 668 / (0.85*5.2) = 151 in^2

a = 151 / b = 151 / 84 = 1.80 in. a/2 = 0.9 in.

d_{BC} = 30 + 5 –1.479 – 0.9 = 32.621 in.

M_{ult} = 668*32.621*(1/12) = 1816 ft-kips

$M_{centerline} = R_L(15’) – 0.1943(15’)(15’/2) – 3.254(5)’ – P_{JLL}(5’)$

$1816 = 6.17(15’) + P_{JLL}(15’) – 21.9 – 16.27 – P_{JLL}(5’)$

$1754.6 = 10\ P_{JLL}$ P_{JLL} = 175.5 kips

Total Load = 2*(175.5) + 2*(6.17) = 363 kips

D.3 Reduced Strength due to Limiting Longitudinal Shear Strength
Nominal Material Properties

$f'_c = 4.0$ ksi $F_y = 50.0$ ksi $b = 46$ in. $b' = 13.5$ in. $A_{cs} = 66.5$ in^2
$A_{mesh} = 0.282$ in^2 $d = 23.6$ in. $b_f = 7.005$ in. $t_f = 0.505$ in. $t_w = 0.395$ in.

$M_u^{calc} = 1180$ ft-kips

Calculated Longitudinal Shear Strength at Critical Shear Plane

$V_r = 0.8 \times 0.282 \times 65000 + 200 \times 366 = 88000$ lbs ~ 88 kips

Equivalent Compressive Force (C) that Produces V_r at Critical Shear Plane

$V_r = \sum Q_n - 0.85 f'_c A_{cs}$ [1 / no. of shear planes]
$\sum Q_n = V_r \times$ [no. shear planes] $+ 0.85 f'_c A_{cs} = C$
$\sum Q_n = 88 \times 1 + 0.85 \times 4 \times 66.5 = 314$ kips ($\sum Q_n = 517$ kips in strength calcs)

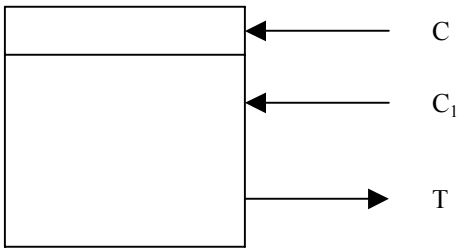

$C + C_1 = T = A_s F_y - C_1$
$314 + 2C_1 = A_s F_y$
$2C_1 = 16.2(50) - 314 = 496$ kips
$T = 562$ kips
$a = 314 / (0.85 \times 4.0 \times 46$ in.$) = 2.00$ in.
$a / 2 = 1.00$ in.

$C_{flg} = 7.005 \times 0.505 \times 50 = 177$ kips < 248 kips ==➔ PNA in web

$d_{web} = (248 - 177) / (0.395 \times 50) = 3.59$ in.

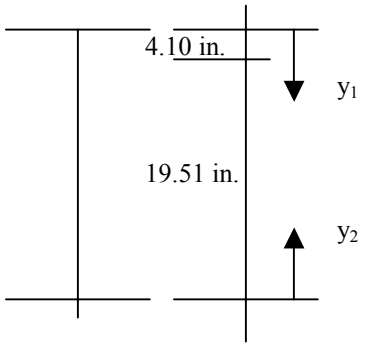

$$y_1 = \frac{3.54(0.253) + 3.59(0.395)(2.30)}{3.54 + 1.42} = 0.84\ in.$$

$$y_2 = \frac{3.54(0.253) + 19(0.395)(10.01)}{3.54 + 7.505} = 6.88\ in.$$

$My_1 = 562\ (23.6\text{-}6.88\text{-}0.84) + 248\ (5\text{-}1.00\text{+}0.84)$
$= 10125$ in-kip ~ 844 ft-kip

$My_1 / M_u^{calc} = 844 / 1180 = 0.72$

VITA

Jason Matthew Piotter was born in Rockford, Illinois on September 30, 1973. He was raised in Omro, WI and graduated from Omro High School in 1992. He attended the University of Iowa from 1992 to 1999 where he received a Bachelor of Science degree in Civil Engineering and a Bachelor of Science Degree in Exercise Science. In the summer of 1999, he entered the Via Department of Civil and Environmental Engineering to pursue a Masters of Science degree.